University of Alberta

Experimental Study of Elastoplastic Mechanical Properties of
Coke Drum Materials

by

Jie Chen

A thesis submitted to the Faculty of Graduate Studies and Research
in partial fulfillment of the requirements for the degree of

Master of Science

Mechanical Engineering

©Jie Chen
Spring, 2010
Edmonton, Alberta

Examining Committee

Dr. Zihui Xia, Mechanical Engineering (Supervisor)

Dr. Chongqing Ru, Mechanical Engineering (Committee Chair)

Dr. Hao Zhang, Chemical and Material Engineering (Committee member)

Abstract

Coke drums are vertical pressure vessels used in the delayed coking process in petroleum refineries. Significant temperature variation during the delayed coking process causes the useful life of coke drums to be shortened. In order to better understand the failure mechanisms, a experimental study of elastic/plastic mechanical properties and deformation behaviors of typical coke drum materials was performed.

A new biaxial thermal-mechanical material testing system has been successfully developed. Basic characterization of mechanical properties of coke drum materials is achieved through uniaxial monotonic and cyclic loading tests. In addition, strain-rate dependence and creep of coke drum materials were further experimentally investigated. Complex thermal-mechanical cyclic tests were conducted. The experimental findings help us to understand the damage mechanisms of coke drums such as bulging. In addition, experimental data serve as benchmark data to verify the predictions of the temperature dependent elastoplastic constitutive model.

Acknowledgements

I wish to express his appreciation to Dr. Zihui Xia for his guidance and patience throughout this endeavor.

Gratitude is extended to Mr. Bernie Faulkner, who gives me great help on developing, using the experimental facility and manufacturing the test specimens.

I also would like to take this opportunity to express my thanks to Dr. Pierre Mertiny, Dr. Feng Ju, Dr. Yejian Jiang, John Aumuller, and other members of the ACME group, for offering great support and discussions. It is a pleasure to be among them.

I am especially grateful to my wife, Shuo Tong, for being so supportive throughout my study.

INDEX

List of Figures

List of Tables

Chapter 1 Introduction

1.1 Introduction of Coke Drum and Problems

1.1.1 Coke Drum and Production Process

Coke drums are vertical pressure vessels used in the delayed coking process in petroleum refineries. They are normally constructed of carbon or low carbon alloy steels internally cladded with AISI 410S or AISI 405 stainless steel to protect the coke drums from corrosion. They range from 4 to 9 meters in diameter and around 25 meters in height. The maximum shell thickness varies from 0.014 to 0.042 meters. The pressure ranges from 100 to 500 kPa, and the maximum operation temperature ranges from 427 to 482°C [1].

A typical coke drum cycle in terms of temperature is shown in Figure 1.1. Firstly, heavy residual is imported into a coker heater and heated to approximately 480 °C. Before directing the heavy oil into the coke drum, the drum is preheated by flowing vapor from the bottom of the drum to the top. (Temperature rises from approximate 93 °C to 427 °C, see Fig. 1). Then, the hot heavy oil is directed into the coke drum to begin the fill cycle. The fill cycle usually takes 14-18 hours. When the filling is complete, light hydrocarbon produced from the coke during the thermal cracking process is removed by steam stripping. (Temperature drops from 480 °C to 149 °C approximately) After that, high rate of quench water is injected into the coke drum, cooling the vessel and possibly extracting the solid coke. After soaking, the solid coke is cut by applying the high-pressure water

steams. After all the coke is removed from the drum, the coke drum is reheated

and checked in order to prepare for a new operation cycle.
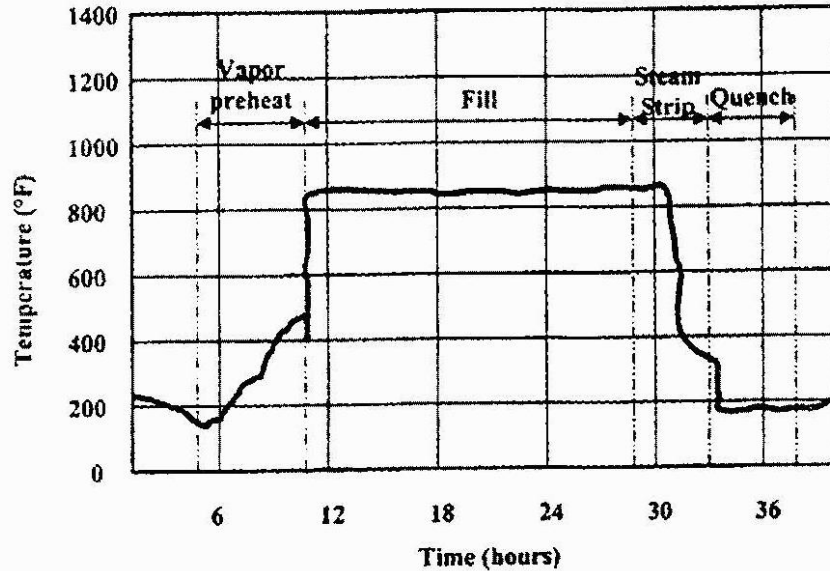
Figure 1.1Typical thermal cycle experienced by coke drums [1]

1.1.2 Problems and Studies Related with Coke Drum

The average operation life of coke drums is above ten years. However,

there are several kinds of service related damages of coke drum components

reported. Several thousands of dollars are spent to repair the units and the loss

from the disrupt of the production could be even much high [1].

The significant temperature variation during the delayed coking process,

such as heating and quenching, causes the useful life of coke drums to be

shortened comparing with other pressure vessels under non-cyclic thermal

condition. The severe cyclic thermal-mechanical load makes coke drums

susceptible to damage. It is also found that shell bulging is one of the causes

leading cracking and failure in the vessel shell of coke drums. Radial bulging is identified as a "reoccurring difficulty" that existed in essentially all operating coke drums of the time [2]. The root cause of the shell bulging is the intense thermal cycling during the operation of filling-quenching cycle [3]. The bulges are normally found near the circumferential weld seams which normally have higher yield strength, and the base material finally tend to become thin and fails via cracking as the result of the restraint caused by the weld seams [4-6]. There is also agreement that low cycle fatigue is considered the failure mode for coke drums. There have been several measuring techniques involved to identify the bulging and cracking problems of coke drums. The traditional inspection method of characterizing the coke drum distortion is performed with an internal visual and dimensional inspection [7]. However, this type of inspection is only performed during major unit turnarounds that occurred once every four years [7]. There are also new inspection methodologies including laser bulging inspection [7], high temperature strain gauge monitoring, and finite element analysis [8], etc. The FEM analysis carried by Rutt and Clark shows a local doubling of axial stress in the area of the weld crack which would significantly reduce the fatigue life of the material in that region [7]. However, there are relative few investigations involving analytical or numerical models to simulate and predict the damage and fatigue life of coke drums.

1.2 Importance of Experimental Study on Elastoplastic Mechanical Properties of the Coke Drum Materials

Most of the researches show that low cycle fatigue is the major factor which causes the failure in coke drums, due to the high stresses generated during the quenching of the operation cycle [1]. In order to extend the life span of coke drums and reduce the undesired cost during the down time, as shown in Table 1.1, coke drums were constructed from carbon steel in early years to low alloys steels such as carbon-1/2 Moly, 1 ¼ Cr or even higher alloys in more recent years. In addition, most coke drums manufactured in recent years are cladded with either 410S or 405 stainless steel to prevent the corrosion caused by the high sulfur content [2].

Table 1.1 Typical materials used in coke drums [9]

Base Metal	Type
A516-70	Carbon Steel
A204 C	Carbon –½ Moly
A387-11, CL2	1 ¼ Cr – ½ Moly
A387-12, CL2	1 Cr – ½ Moly
A387-22, CL2	2 ¼ - 1 Moly
405 (clad)	13 Cr
410S (clad)	12 Cr

New drum material selection has been towards increasing Chrome Moly alloy content [6]. Steels with higher Cr and Mo contents are considered to have better thermal cycling resistance because of their higher yield strength and better creep resistance. However, there is still not enough evidence to demonstrate the

improved reliability due to use of these materials. The coke drums constructed from these materials still experience same type of damage or failure. In addition, there are a few papers dealing with the fatigue life estimation for the coke drums [10-12], these are only based on unaxial strain-fatigue life curves which do not consider biaxial loading cases. Therefore, Experimental study of typical coke drum materials (e.g. Cr-Mo material) plays an important role to characterize the mechanical properties and deformation behaviors of these materials under both uniaxial and biaxial loadings. In addition, the more accurately characterized basic mechanical properties of coke drum materials serve as a basis for further more accurate thermal-mechanical stress/strain analysis of coke drums. The experimental study of elastic/plastic deformation behaviors of these materials under complex thermal-mechanical cyclic loading conditions can also help in understanding damage and failure mechanisms of coke drums. Moreover, the experimental data could serve as benchmark data to verify the predictions of the temperature dependent elastoplastic constitutive models because the reliability of the FEM analysis on coke drums largely depends on the accuracy of the materials' constitutive models.

1.3 Objectives and Scope of the Research

Objectives of the research are summarized in the following:

- to develop a thermal-mechanical testing system;

- to characterize basic mechanical properties of typical coke drum materials;

- to study the deformation behaviors of coke drum materials under complex thermal-mechanical cyclic loadings;

- to provide reliable benchmark experimental data for verification of materials' constitutive models;

Coke drums are usually constructed of low alloy steel internally cladded with stainless steel as introduced in the previous section. In order to obtain a deeper understanding of mechanical properties and deformation behaviors of coke drum materials, experimental investigations of coke drum materials are crucial. In the beginning, development of a biaxial thermal-mechanical testing system is required to carry out both uniaxial and biaxial tests at ambient and elevated temperatures. Subsequently, uniaxial monotonic and fully-reversed cyclic tests are needed at different temperatures, up to $427\,^{\circ}\text{C}$, to characterize basic mechanical properties, such as yield strength and Young's modulus. Furthermore, the cyclic deformation properties of the coke drum material could be experimentally identified from stress-strain hysteresis loops of the fully-reversed cyclic experiments. To better understand the damage mechanisms of coke drums, such as bulging, complex thermal-mechanical cyclic tests are required. However, there is still lacking of reliable theoretical constitutive models which can properly simulate the initiation and growth of the bulging deformation. These test results will serve as benchmark experimental data for verification of the theoretical constitutive models. All the above mentioned experimental studies were carried

out on the thermal-mechanical testing system newly-developed in our laboratory as mentioned.

The thesis is organized as the following: in Chapter two, the details of the developed thermal-mechanical testing system, including furnace, gripping system, and axial and diameter extensometers, are introduced. In Chapter three, test materials and specimen geometry are firstly introduced. Then, the experimentally-obtained mechanical properties of both base and cladding materials are summarized and discussed. In addition, strain-rate dependence tests of coke drum materials and creep tests of base materials are presented. In Chapter four, test materials and specimen geometry in complex thermal-mechanical tests are also firstly introduced. Then, the test programs of complex thermal-mechanical cyclic tests are described. They include constant stress with cyclic thermal loading, in-phase and out-of-phase thermal-mechanical loadings, strain- or stress-controlled axial cycling with constant internal pressure, etc. In addition, certain experimental results are compared with the predictions of the newly-developed constitutive model. In Chapter five, the conclusion and future work are summarized.

Chapter 2 Development of a New Biaxial Thermal-Mechanical Material Testing System

2.1 Introduction

Material properties are one of the important factors in the design and numerical modeling of structures [13]. To obtain the basic mechanical properties of the coke drum material at room and elevated temperatures and to better understand the deformation behaviors of materials under complex thermal-mechanical loadings which are similar to the loadings experienced by the coke drums in operation, a biaxial thermal-mechanical material testing system has first been developed in our lab. Although some biaxial loading tests were conducted [14-20], there are few testing systems capable of simulating complex thermal-mechanical loading, especially with biaxial loading combined. The developed material testing system is primarily designed for performing tests under biaxial thermal-mechanical loadings, but tests under uniaxial loadings, such as tensile or cyclic loading, can also be performed. The uniquely designed material testing system has been successfully developed and installed. It consists of a MTS machine, a furnace, a water cooled gripping system, extensometers, and a data acquisition and control system, which will be introduced in the following sections.

2.2 Testing Apparatus

2.2.1 MTS Machine

As shown in Fig. 2.1, a servo-controlled electro-hydraulic closed-loop system- a modified MTS machine for bi-axial thermal-mechanical loading tests is implemented and tuned. The crosshead of the MTS machine supports all components of the testing system. The load cell is firmly connected with the crosshead, and the maximum loading capacity of the load cell is 10,000 lbs. A hydraulic-operated piston is installed on the base compartment of the MTS machine to apply the uniaxial tensile or compressive loading. A MTS 442 controller is used, by which load or strain controlled static and dynamic testing can be simulated.
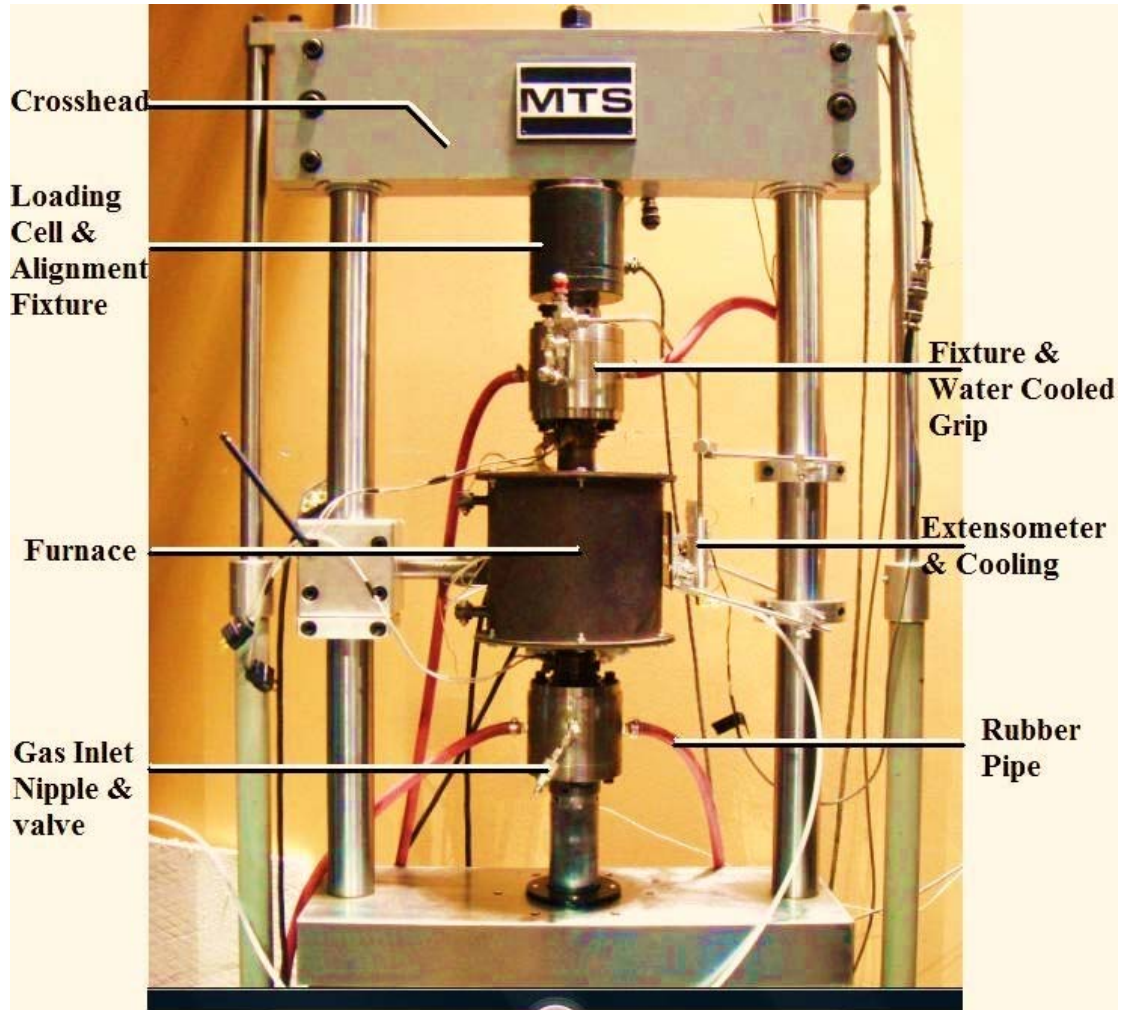
Figure 2.1 New developed thermal-mechanical material testing system

2.2.2 Furnace

The furnace, as shown in Fig. 2.2, with control equipment (not shown in the figure) was designed and manufactured for the elevated temperature tests. The furnace is mounted on one column of the existing MTS test machine. The position of the furnace can be altered easily in two degrees of freedom to appropriately cover a test specimen. The furnace consists of two separated metal covers, heating coil which is embedded in a ceramic mold, an insulation layer which is placed in between the metal cover and the heating coil, and a temperature controller. There is 0.0635 x 0.00635 m groove cut through one side of the furnace to fit the extension rods of the extensometer. The two metal covers are connected by a hinge, and two pieces of metal covers can be properly engaged after installation of the specimen and the extensometers. The metal cover is 0.2286 m in outer diameter and 0.2794 m in height. The designed furnace with controller has a capability of adjusting temperature inside the furnace to any desired value between ambient temperature to 500°C. The temperature sensor is bonded to the center of the gage length of the test specimen. The digital temperature controller allows for accurate monitoring and controlling of the specimen temperature during elevated temperature test. Two 0.0635 m holes in diameter are cut through the centers of the top and the bottom of the metal cover to allow the grip and specimen suitably housing in the furnace. This kind of design provides easiness of specimen installation and minimization of heat loss.
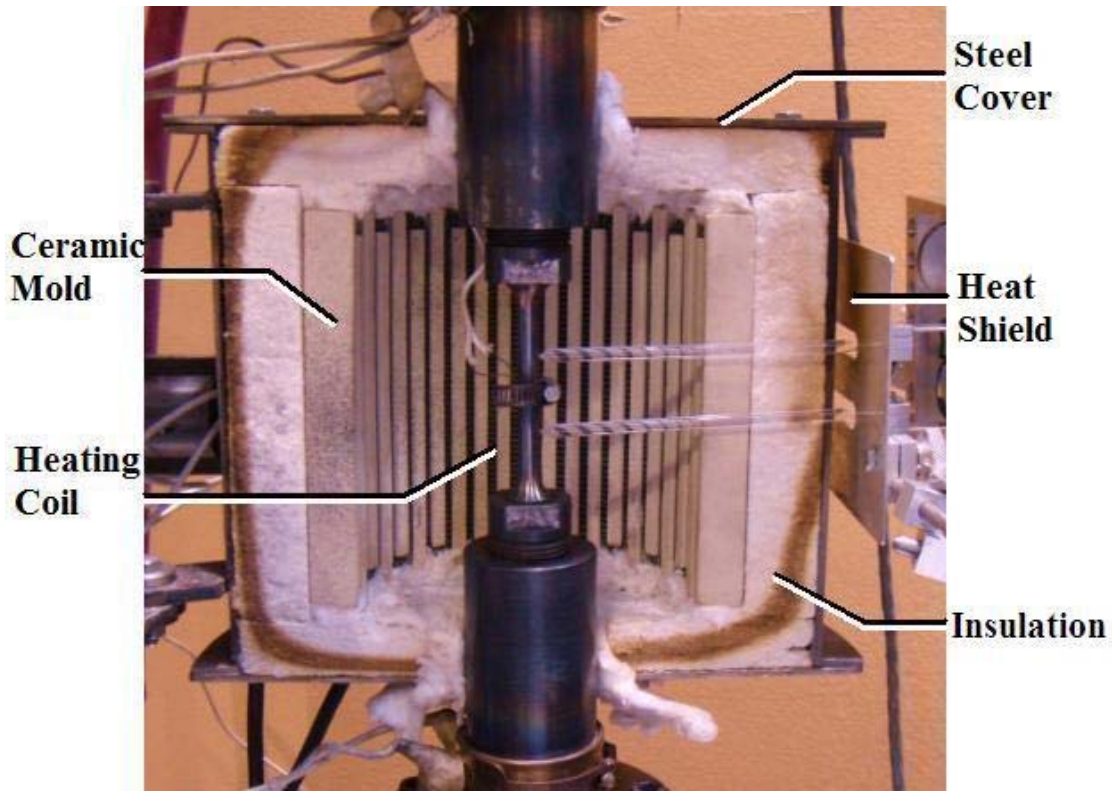
Figure 2.2 A photo of the furnace

2.2.3 Extensometer

2.2.3.1 Design of Cantilever Beam

Extensometers are devices which could quantitatively measure the deformation of test specimens during loading tests. Most commercial ambient temperature extensometers are closely attached to test specimen. Some existing extensometers are designed to perform remote operation because of the environment requirement [21]. However, in order to properly implement the measurement at elevated temperatures and collaborate with the designed furnace, a set of high temperature extensometers is developed to measure the strain of test specimen in axial and diametral directions.   The arm of the designed extensometers primarily includes two parts, a solid rod (A-B) and a cantilever beam (B-C) as shown in Fig. 2.3. The solid rod is made of quartz which is stiff enough to neglect the deflection and also can survive at fairly high temperature (melting point 1600 ^{o}C), and the cantilever beam is delicately machined from aluminum alloy. A full-bridge strain gage is glued on the far-end (point C in Fig. 2.3) of the cantilever beam. It measures the strain of test specimen by transferring the elongation of the specimen to the deflection of the cantilever beam. The dash line shows the deflected arm due to the tensile or compressed force applied on the specimen which firmly attached with the end of the extensometer (point D in Fig. 2.3). In order to find a proper dimension of the cantilever beam to optimize the strain measurement of the test specimen, a mechanics model is developed for this special case.
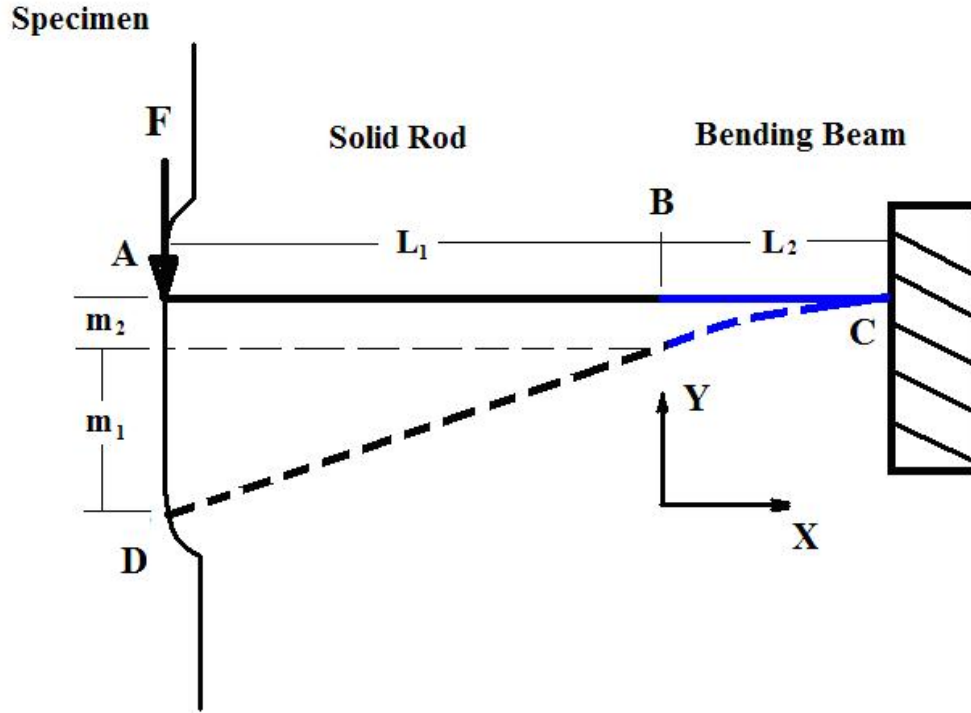
Figure 2.3 Schematic of cantilever beam deflection

The length of the cantilever beam is assigned to be L_2, and the length of the quartz rod is L_1. The total deflected distance is m which consists of m_1 and m_2 as shown in figure 2.3. The origin of the x-y coordinate is assumed at point B.

Assuming a constant force F is applied at point A in vertical direction.

Moment (M):

$$M_B = -FL_1 \tag{1}$$

$$M_C = -F(L_1 + L_2) \tag{2}$$

Between BC, $M(x) = -F(L_1 + x)$ (3)

$$M(x) = \frac{d^2 y}{dx^2} EI \tag{4}$$

Combine (3) and (4)

$$EI\frac{d^2y}{dx^2} = -F(L_1 + x) \tag{5}$$

Integrate in x once,

$$EI\frac{dy}{dx} = -FL_1x - \frac{1}{2}Fx^2 + C_1 \tag{6}$$

At point C, $x = L_2$ and $\frac{dy}{dx} = 0$

Put into equation (6), we get

$$C_1 = FL_1L_2 + \frac{1}{2}FL_2^2$$

Then,

$$EI\frac{dy}{dx} = -FL_1x - \frac{1}{2}Fx^2 + FL_1L_2 + \frac{1}{2}FL_2^2 \tag{7}$$

Integrate in x again,

$$EIy = -\frac{1}{2}FL_1x^2 - \frac{1}{6}Fx^3 + FL_1L_2x + \frac{1}{2}FL_2^2x + C_2 \tag{8}$$

At point C, $x = L_2$, y=0,

Put into equation (8), we get

$$C_2 = \frac{1}{2}FL_1L_2^2 + \frac{1}{6}FL_2^3 - FL_1L_2^2 - \frac{1}{2}FL_2^3$$

Then,

$$y = \frac{F}{6EI}(-3L_1x^2 - x^3 + 6L_1L_2x + 3L_2^2x + 3L_1L_2^2 + L_2^3 - 6L_1L_2^2 - 3L_2^3) \tag{9}$$

Deflection at point B by letting x=0

$$y_B = -\frac{F}{6EI}(3L_1L_2^2 + 2L_2^2) \tag{10}$$

$$\theta_B = \left(\frac{dy}{dx}\right)_B = \frac{F}{2EI}(2L_1L_2 + L_2^2) \tag{11}$$

$$m_2 = -y_B = \frac{F}{6EI}(3L_1L_2^2 + 2L_2^2) \tag{12}$$

$$m_1 = L_1 \tan\theta_B = L_1 \tan\left[\frac{F}{2EI}(2L_1L_2 + L_2^2)\right] \tag{13}$$

The total deflection,

$$m = m_1 + m_2 = L_1 \tan\left[\frac{F}{2EI}(2L_1L_2 + L_2^2)\right] + \frac{F}{6EI}(3L_1L_2^2 + 2L_2^2) \tag{14}$$
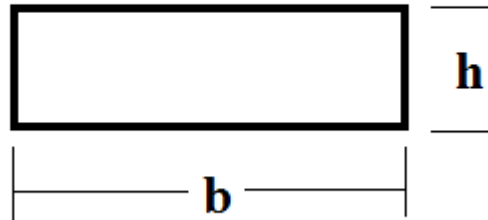
Figure 2.4 Cross-section of bending beam

Cantilever beam material: Alloy 6061-T6

Alloy 6061-T6 at room temperature, Young's modulus (E) = 70 GPa.

$$I = \frac{1}{12}bh^3$$

Assumption: put strain gage very closed to point C

$$M_C = F(L_1 + L_2)$$

$$\varepsilon_C = \frac{6M_C}{Ebh^2} = \frac{6F(L_1 + L_2)}{Ebh^2}$$

From numerical iteration (Appendix A), the reasonable dimension of the cantilever beam are determined as 0.02 m in length, 0.0009 m in thickness and 0.009525 m in width. The detailed engineering drawing of the designed cantilever beam for machining is also provided in Appendix A.

2.2.3.2 Uniaxial Extensometer

Uniaxial extensometers were designed to implement in high temperature tests to measure the axial strain. As shown in Fig. 2.5, the uniaxial extensometer consists of two quartz rods with sharpened pin tips, two aluminum bending beams and a C-shaped frame. The aluminum bending beam is connected with C-shaped frame with one end and quartz rod with the other end. Two strain gages are in pair mounted on the top and bottom of the beam. The strain gages are positioned toward to the C-shaped frame side as close as possible. The length of the quartz rod is 0.127 m which provides sufficient extension to reach to the test section of the specimen from outside of the furnace. The designed gage length of the extensometer is 0.0508m or 0.0254m. The latter length can be achieved by flipping over the tightening blocks of the extension rods attached to the inner face

of the coupon, see Fig. 2.6. The design of cantilever beams is significantly critical to ensure the accuracy of measurement.
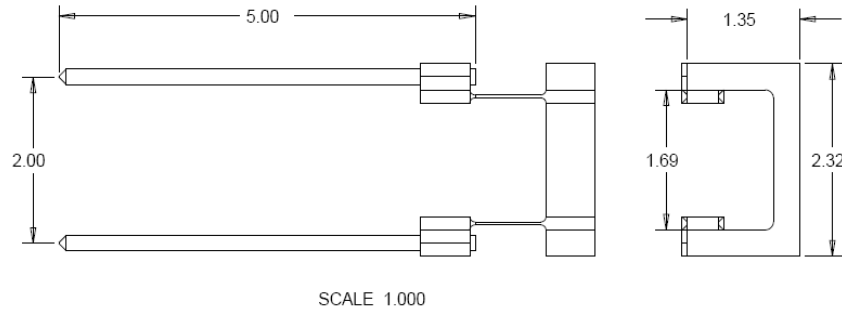
Figure 2.5 Drawing of high temperature uniaxial extensometer

The entire uniaxial extensometer system consists of a fixture frame, a uniaxial extensometer, two spring loops, and an air duct, as shown in Fig. 2.6. The uniaxial extensometer is connected with an aluminum fixture frame by two spring loops which can apply compression force when mounting the extension quartz rods onto the test specimen. The fixture frame directly attaches to one column of the MTS testing system by a solid rod. Extensometer may be adversely affected by air density changes associated with thermal gradients and turbulence, especially at high temperature testing [22]. The heat shield is placed in between the furnace and the extensometer, as shown in Fig. 2.2, to reduce the effect of heat radiation to the extensometer. In addition, an air duct is introduced in the extensometer system to minimize the effect of heat to the accuracy of the extensometer measurement. There are four small round conducting holes on the duct, which constantly blows the air to the strain gage of the extensometer to cool down and maintain the constant temperature of the coupons.
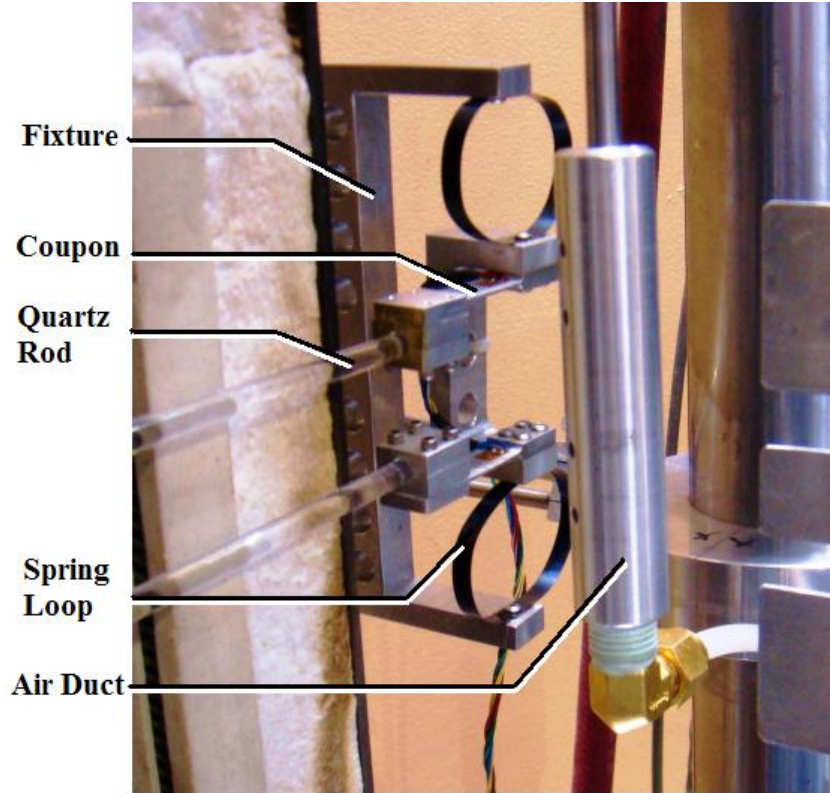
Figure 2.6 A photo of the complete uniaxial extensometer system

2.2.3.3 Diametral Extensometer

Diametral extensometer is diametral strain measurement device. It could accurately measure the specimen deformation in diametral direction. The developed diametral extensometer consists of a designed cantilever beam, two quartz extension rods, a fixture frame and a spring loop as shown in Fig. 2.7. One quartz rod is attached with fixture frame which hangs on a spring loop, and the spring loop can provide three degrees of freedom for the entire structure. The conical tip of the other extension rod is placed in the dimple of the upper edge of the cantilever beam. A spring which attaches the opposite side of upper edge of

the cantilever beam could provide adjustable compressive force, and this force

can secure the two ends of the extension rods attached to the surface of the test

specimen.
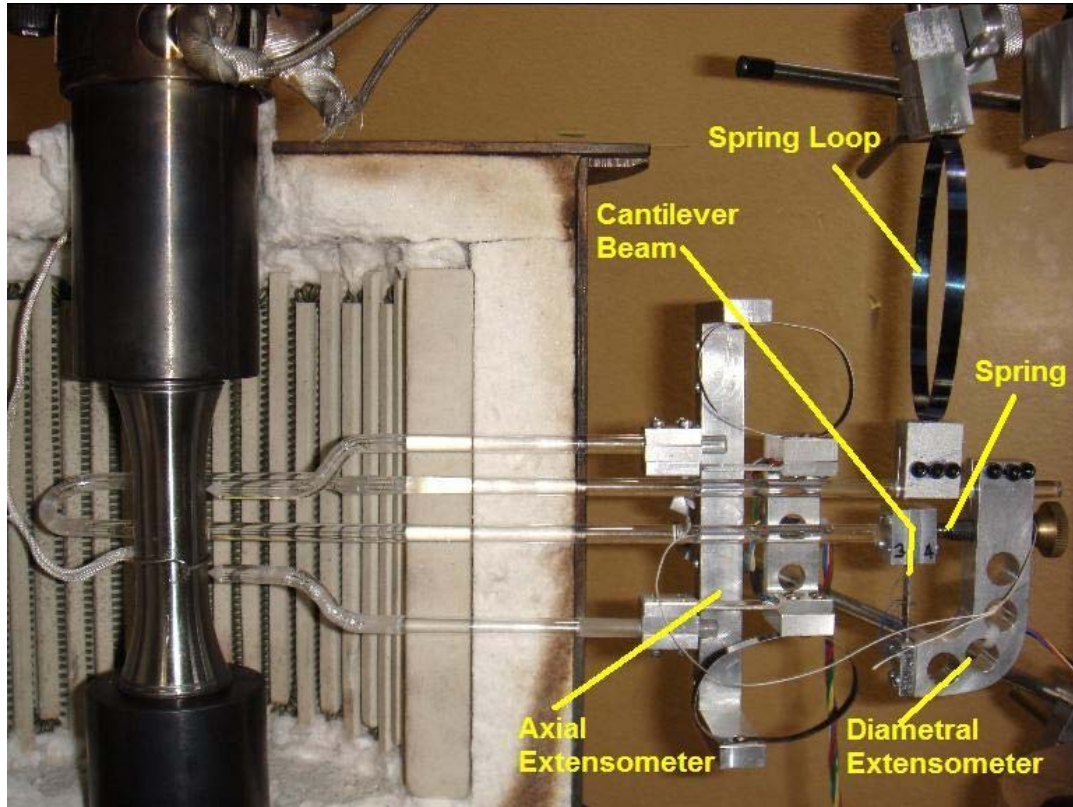
Figure 2.7 A photo of installed axial and diametral extensometers

2.2.4 Gripping System

The gripping system, as shown in Fig. 2.8, was designed to fit monotonic test,

cyclic test, and bi-axial test at ambient and elevated temperatures. The capability

and quality of conducting the high temperature bi-axial test, which is the most

complicated test among those tests, are set to the goal and key factor of this

design. The gripping system mainly contains two water cooled fixtures, two grips,

two gas intake tubes, two bolts, and a set of grip adaptors for different sizes of

specimens. The entire gripping system securely mounted on the MTS testing

system by connecting upper and lower water cooled fixtures directly with the load

cell and the hydraulic piston. The flange grips are firmly attached with upper and

lower alignment fixtures by six bolts on each side. The specimen is tightly fixed

with the extension arms of the grips by threading grips, and two bolts inside the

flanges are forced to compress the ends of the specimen to ensure the tightness of

the installed specimen.
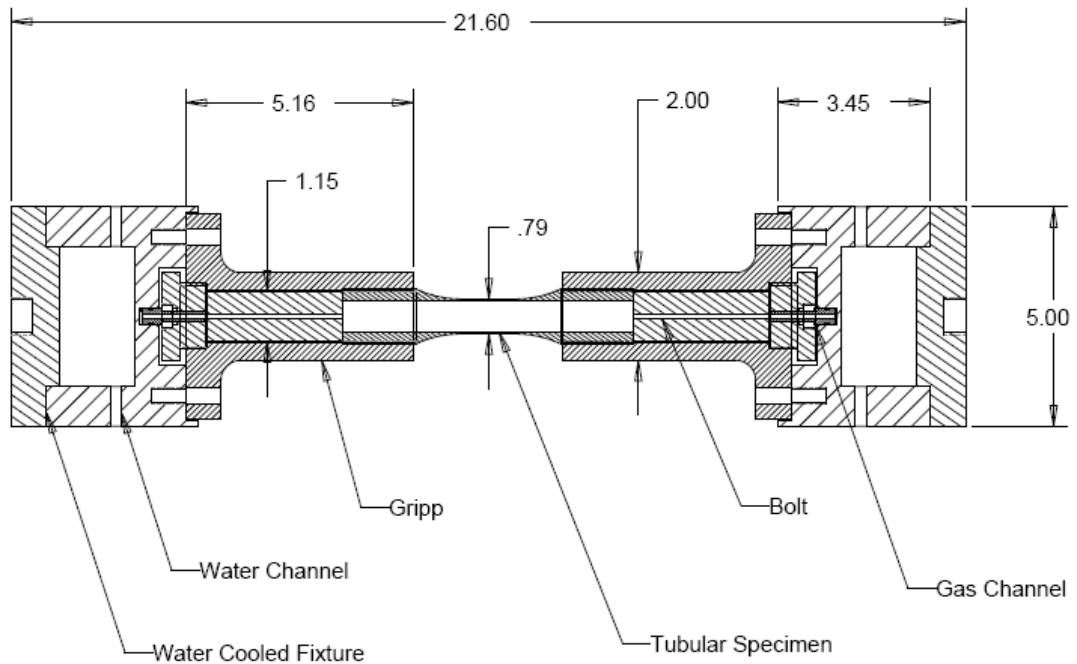
Figure 2.8 Engineering drawing of high temperature gripping system

As shown in Fig. 2.9, the water cooled alignment fixture consists of an

automatic pressure relief valve, a manual pressure relief valve, two water hoses, a

coolant cell, and a metal heating belt. The main purpose of the water cooled

alignment fixture is to cool down the contact surface between the grip and the

load cell during high temperature tests, and it is necessary to eliminate the heat effect to the accuracy of the load cell response. The cooling rate could be manually adjusted by altering water flow rate through the water hose. Tubular specimen is feasibly introduced to achieve room and high temperature bi-axial tests. Constant internal pressure inside the tubular specimen can be accurately and gently generated by conducting gas through the gas channel of the lower water cooled alignment fixture. It is equipped with a needle valve to provide precious gas release to the tubular specimen. Two pressure relief valves (see Fig. 2.9) installed on the upper water cooled alignment fixture connect with an air flow channel under the coolant reservoir of the cell, and the channel is extended to the center of the fixture cell and hermetically connected with gas channel (gas conductive tube). The automatic pressure relief valve can be preset to a certain value, and the gas will be automatically released when the internal pressure of the specimen exceeds this preset value. This valve helps to maintain the internal pressure inside the tubular specimen constant. From the specimen temperature gradient test, it is found that there is significantly large temperature gradient between the center of the gage length and 0.0254 m away from the center. To eliminate the large temperature gradient of the specimen, an additional heating supplement, metal heating belt, is wrapped around the end of each grip, as shown in Fig. 2.9. From the experiment, it is shown that the temperature gradient on the test section is extensively reduced.
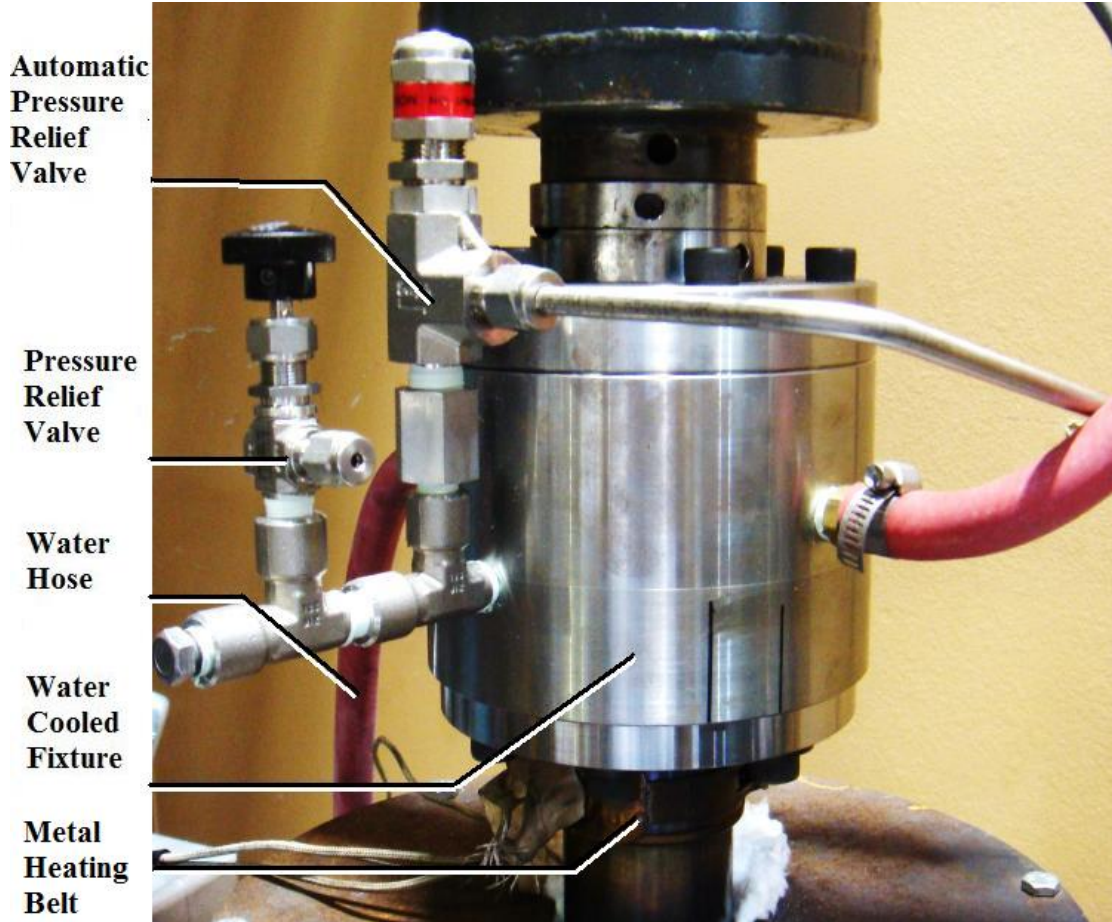
Figure 2.9 A photo of water cooled alignment fixture

The gas conductive tube directs the gas through gas channel into the air channel inside the bolt (see Fig. 2.8) which connected and sealed with a o-ring. The gas will flow through the tubular specimen to generate the internal pressure. The total length of the gripping system with a designed tubular specimen is 0.54864 m. The approximate length of the gripping system sitting in the furnace is 0.2794 m. The two water cooled cells are located outside of the furnace. The design of the gripping system was aimed on carrying out different types of tests, such as bi-axial loading test which involves axial cyclic stress/strain loading with

constant internal pressure at elevated temperatures up to 500 $^{\circ}$C. High temperature monotonic and cyclic tests can also be tested using this system, simply by ignoring the internal pressure section. The cylindrical-threaded and pin-loaded uniaxial test specimens, for example, can be mounted on the gripping system by introducing two different specimen grip adaptors, as shown in Fig. 2.10. Two bolts on each side of the flat specimen grip provide sufficient shearing force during axial loading. The external-threaded adaptors can be installed in the internal-threaded grip preciously, and the design of grip adaptor insures the maximization of gripping force and minimization of the specimen bending.
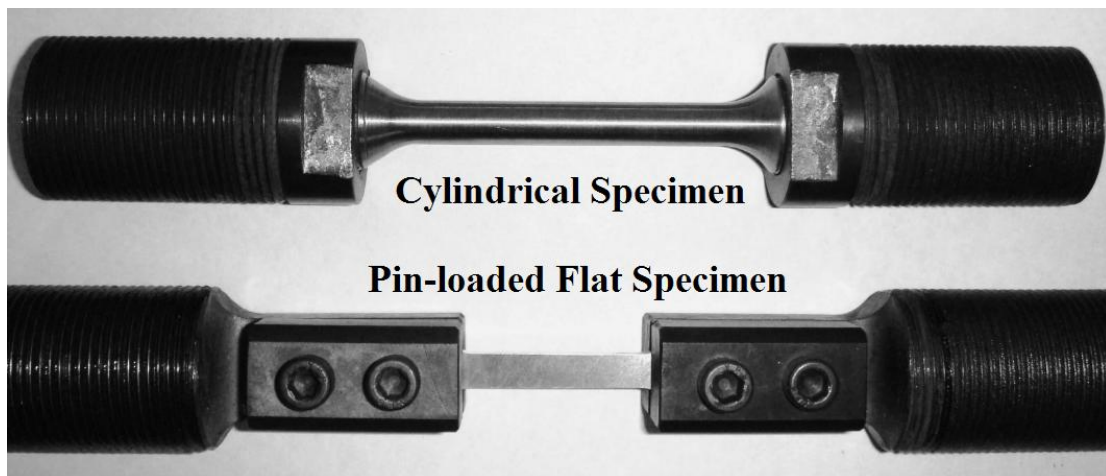
Figure 2.10 Specimen grip adaptors

2.2.5 Data Acquisition and Control System

2.2.5.1 Data Acquisition

Commercial software, LabView SignalExpress [23], is used as a tool for test data acquisition through out all tests. Three channels of signals as voltages are collected for load, axial strain, and temperature or circumferential strain. The software interface mainly consists of toolbars, data view window, logs window, and step setup dialog box (Fig. 2.11). The program can be manually controlled by clicking on execution control buttons to start, stop and record test signals. The data view window can display the test signals simultaneously while conducting the experiment. The experimental signals can be recorded by using the record button. After clicking record button, the logging signals selection dialog box will open, and one or multiple signals can be selected to be recorded. The data recording process will continue until clicking on stop button. The recorded data is written in the logs, and it can be exported to windows Excel spreadsheet by dragging the log file directly from the logs window. All logged signals analysis will be processed in the Excel spreadsheet. The data acquisition rate can be adjusted from the step setup dialog box. The signal input range can also be altered from the step setup box to suit different input voltage ranges.
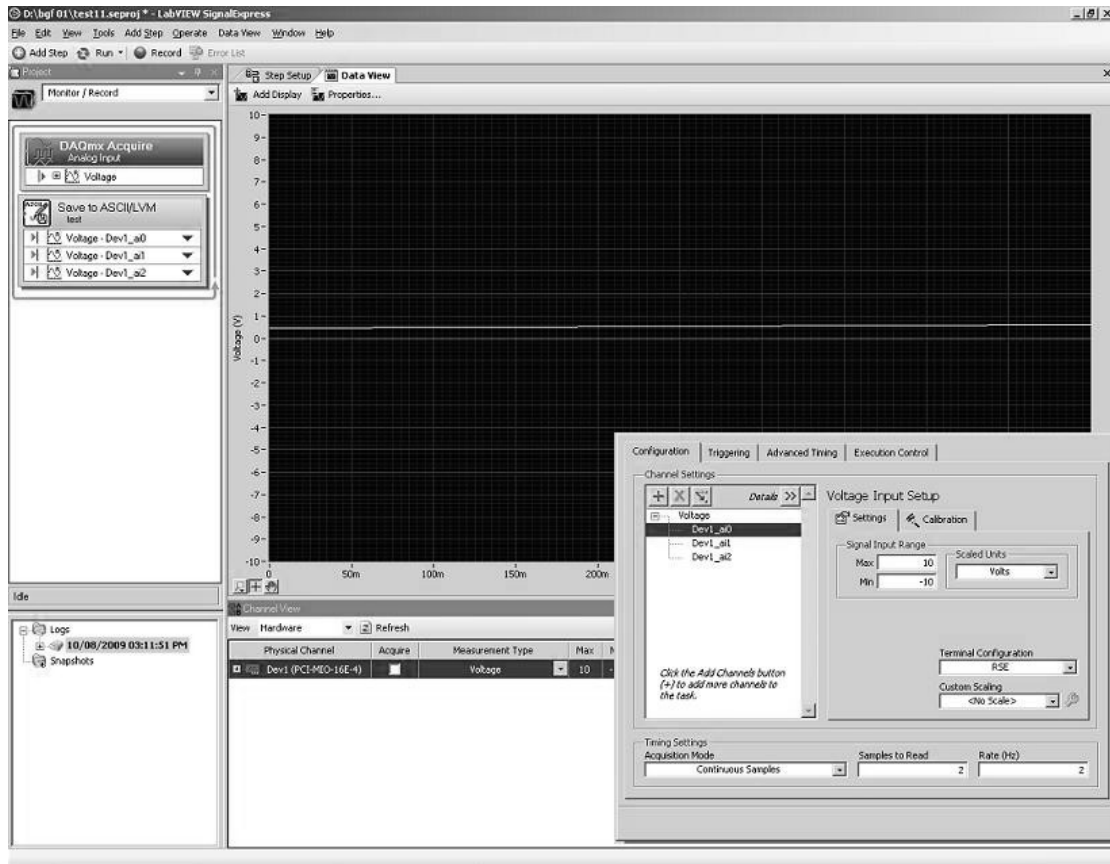
Figure 2.11 The LabView SignalExpress Interface

2.2.5.2 Control System

A MTS 442 controller is used as a main controller, and simple direct load or strain controlled tests could be performed by this controller. However, more complicated thermal-mechanical loading tests, e.g. in-phase thermal-mechanical loading test, require temperature-load or temperature-strain controlled loading conditions. Therefore, a set of home-built gain amplifier and inverter are used in the temperature-controlled tests, such as in-phase and out-of-phase thermal-mechanical loading tests. Figure 2.12 is the brief flow chart of temperature-load controlled tests. The same devices and principles are used for the temperature-

strain controlled tests as well. The temperature sensor senses the instantaneous temperature from the specimen and outputs the signal as voltage. The cycling temperature range ΔT is first determined by subtracting T_{low} from T_{high}, and the corresponding Δ Voltage can be obtained. Then, the predetermined cycling load range $\Delta \sigma$ can be found by subtracting σ_{low} from σ_{high}, and the corresponding Δ Voltage can also be determined. By implementing the gain amplifier, $\Delta V_{temperature} + V_{gain} = \Delta V_{load}$ the in-phase thermal-mechanical loading test can be conducted by temperature-load controlled or temperature-strain controlled mode. Similarly, the out-of-phase thermal-mechanical loading test can be achieved by adding one inverter after the gain amplifier to obtain the inverted load signal.

In-Phase Thermal-Mechanical Loading Test

| Temperature Sensor 100°C=1volt | → | Gain Amplifier ΔT + Gain = Δ Load | → | Load - Controlled 1volt=1000lb |

Out-of-Phase Thermal-Mechanical Loading Test

| Temperature Sensor 100°C=1volt | → | Gain Amplifier ΔT + Gain = Δ Load | (-1) → | Load - Controlled 1volt=1000lb |
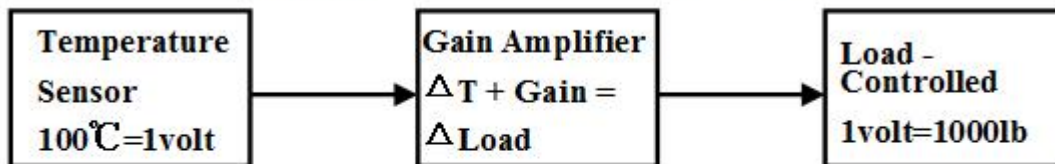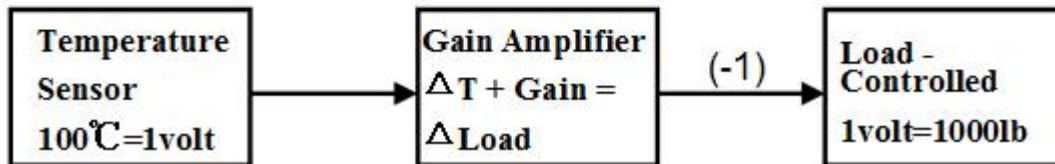
Figure 2.12 Flow chart of temperature controlled load

2.3 Summary

A biaxial thermal-mechanical material testing system is successfully designed and developed. The developed testing system primarily consists of a MTS machine, a furnace, a set of extensometers, a gripping system, and a set of data acquisition and control system. The new biaxial material testing system is developed based on an existing servo-controlled electro-hydraulic closed-loop MTS machine. An electricity-powered furnace is mounted on the MTS machine, and test specimen inside the furnace could be heated up to a controllable temperature (up to 500 ^{o}C). Two cantilever beam extensometers, uniaxial and diametral extensometers, are successfully designed and manufactured. A mechanics model of the cantilever beam is derived to help us to find the dimensions of the cantilever beam of the extensometers. A set of water-cooled gripping system is also designed and developed. It is capable of eliminating heat effect to the connected load cells, channelling the gas to tubular specimen to generate internal pressure, and adapting specimens with different geometries. The control system can provide load or strain controlled loading conditions, furthermore, temperature-load or temperature-strain controlled loading conditions could also be achieved by implementing additional electronics. There are three channels used in the data acquisition system which could simultaneously collect load,

strain, or temperature as voltages.

Chapter 3 Characterization of Mechanical Properties of Coke

Drum Materials

3.1 Introduction

To characterize the basic mechanical properties of the coke drum materials, tests were carried out under eight types of material and temperature combinations as shown in Table 3.1. In addition, the different strain rates of the coke drum materials in monotonic tensile tests were compared to identify the strain-rate dependence of the coke drum material. Furthermore, creep tests of the base material were carried out at different elevated temperatures.

Table 3.1 Selected test materials and temperatures

		22°C	427°C
SA 387-11 (Base)	Weld Zone	Tested	Tested
	Non-weld zone	Tested	Tested
SA240-410S (Cladding)	Weld Zone	Tested	Tested
	Non-weld zone	Tested	Tested

3.2 Test Material and Specimen Geometry

3.2.1 Test Material

The test plates which include base metal SA387-11 and Alloy SA 240 type 410S cladding were provided by Cessco Fabrication & Engineering Limited, and the plates also include the welded-plate sections. The thickness of the base metal is 30 mm and alloy cladding is 3 mm. The material characteristics of base metal

SA387-11 (1 ¼ Cr- ½ Moly) and alloy SA 240 type 410S cladding were determined experimentally from monotonic and stepped fully reversed cyclic tests. Table 3.2 shows the typical chemical composition of the base material and alloy cladding. The specified mechanical properties of SA387-11 and 410S at ambient temperature are provided in Table 3.3.

Table 3.2 Chemical composition of coke drum materials [24-26]

Material	% C	% S	% Mn	% Si	% Cr	% Ni	% Mo
SA387-11 (base)	0.04-0.17	0.035	0.35-0.73	0.44-0.86	0.94-1.56	-	0.40-0.70
410S (cladding)	0.08	0.03	1.00	1.00	11.5-13.5	0.60	-

Table 3.3 Specified mechanical properties at ambient temperature and 427 ^{o}C [27-30]

a. ambient temperature

Material	Tensile Strength, (MPa)	Yield strength, (MPa) -0.2%	Density, g/cm^3 (25° C)	Poisson's ratio (25° C)	Elastic Modulus (GPa) 25° C
SA387-11	515-690	310	7.7-8.03	0.27-0.3	190-210
410S(clad)	444	290	7.7-8.03	0.27-0.3	200

b. 427 ^{o}C

Material	Tensile Strength, (MPa)	Yield strength, (MPa) -0.2%	Density, g/cm^3 (427° C)	Poisson's ratio (427° C)	Elastic Modulus (GPa) 427° C
SA387-11	414	174	-	-	176
410S(clad)	340	157	-	-	170

3.2.2 Specimen Geometry

Coupon specimens were designed and manufactured for the testing of mechanical properties for base material, cladding, and the base and cladding materials at weld zones. Due to the thickness limitation of the test plate which is

described in the previous section, there are several different geometries of specimens designed which will be demonstrated in the following sections.

As shown in Table 3.4, for each monotonic and cyclic test, six specimens were prepared and tested at room temperature (25°C) and elevated temperature (427°C) respectively. Two specimens were manufactured from weld zone of the base metal, two from non-weld zone of the base metal, one from weld zone of the cladding, and the other one was made from non-weld zone of the cladding. Cylindrical and rectangular specimens were designed and machined from the base metal of the test plate, and only rectangular specimens were made for the cladding due to the limited thickness of the test plate.

Table 3.4 schedule of tests at room temperature and 427°C

Test Type	Base Material- A387-11		410S (cladding)
Monotonic test	CW	RW	RW
	CN	RN	RN
Fully-reversed cyclic test	CW	RW	RW
	CN	RN	RN

Note:

CW - cylindrical specimen from weld zone of the test plate
CN - cylindrical specimen from non-weld zone of the test plate
RW - rectangular specimen from weld zone of the test plate
RN - rectangular specimen from non-weld zone of the test plate

Room Temperature Monotonic Test Specimen

Two types of tensile specimens designed for uniaxial monotonic tests: round and rectangular cross-section, respectively. As shown in Fig. 3.1, the diameter of the test section is 0.0127 m, and the gage length of the specimen is 0.0508 m which is four times of the diameter. The radius of fillet is 0.009652 m, and the length of reduced section is 0.05715 m. The designed specimens were tested on

the testing machine which is equipped with round wedge grips. The round

specimen was designed according to ASTM E8 standard.
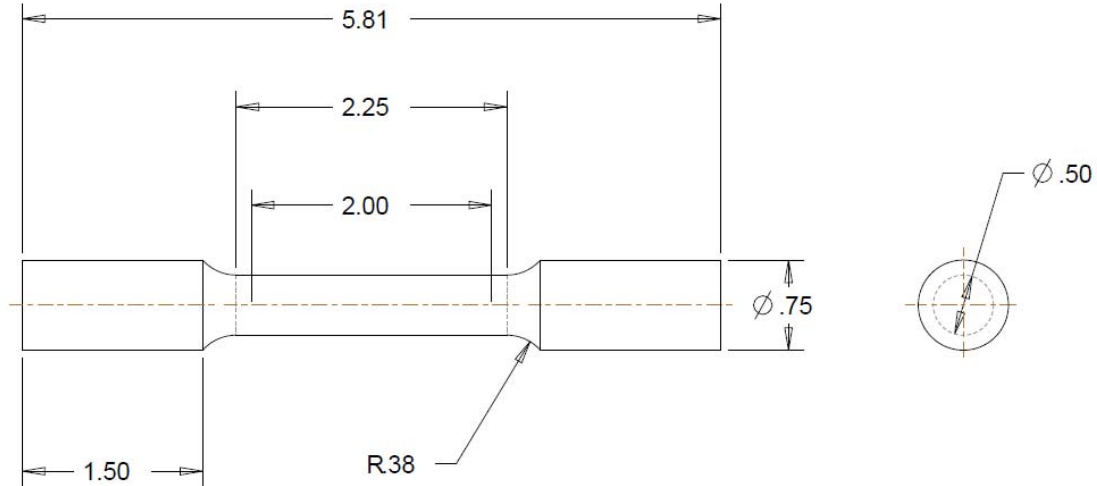
All Dimensions are in inches;

Figure 3.1 Round tension test specimen

As shown in Fig. 3.2, the subsize rectangular specimen was designed

according to ASTM E8 standard. Four specimens, two from base metal and the

other two from cladding, were prepared according to this geometry. The thickness

of the cladding (0.003 m) is the key design factor. According to ASTM E8

standard [31], for material with a nominal thickness between 0.00013 to 0.005 m,

the sheet-type specimen should be implemented. The thickness is 0.003048 m,

and the width of grip section is 0.009652 m. The gage length is 0.0254 m, and the

width of the test section is 0.00635 m. The overall length is 0.1016 m, and the

length of reduced section is 0.03175 m. The subsized rectangular specimens were

tested on the material test system which is equipped with flat wedge grips.
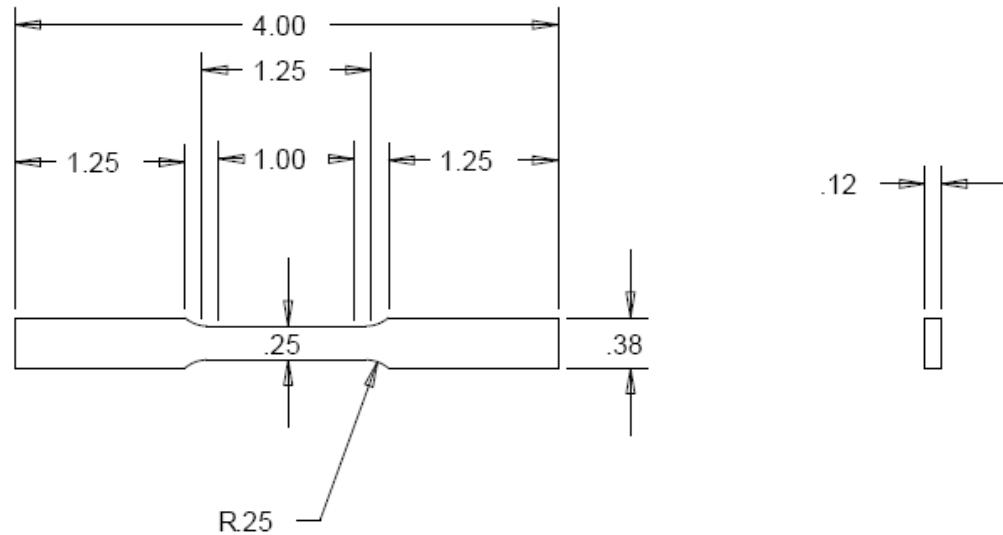
All Dimensions are in inches;

Figure 3.2 Subsized rectangular tension specimen

Room Temperature Stepped fully-Reversed Cyclic Test Specimen

As shown in Fig. 3.3, round stepped cross section specimen was designed for the fully-reversed cyclic test. The much-shortened gauge length was adopted to minimize the effect of buckling to the test result in the fully-reversed cyclic tests. Please refer Appendix B for details of the buckling load calculation. The gage length is reduced to 0.01905 m, and the corresponding diameter is 0.00635 m. The length of the grip is enlarged to 0.043942 m to enhance the alignment and stability of the specimen during the continuous cyclic loading. The stepped cylindrical specimens were tested on the material test system which is equipped with round wedge grips.
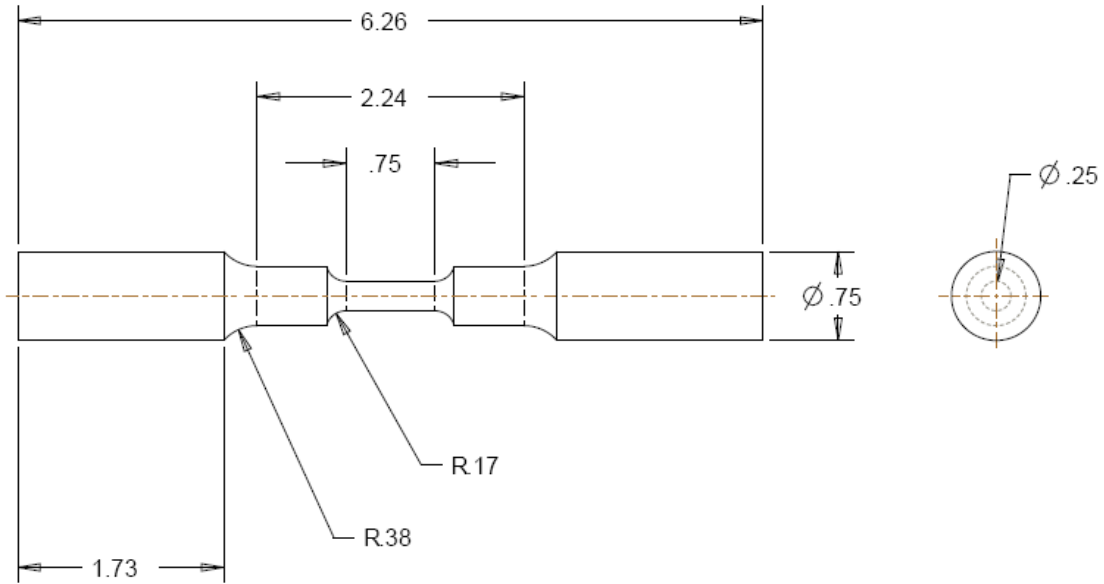
All Dimensions are in inches;

Figure 3.3 Modified round stepped cyclic test specimen

Rectangular specimens were also prepared for the fully-reversed cyclic tests according to the geometry shown in Fig. 3.4. The gage length is 0.0127 m, and width is 0.00635 m. The length of the grip is 0.033782 m, and the corresponding width is 0.0127 m which is greatly enlarged to provide good gripping during the cyclic loading conditions. Due to the thickness constraint of the raw material (pre-cut to 3 mm in thickness) and the limited gage length of the existing MTS extensometer, this geometry was designed to minimize the buckling effect according to the calculation in the Appendix B, but from the test results, buckling effect was still unable to be avoided under the cyclic tests with larger compressive strains (> 1.25%).
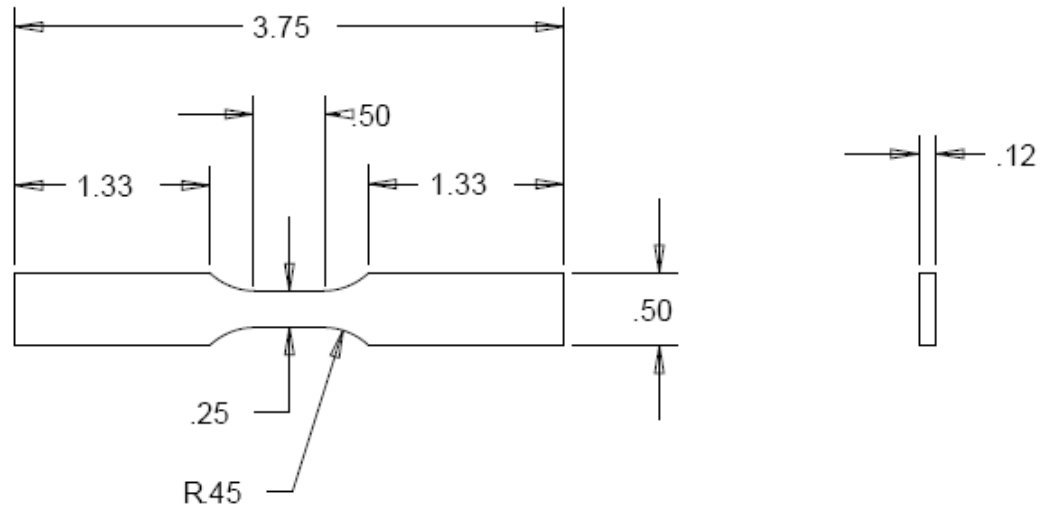
All Dimensions are in inches;

Figure 3.4 Subsized rectangular cyclic test specimen

Elevated Temperature Monotonic and Cyclic Test Specimen

Cylindrical-threaded and pin-loaded test specimens were designed for both monotonic and fully-reversed cyclic test at elevated temperature. The effect of specimen buckling to the test result at large stepped strain (>1%) was hardly eliminated during the compression of the cyclic loading. Monotonic and cyclic test specimens of base material at elevated temperature were designed identically, as shown in Fig. 3.5. The gage length is 0.0508 m, and the diameter is slightly reduced to 0.008255 m (comparing with ASTM E8 [31] standard round tension test specimen) due to the limitation of the load cell capacity of the modified high temperature testing system.
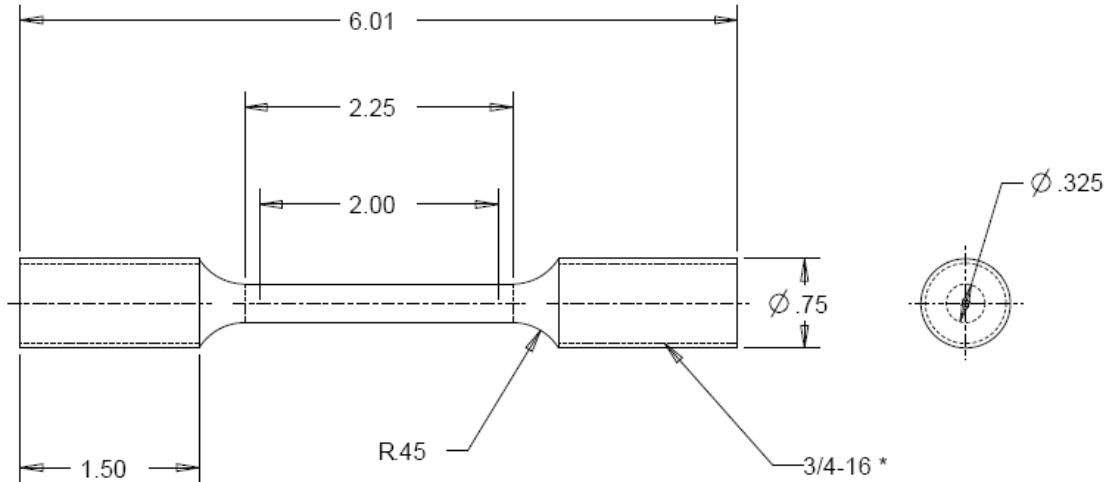
All Dimensions are in inch:

Figure 3.5 Cylindrical-threaded elevated temperature test specimen

Pin-loaded thin test specimens from base and cladding materials were designed for elevated temperature monotonic and cyclic tests to reduce significant buckling in cyclic tests. As shown in Fig. 3.6, the gage length is 0.0381 m, and the width is 0.00635 m. The length of grip section is 0.0381 m, and width of grip section is 0.01524 m. The pin whole is 0.00635 m in diameter, and two pin holes are on each grip which provide sufficient pin-loaded force and accurate alignment with the center line of the heads of the testing machine. In addition, the surfaces of two grip sections are treated with sandblasting to enhance friction between the specimen and the home made flat-surface grips.
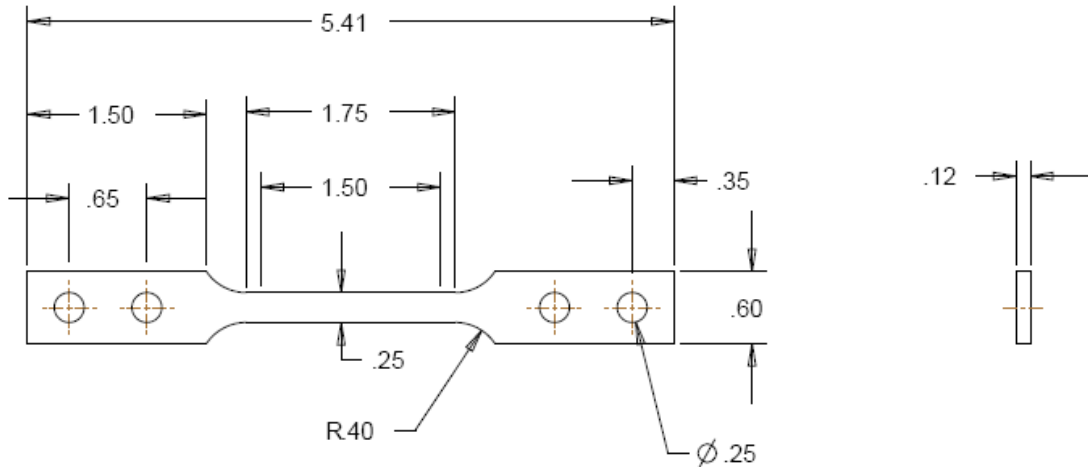
All dimensions are in inch;

Figure 3.6 Pin-loaded elevated temperature test specimen

The designed room temperature and elevated temperature test specimens are properly prepared for satisfactory and correct test results. The specimen surface is well finished to maximize precision and minimize bias in test results.

The room temperature test specimens are tested on MTS 810 with commercial MTS extensometer. The elevated temperature test specimens are tested on the newly-developed thermal-mechanical testing system described in Chapter 2. In order to fix the placement of the extensometer on the test specimen, two small dimples are carefully prepared by implementing height gage and nail punch to minimize the damage to the test specimens. Two dimples with 0.0254 m distance, as shown in Fig. 3.7, are prepared to joint the conical tip of the extension rod of the extensometer.
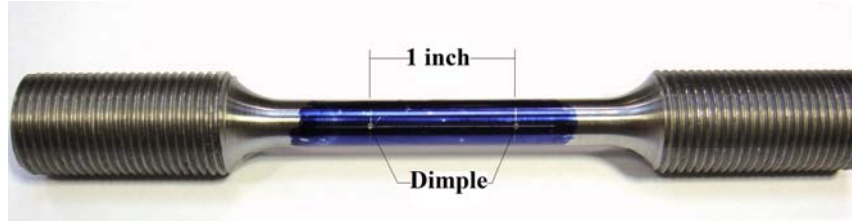
Figure 3.7 A photo of high temperature cylindrical specimen with two dimples

3.3 Determination and Discussion of Mechanical Properties of Coke Drum Materials

3.3.1 Introduction

There are various uses of tensile and cyclic tests. The mechanical properties of testing materials can be determined from tensile and cyclic test, such as yield strength, young's modulus, tensile strength, and so on. In addition, tensile stress-strain curves can be used to predict a specified material's behaviour under forms of loading other than uniaxial tension. The term of yield strength can be defined as the level of stress which causes certain plastic deformation of a material. Young's modulus is a measure of the stiffness of an isotropic elastic material, and it is defined as the ratio of uniaxial stress over the uniaxial strain in the range of stress in which Hooke's law holds. The tensile strength is defined as the maximum stress value in the engineering stress strain curve of a material. Tension testing of coke drum materials was performed under guidance of ASTM 8M Standard Test Methods for Tension Testing of Metallic Materials [31]. Elevated temperature tension tests were conducted according to ASTM E21 [32, 33].
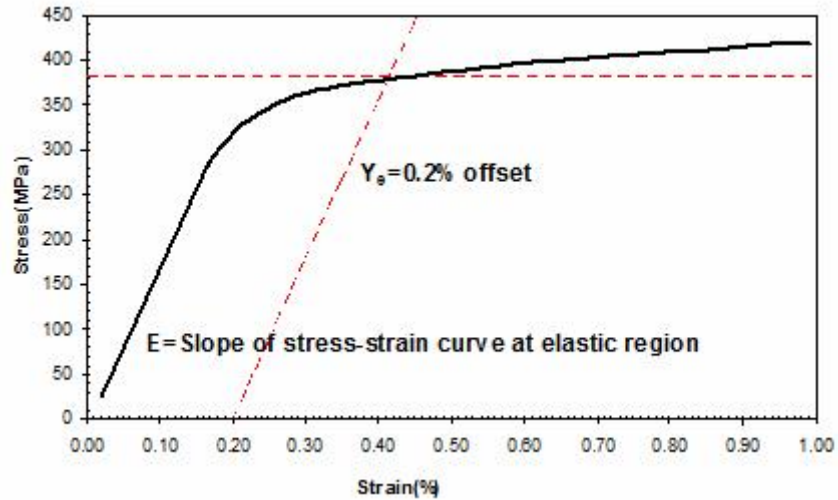
Figure 3.8 A typical engineering stress-strain curve

Figure 3.8 shows a typical engineering stress-strain curve from one of the monotonic test of coke drum material at 427 $^{\circ}$C. The yield strength can be found from constructing a straight line parallel to the initial linear portion (elastic portion) of the stress-strain curve, but offset from it by 0.2% strain. Then the yield strength is the stress level at which the created straight line intersects the stress-strain curve. The Young's modulus can be determined by calculating the slope of stress-strain curve at initial elastic portion, and if both initial stress and strain are at zero state, it can be conveniently determined by calculating the ratio of proportional limit which is the stress that causes the first plastic deformation over the corresponding strain level in the stress-strain curve.
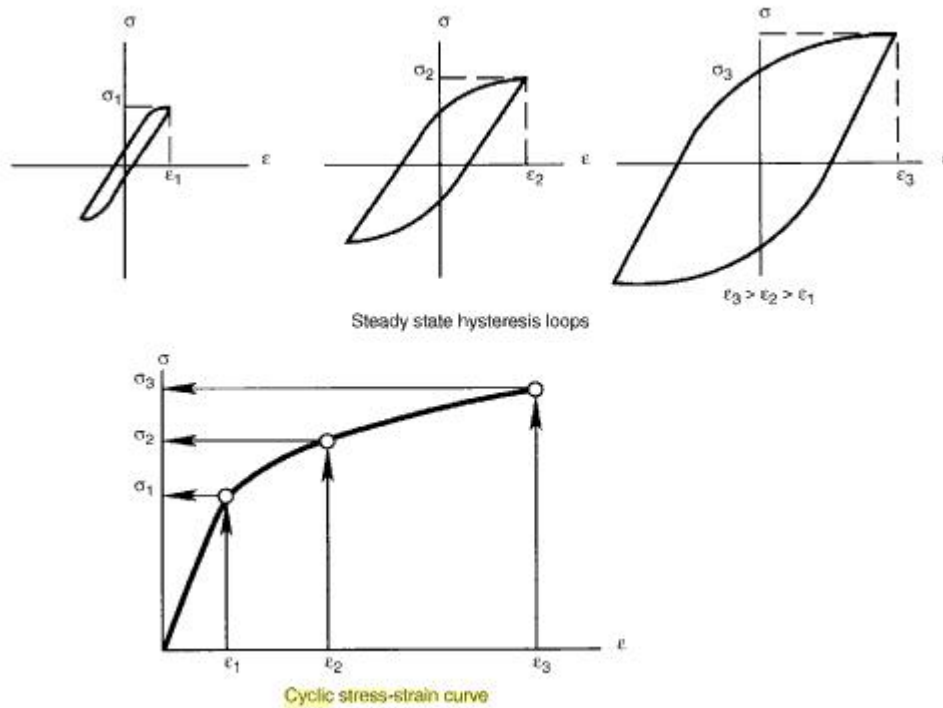
Figure 3.9 Formation of cyclic stress-strain curve [34]

The fully-reversed cyclic tests are conducted by cycling at one strain amplitude until stress level saturates and then repeating this at increasing strain amplitudes. The cyclic stress-strain curve, as shown in Fig. 3.9, is obtained by connecting the saturated stresses corresponding to the strain amplitudes.
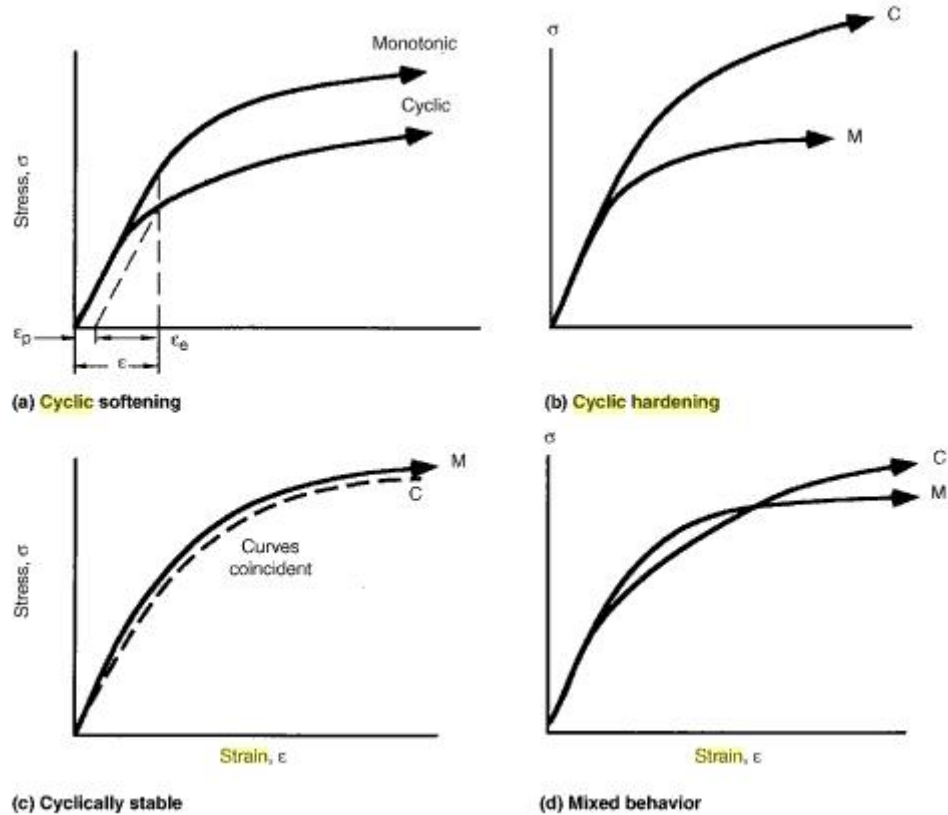
Figure 3.10 Comparisons between cyclic and monotonic stress-strain curves [34]

The cyclic stress-strain curve can also directly compare with the monotonic stress-strain curve of a material to show cyclically induced changes in mechanical properties of a material. There are normally four cases which are cyclic softening, cyclic hardening, cyclically stable, and mixed behaviour involved during the cyclic loading conditions as shown in Fig. 3.10. If the cycling is done at constant strain amplitude (strain-controlled condition), strain hardening is verified if an increase of stress amplitude occurred during the test. Conversely, a material behaves cyclic strain-softens if a decrease of stress amplitude during the test.

3.3.2 Summary of Mechanical Properties of Coke Drum Materials

Table 3.5 Summary of mechanical properties of coke drum material (25 ^oC)

			E (GPa) 25 °C	$\sigma_{y,0.2}$ (MPa)	σ_{ult} (MPa)
Monotonic Stress Strain Curves	SA387-11	weld zone (C)*	213	449	598
		weld zone (R)*	210	443	599
		non-weld (C)	222	445	593
		non-weld (R)	208	422	577
	410S	weld zone (R)	200	397	544
		non-weld (R)	197	366	526
Cyclic Stress Strain Curves	SA387-11	weld zone (C)	206	496	-
		weld zone (R)	210	524	-
		non-weld (C)	220	447	-
		non-weld (R)	204	442	-
	410S	weld zone (R)	216	450	-
		non-weld (R)	194	370	-

*weld zone (C) - "C" means the designed cylindrical (x-section) specimen is tested
 Weld zone (R) – "R" means the designed rectangular (x-section) specimen is tested

Ambient temperature mechanical properties of base and cladding materials

of the coke drum is obtained from the experimental monotonic and cyclic stress-

strain curves and summarized in Table 3.5. Comparing with specified mechanical properties of the coke drum material in Table 3.3, it is found that the yield strengths of the base and cladding materials are much higher (~ 20-30%) than the specified values of the materials, and the ultimate strength of base material is at the upper limit of the specified ranges and the ultimate strength of cladding material is approximate 15% higher than the specified value.

Figure 3.11 is the comparison of mechanical properties of coke drum materials between the base and cladding materials and also between weld and non-weld zones. The differences of Young's modulus of weld and non-weld zones of base and cladding materials are relative small. The yield strength from the weld zone of the cladding material is 10% less than the one from the weld zone of the base material, and the yield strength from the non-weld zone of the cladding material is 18% less than the one from the non-weld zone of the base material. In addition, the ultimate strength of cladding material is obviously smaller than base metal. Overall, it is found that cladding (410S) has less strength than base metal (SA387-11) in the coke drum construction. The weld zones of the base and cladding materials have higher yield strength than corresponding non-weld zone at ambient temperature.
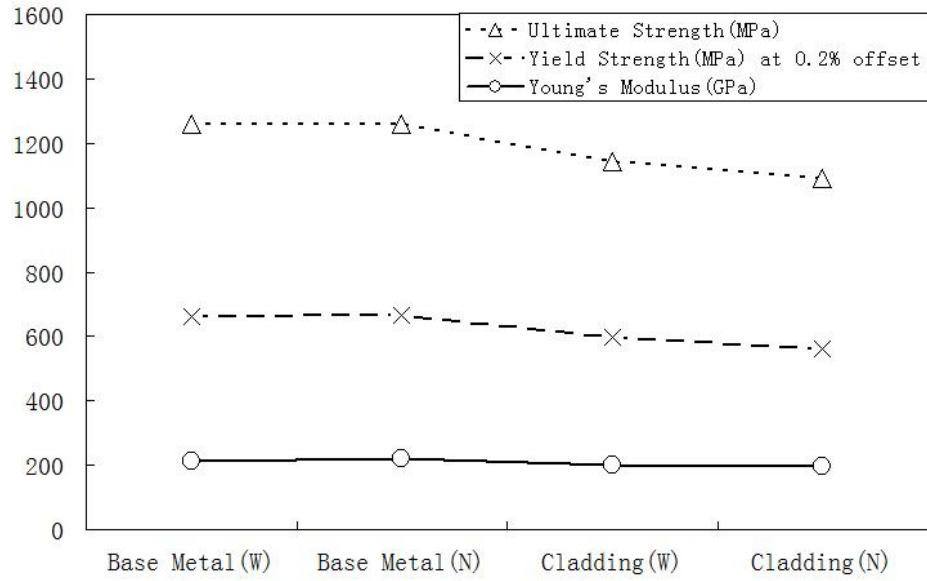
Figure 3.11 Comparison of mechanical properties of coke drum materials at 25 $^{\circ}$C

Table 3.6 Summary of mechanical properties of coke drum material (427 ^{o}C)

		427ºC	E (GPa) 427 °C	$6_{y,0.2}$ (MPa)
Monotonic Stress Strain Curves	**SA387-11**	weld zone (C)*	180	446
		weld zone (R)	150.9	387
		non-weld (C)	177	381
		non-weld (R)	147.2	376
	410S	weld zone (R)	167.1	334
		non-weld (R)	115	267
Cyclic Stress Strain Curves	**SA387-11**	-	-	-
		weld zone (R)	167.6	475
		non-weld (C)	176.8	380
		non-weld (R)	203.4	363
	410S	weld zone (R)	162.5	332
		non-weld (R)	198.2	303

*weld zone (C) - "C" means the designed cylindrical (x-section) specimen is
tested
Weld zone (R) – "R" means the designed rectangular (x-section) specimen is
tested

The mechanical properties of coke drum materials at 427ºC are tabulated in

Table 3.6. Yield strength and Young's modulus are obtained separately from the

monotonic tensile and cyclic stress-strain curves. By comparing with specified

minimum mechanical properties of the coke drum material at 427ºC (Table 3.3 b),

it is found that most the yield strength and Young's modulus of the base and

cladding materials at 427ºC are greater than the specified minimum values of the

materials except the results from the non-weld zone of the cladding. In addition, it is observed that larger scatter found in the Young's modulus and yield strengths of same testing zone with different specimen geometries.

The comparison of elevated temperature ($427^{o}C$) mechanical properties of coke drum materials from the tensile tests is charted in Fig. 3.12. The input values are from monotonic stress-strain curves which are obtained from the cylindrical specimens of base metal and rectangular specimen of cladding. The difference of Young's modulus of weld and non-weld zones of base and cladding material are relative small, with the exception of suddenly decreasing in non-weld zone of cladding. The yield strength from the weld zone of the cladding material is 20% less than the one from the weld zone of the base material, and the yield strength from the non-weld zone of the cladding material is 15% less than the one from the non-weld zone of the base material. Therefore, it is found that cladding (410S) has less strength than base metal (SA387-11) at elevated temperature in the coke drum construction. Additionally, temperature seems have larger impact on the mechanical properties of cladding material than that of the base material. The weld zones of the base and cladding materials also have higher yield strength than corresponding non-weld zones at $427^{o}C$. However, due to the shortage of virgin test plate, there is only one or two tests conducted for each kind of tests. More tests of monotonic and cyclic tests should be carried out to obtain more confident mechanical properties of the specified materials.
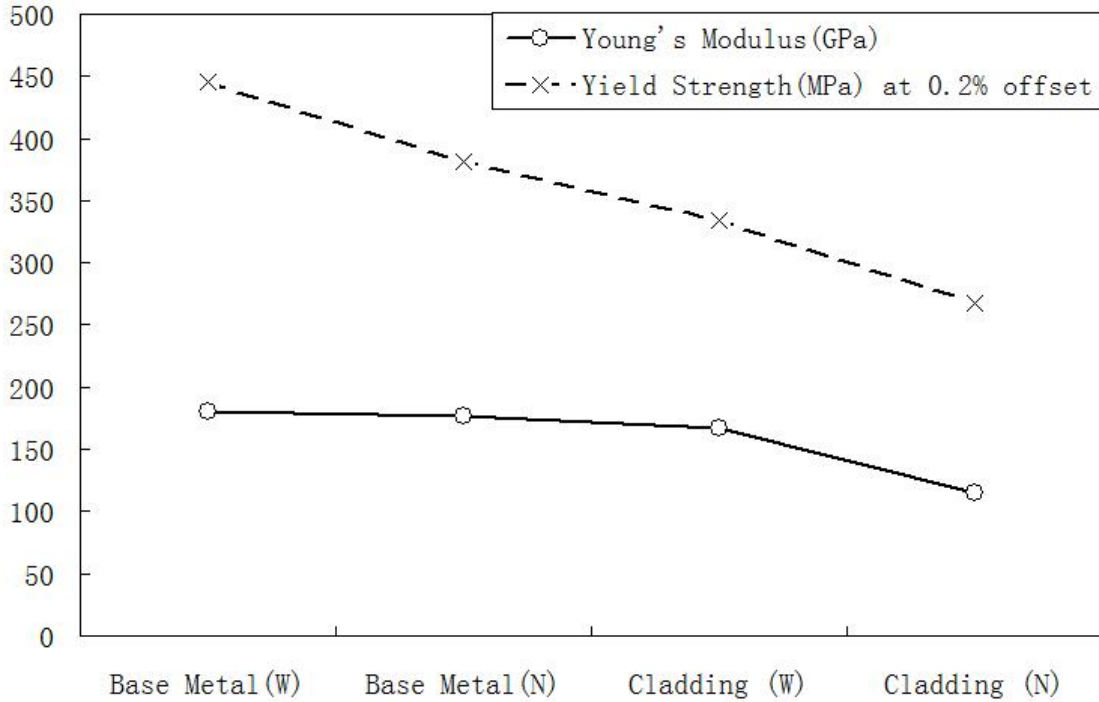
Figure 3.12 Comparison of mechanical properties of coke drum materials at 427°C

The temperature effect on the Young's modulus and yield strength of the base and cladding materials at non-weld zone from the monotonic stress-strain curves is demonstrated in Fig. 3.13. The values in the Fig. 3.13 are those at 427°C in comparison to the corresponding values at 25°C. It can be seen that the increase of temperature causes significant drop of the mechanical properties for both base and cladding materials. The drops of Young's modulus and yield strength are even larger for the cladding material.
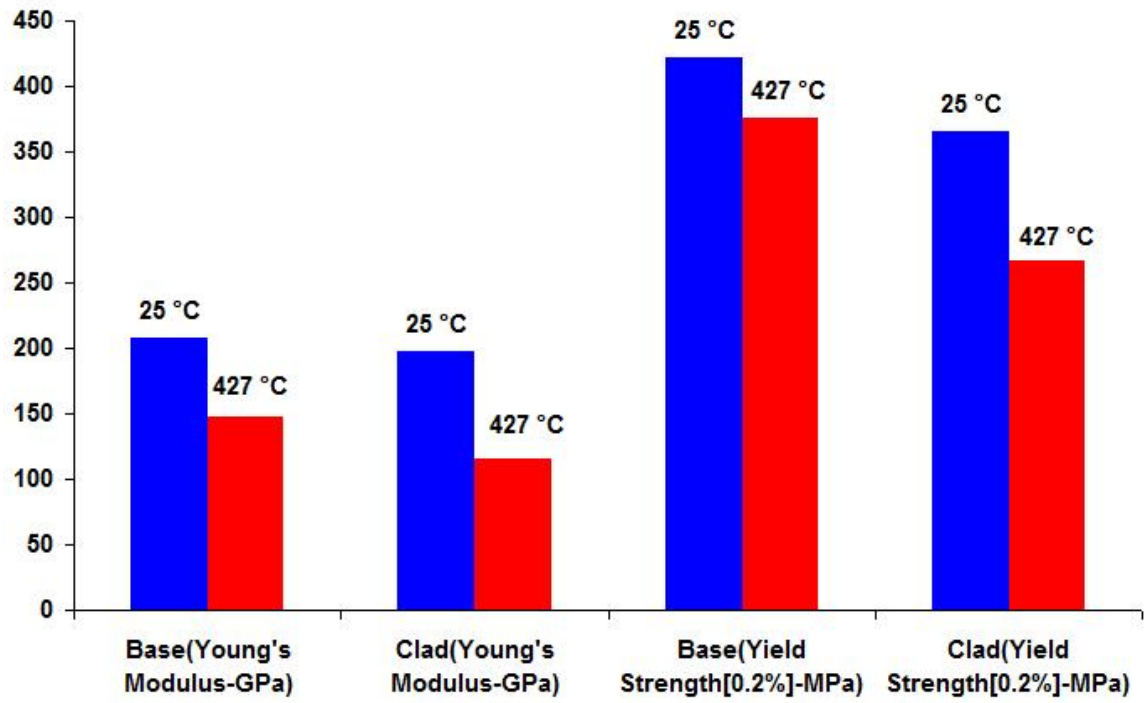
Figure 3.13 Mechanical properties of coke drum materials at 25 ^{o}C, 427 ^{o}C

3.3.3 Discussion on Monotonic and Cyclic Stress-Strain Curves

A comparison between room temperature monotonic and cyclic stress-strain curves of base material is shown in Fig. 3.14. The Young's modulus calculated from the monotonic and cyclic stress-strain curves are 208 GPa and 204 GPa, and the yield strength obtained from the monotonic and cyclic stress-strain curves are 422 MPa and 442 MPa respectively. From Fig. 3.14, it is observed that the cyclic stress-strain curve is below monotonic stress-strain curve between strains of 0.18% and 0.22%, and the cyclic stress-strain curve is above the monotonic stress-strain curve after strain of 0.22%. Therefore, the base material has mixed cyclic behaviour, and it first behaves cyclic softening and then cyclic hardening at ambient temperature.
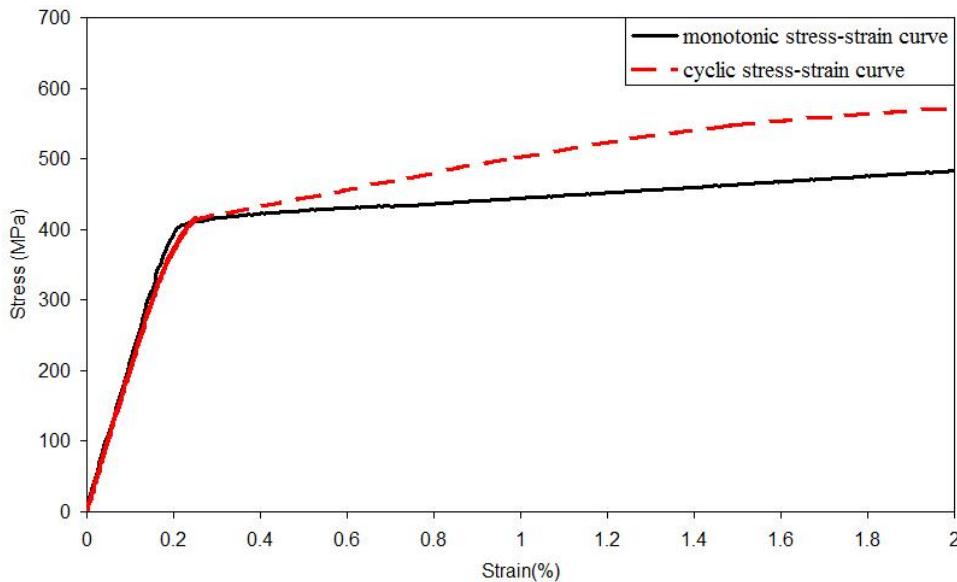
Figure 3.14 Monotonic and cyclic stress-strain curves of base material (25°C)

An assessment of room temperature monotonic and cyclic stress-strain curves of the cladding material is presented in Fig. 3.15. The Young's modulus of

the cladding obtained from the monotonic and cyclic stress-strain curves are 197 GPa and 194 GPa. The yield strength of the cladding evaluated from the monotonic and cyclic stress-strain curves are 366 MPa and 370 MPa. By comparing the monotonic and cyclic stress-strain curves, it is shown that the cladding of the coke drum also has mixed cyclic behaviour at room temperature. The cyclic stress-strain curve is below the monotonic stress-strain curve between strains of 0.1% and 0.4%, and thereafter the cyclic stress-strain curve is above the monotonic stress-strain curve. Therefore, the cladding of the coke drum has mixed cyclic behaviour, and it first behaves cyclic softening and cyclic hardening afterward.

By comparing of cyclic behaviours of the base and cladding materials at room temperature, it is found that both the coke drum materials have mixed cyclic behaviour, and the cladding has more noticeable initiated cyclic softening than the base material.
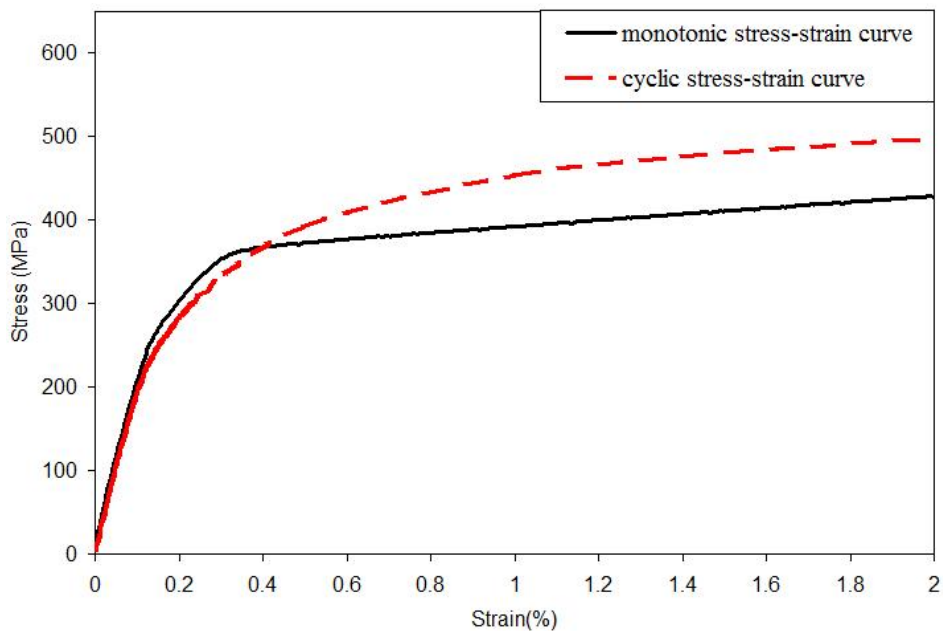
Figure 3.15 Monotonic and cyclic stress-strain curves of cladding (25 ^{o}C)

The monotonic and cyclic stress-strain curves of the base material at evaluated temperature of 427 ^{o}C are presented in Fig. 3.16. The Young's modulus of the base metal obtained from the monotonic and cyclic stress-strain curves are 177 GPa and 176.8 GPa respectively. The yield strength of the base material obtained from the monotonic and cyclic stress-strain curves are 381 MPa and 380 MPa. By comparing the monotonic and cyclic stress-strain curves, it is established that the base metal of the coke drum at elevated temperature (e.g. 427 ^{o}C) has a moderate cyclic hardening. The cyclic stress-strain curve is slightly above the monotonic stress-strain curve before the proportional limit, and at 1% strain, the cyclic stress-strain curve is 13.6% higher than the monotonic stress-strain curve. Therefore, the base metal of the coke drum behaves cyclic hardening at 427 ^{o}C.
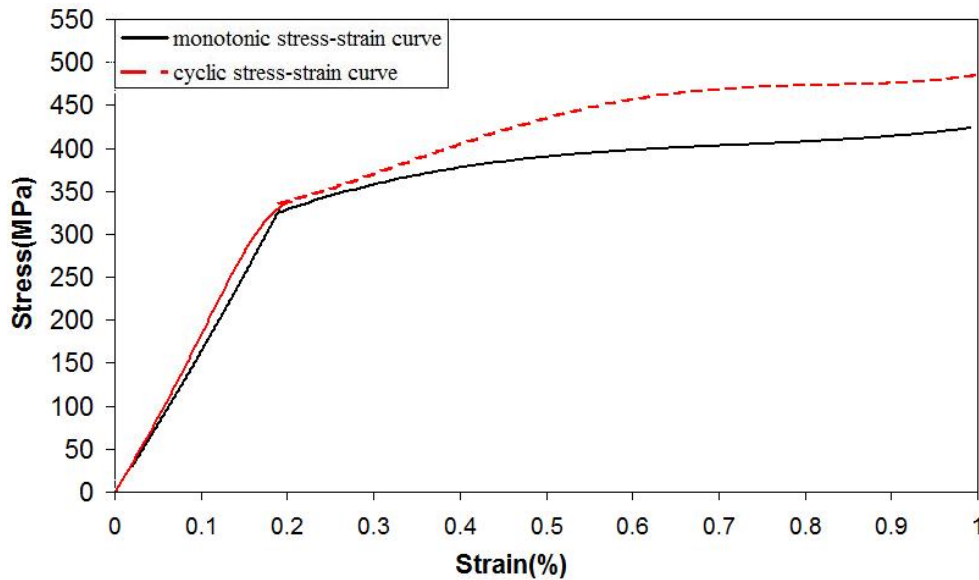
Figure 3.16 Monotonic and cyclic stress-strain curves of base material (427 ^{o}C)

An assessment of monotonic and cyclic stress-strain curves of the cladding at elevated temperature of 427 ^{o}C is presented in Fig. 3.17. The Young's modulus of

the cladding obtained from the monotonic and cyclic stress-strain curves are 167 GPa and 162.5 GPa. The yield strength of the cladding evaluated from the monotonic and cyclic stress-strain curves are 334 MPa and 332 MPa. By comparing the monotonic and cyclic stress-strain curves, it is shown that the cladding of the coke drum also has mixed cyclic behaviour at 427 ^{o}C. The cyclic stress-strain curve is below the monotonic stress-strain curve between the strain range of 0.08% and 0.45%, and the cyclic stress-strain curve is above the monotonic stress-strain curve thereafter. Therefore, the cladding of the coke drum has mixed cyclic behaviour, and it first behaves cyclic softening and cyclic hardening afterward.
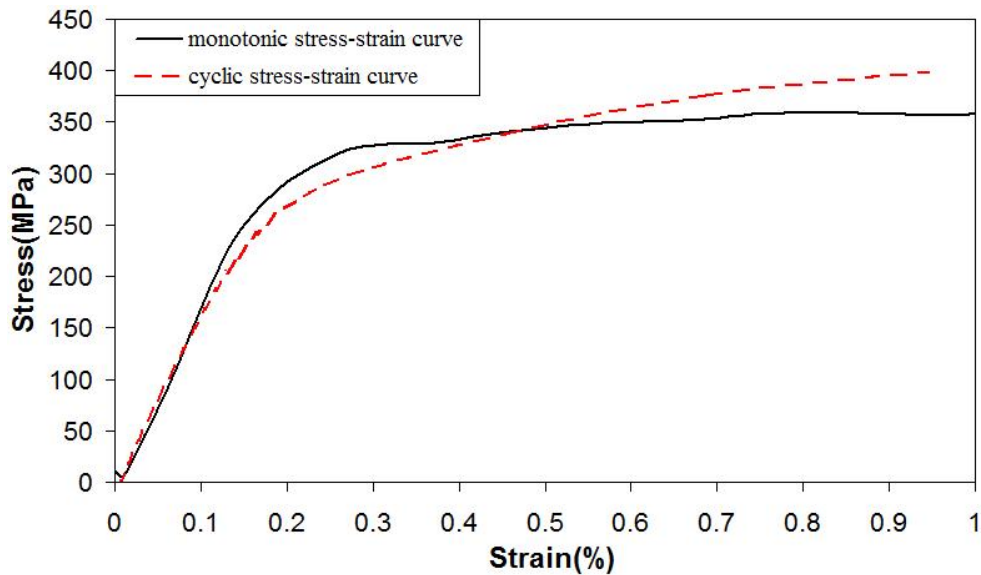
Figure 3.17 Monotonic and cyclic stress-strain curves of cladding (427 ^{o}C)

3.4 Strain-Rate Dependence Test

For most materials, an increase of strain rate increases flow stress, and the amount of the effect depends on the material and the temperature [35]. The construction materials of modern coke drums experience in temperature between room temperature and 427 ^{o}C. Therefore, it is significant to study the effect of different strain-rates and temperatures to the mechanical behaviours of the coke drum materials.
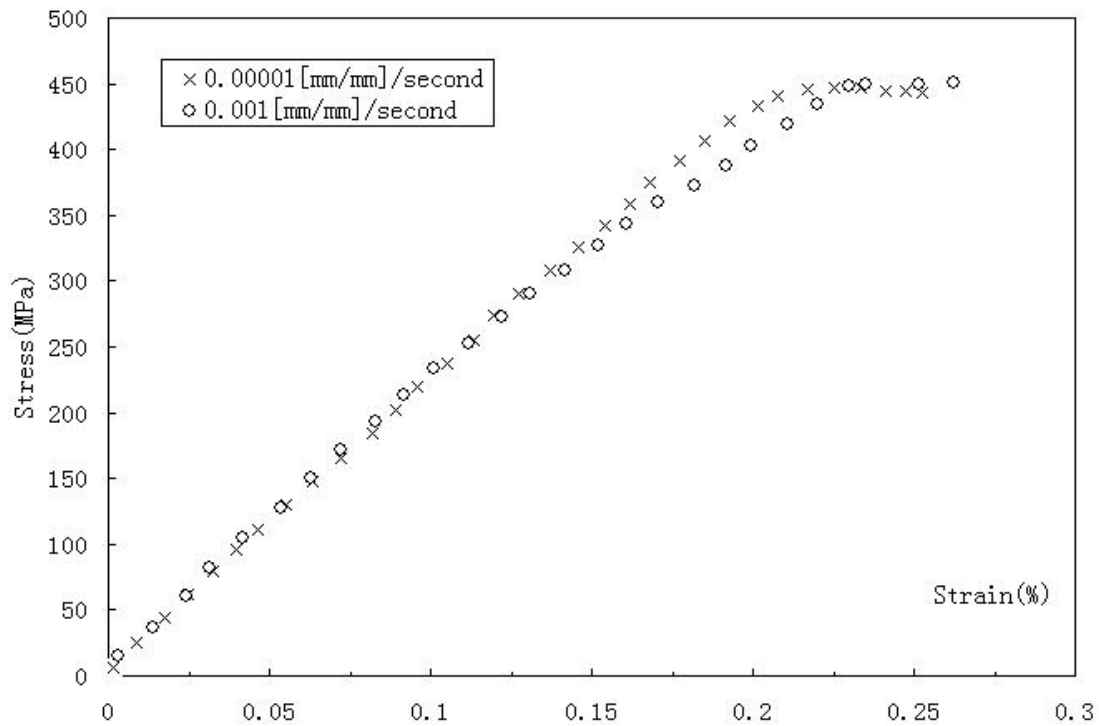
Figure 3.18 Comparison of monotonic stress/strain curves of base material (25°C)

As shown in Fig. 3.18, two room temperature tensile stress-strain curves of base material (SA387-11) with different strain rates are compared. The tensile tests were tested under strain-controlled condition up to the strain of 0.25% (past the proportional limit). One strain rate used is 0.00001 [mm/mm]/second and the

other strain rate tested is 0.001 [mm/mm]/second, and there is a factor of 100 of strain rate difference between two tested strain rates. The difference of the stress-strain curves occur in the strain range between 0.16% and 0.22%, and it corresponds a 5% differences in stress level which is not significant.
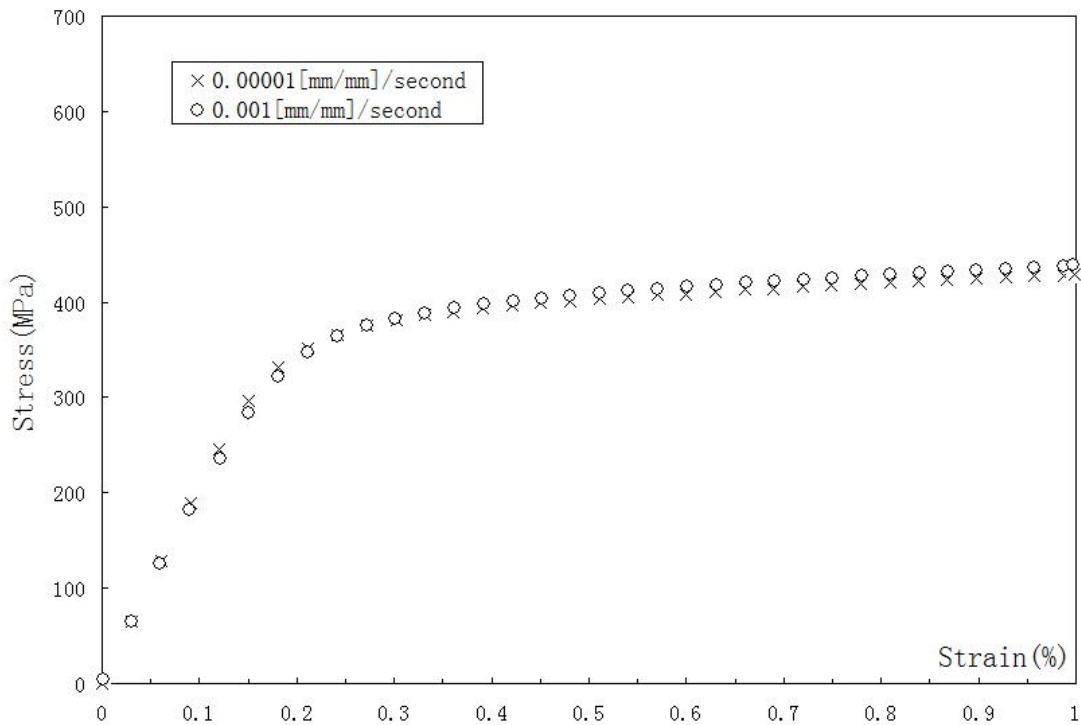
Figure 3.19 Comparison of monotonic stress/strain curves of cladding (25°C)

Two room temperature tensile stress-strain curves of cladding material (SA240 type 410S) with different strain rates are compared, as shown in Fig. 3.19. One strain rate used is 0.00001 [mm/mm]/second and the other strain rate tested is 0.001 [mm/mm]/second, and there is a factor of 100 of strain rate difference between two tested strain rates. It can be seen from Fig. 3.18 and 3.19 that at room temperature, both base and cladding materials are strain-rate insensitive.
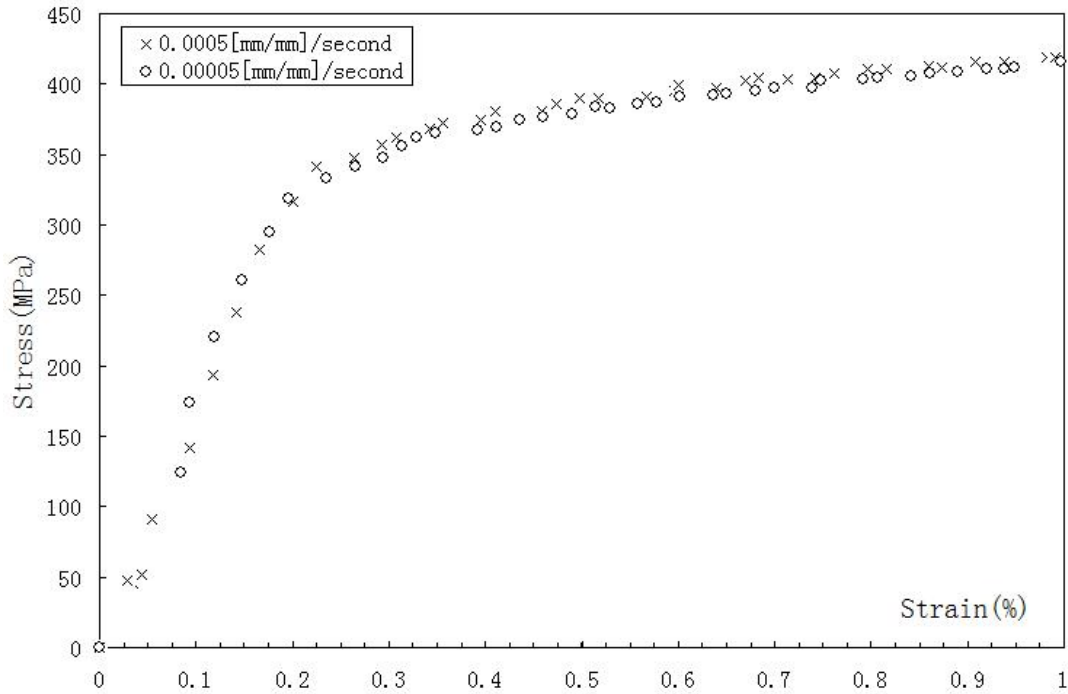
Figure 3.20 Comparison of monotonic stress/strain curves of base material (427°C)

Normally, at elevated temperatures, the effect of strain rate on flow stress is much greater, and increasing the strain rate at elevated temperature should have greater effect on raising the stress-strain curve. Two tensile stress-strain curves of base material (SA387-11) at elevated temperature (427 ^{o}C) with different strain rates are evaluated, as shown in Fig. 3.20. One strain rate used is 0.00005 [mm/mm]/second and the other increased strain rate is 0.0005 [mm/mm]/second, and there is a factor of 10 of strain rate difference between two tested strain rates. A factor of 10 increase of strain rate raises the level of the stress-strain curve by only 2 to 3% approximately at 427 ^{o}C which is quite small and can be neglected. Therefore, at elevated temperature of 427 ^{o}C, the base material is strain-rate insensitive as well from the observation of the experimental result.

3.5 Creep Test

Creep is time dependent plastic deformation, which is often more obvious at high temperature [36]. Creep usually involves three stages after the constant load is applied. First, after the load is applied, there is an instantaneous linear respond of the strain, followed by a period of transient creep. After that, the creep rate gradually decreases to a fairly steady state. Finally, the strain rate may increase again, accelerating to the material failure [35]. In order to deeply study the mechanical behaviours of the coke drum material under different loading conditions and at the request of industrial partner of the research project, creep tests of SA387-22 (base metal) were conducted at elevated temperatures of $427\,^{\circ}$C and $500\,^{\circ}$C, respectively.

Figure 3.21 shows the result of a stepped creep test at constant temperature of 427°C. The thermal strain had been deducted from the total strain at the beginning of the test. The proportional limit of SA387-22 experimentally determined is approximately 300 MPa at 427°C, and the stepped stress levels of 385 MPa, 400MPa and 415 MPa are used to study the creep behaviour of the base material. After each constant stress applied, there is one hour holding period to observe the material deformation. At the initial load of 385 MPa is applied, there is an instantaneous response of the strain, followed by a period of small strain increment but the creep seems stopped after holding time of 40 minutes. In the subsequent to stress level of 400 MPa, there is total 0.07% strain increment during the one-hour holding period. After increasing the load to the third stepped stress level, there is rapid strain rise, and subsequently, the creep rate gradually

decreases to a stable value. There is 0.25% strain increment observed in one-hour

holding period. Therefore, there is negligible creep strain at temperature of 427°C

when the stress level is below 385MPa. However, obvious creep is observed at

the higher stress levels.
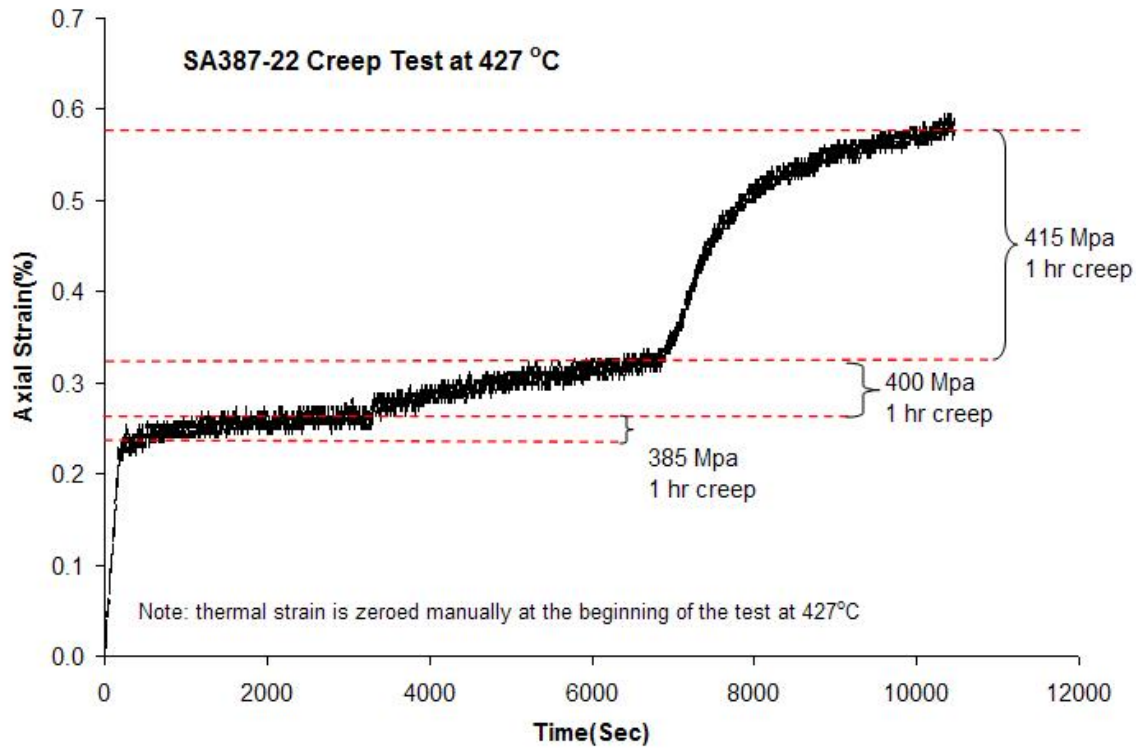
Figure 3.21 Creep test result of SA387-22 at 427°C

Another creep test of SA387-22 was conducted at 500°C, as shown in Fig.

3.22. The same stress levels of 385MPa, 400MPa and 415 MPa are used in 500°C

creep test of the base metal. After the initial constant load of 385 MPa is applied,

there is approximate 0.25% creep strain in the one-hour holding period.

Subsequently, at the second constant stress level, there is also 0.25% creep strain

accumulated in the corresponding holding period. Finally, at the third constant

stress level of 415 MPa, the creep strain increases in an amount of 0.45% in one hour.

By comparing the creep phenomenon between 427°C and 500°C, it is found that the accumulated creep strain at 500°C with stress level of 385 MPa is approximately equal to that at 427°C with stress level of 415 MPa within the one-hour holding period. Therefore, creep of SA387-22 is more obvious at higher temperature, and the temperature is an important influence factor on the creep of the base material.
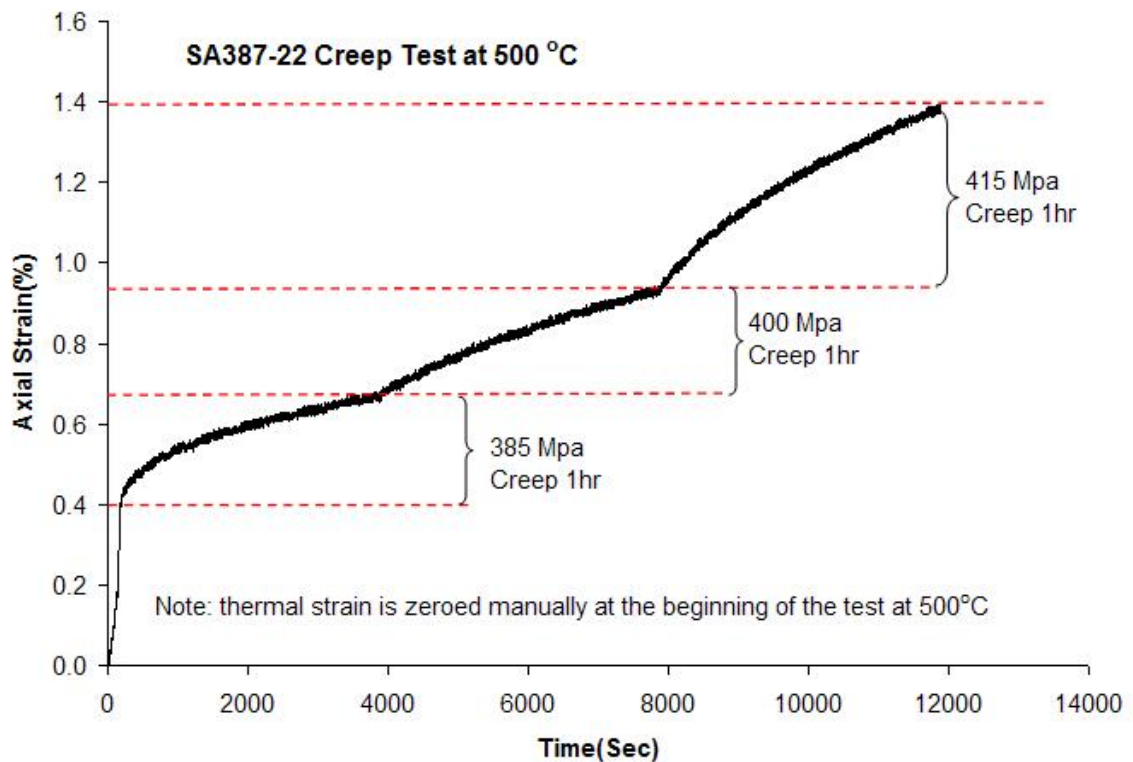
Figure 3.22 Creep test result of SA387-22 at 500°C

3.6 Summary

Relatively large scatter in ultimate strains of the tested specimens were observed while the scatter in the yield and ultimate strengths are relatively small. There is even larger scatter for the specimens cut from weld zone. This may be attributed to the inherent defects in the materials and inhomogeneity in the weld zone;

All ambient and elevated temperature mechanical properties of coke drum materials obtained from the experimental results are higher than the specified minimum values. By comparing the yield strength and Young's modulus of the coke drum materials, it is experimentally found that the base metal has higher strength than the cladding at both ambient and elevated temperature. In addition, temperature seems have larger impact on the variation of the mechanical properties of cladding material than that of base metal of the coke drum. The yield strength and Young's modulus of base and cladding obtained from the ambient temperature stress-strain curves are approximate 10% to 30% higher than the corresponding values obtained from the 427 ^{o}C stress-strain curves in both monotonic and cyclic tests. The weld zones of the base and cladding materials have higher yield strength than corresponding non-weld zones. Finally, it is found that the base and cladding materials at ambient temperature and the cladding at elevated temperature have mixed cyclic behaviours (cyclic softening at smaller strain amplitude and cyclic hardening at larger strain amplitude), and the base metal at elevated temperature has a distinguished cyclic hardening behaviour.

Both SA387-11 (base material) and SA240 TP410S (cladding materials) show negligible rate-dependence as the stress-strain curves with two order differences in loading rate are almost coincided each other.

SA387-22 base material has a negligible creep at stress level up to 385 MPa and at temperature up to 427°C. However, at a higher temperature of 500°C, the creep is obvious at the stress level of 385 MPa.

Chapter 4 Experimental Study of Material Behaviors under Complex Thermal-Mechanical Loading Conditions

4.1 Introduction

The coke drum operation involves high temperature (500°C) oil filling in, water quenching, etc, and the coke drum components experience complex thermal-mechanical cyclic loading conditions. Coke drum materials responses under uniaxial as well as biaxial cyclic thermal–mechanical loadings are experimentally investigated. Several experiments are designed to simulate the cases which coke drum materials may experience in the operation, such as the test on tubular specimens by applying in-phase thermal-mechanical cyclic loading with constant internal pressure. These tests will help us to understand the damage and failure mechanisms of coke drums, especially in the form of shell bulging. All together three types of uniaxial thermal-mechanical cyclic tests on the solid specimens and three types of biaxial thermal-mechanical cyclic tests on the tubular specimens were carried out. The obtained experimental results of these specially designed tests could serve as benchmark data for verifying the temperature dependent elastoplastic constitutive models. They are currently available in the commercial FEM analysis codes and the one recently developed in our lab through this research project. In this chapter, the testing material and the specimen geometry are first introduced and the test programs for the six types of thermal-mechanical cyclic tests are described. The experimental results and discussion are then presented to summarize the key findings of the material

behaviors under the different loading conditions. Finally, a comparison between uniaxial experimental results and the predictions of the multilinear kinematic hardening model in ANSYS FEM code and the newly-developed model in our lab is presented. The model predictions are provided by Dr. Yejian Jiang [37].

4.2 Test Material and Specimen Geometry

The material used is ASTM SA387 grade 22 (chromium-molybdenum) which is used as the base metal of some modern coke drums.

Table 4.1 Chemical composition of ASTM SA387-11&22 [24-26]

Material	% C	% S	% Mn	% Si	% Cr	% Ni	% Mo
SA387-11	0.04-0.17	0.035	0.35-0.73	0.44-0.86	0.94-1.56	-	0.40-0.70
SA387-22	0.04-0.15	0.035	0.25-0.66	0.5	1.88-2.62	-	0.85-1.15

The chemical compositions of ASTM A387 grade 11 and grade 22 (chromium-molybdenum) are shown in Table 4.1. The major difference of grade 11 and grade 22 is chemical composition which is the composition percentage of chromium-molybdenum. The composition percentages of Cr.-Mo. in grade 11 are 0.94-1.56% and 0.4-0.7%, and the composition percentages of Cr.-Mo. in grade 22 are 1.88-2.62% and 0.85-1.15%. The nominal chromium and molybdenum percentages of grade 11 are 1.25% and 0.5%, and the nominal chromium and molybdenum percentages of grade 22 are 2.25% and 1%. The specified nominal yield strength and tensile strength of grade 11 and grade 22 are identical which are 310 MPa and 515-690 MPa.

The solid cylindrical-threaded specimens of the base metal are designed for the uniaxial thermal-mechanical loading tests, as shown in Fig. 4.1. The gage length is 0.0508 m, and the diameter is designed to 0.008255 m to prevent the operated load cell from overloading under strain-controlled test on the modified

elevated temperature testing system. Two 0.0254 m-span dimples are carefully

nail punched in the middle of the test section for placement of the conical tips of

the home-made extensometer on the test section.   In addition, the home-made

external-internal socket (see Fig. 2.10) is implemented which allowed the

cylindrical-treaded specimen mounted on the testing system securely and firmly.

The specimen are prepared and machined according to the ASTM E-8 standard.

The specimen surface is well finished to maximize precision and minimize bias in

test results.
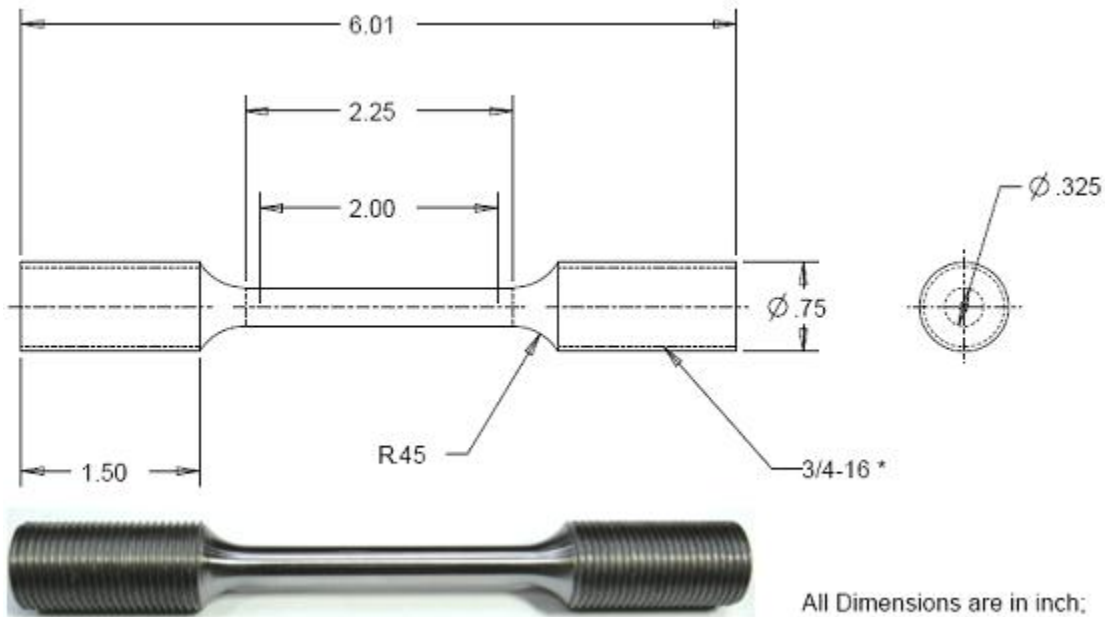
Figure 4.1 Picture of cylindrical-threaded specimen

        As shown in Fig. 4.2, the thin-walled tubular specimen is specially

designed for the biaxial thermal-mechanical loading tests. The cross section area

of the test section is 5.969E-5 m^2. The length of the test section is 0.03 m. The

total length of the tubular specimen is 0.167 m. The length of the threaded grip is

0.04191 m. The designed external threads of the specimen can be tightly engaged

with the internal threads of extension heads of the gripping system. The specimen

geometry is designed based on a FEM buckling analysis to the specimen

(Appendix C) in order to avoid buckling effect during compressive loading stages

in the relevant tests. The thin-walled tubular specimen was designed according to

ASTM E2207 standard. [38]
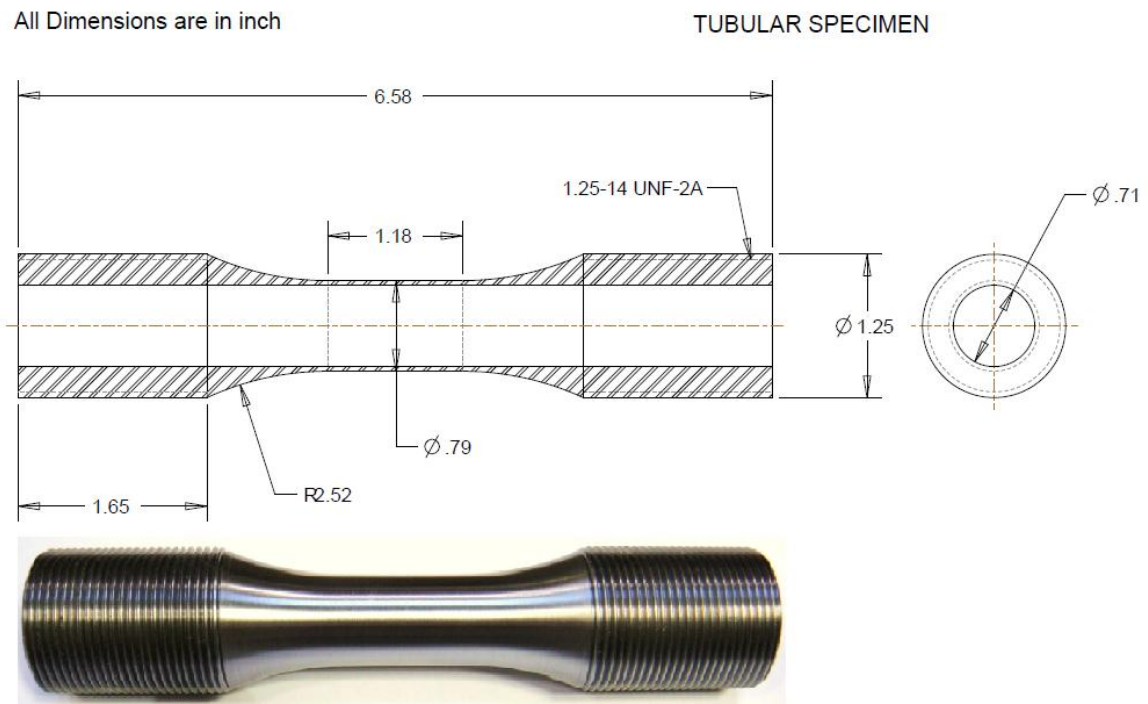
Figure 4.2 Picture of thin-walled tubular specimen

4.3 Test Program

The following six types of thermal-mechanical cyclic tests were

experimentally conducted:

Uniaxial Thermal-Mechanical Loading Test

1. Constant stress with cyclic thermal loading

2. In-phase thermal-mechanical loading

3. Out-of-phase thermal-mechanical loading

Biaxial Thermal-Mechanical Loading Test

4. Strain-controlled fully reversed cyclic loading with constant internal

    pressure

5. Stress-controlled fully reversed cyclic loading with constant internal

    pressure

6. In-phase thermal-mechanical fully-reversed cyclic loading with constant

    internal pressure

    o   Strain-controlled

    o   Stress-controlled

1. Uniaxial constant stress with cyclic thermal loading

The brief testing procedure of constant stress with cyclic thermal loading

test is shown in Fig. 4.3. The specimen is firstly raised to 70$^{\mathrm{o}}$C under zero

mechanical load condition, and the strain is tuned to zero at the stabilized

temperature of 70$^{\mathrm{o}}$C. After that, the temperature is ramped up to 235$^{\mathrm{o}}$C (mid

temperature of 70$^{\mathrm{o}}$C and 400$^{\mathrm{o}}$C), and the stress amplitude of 345 MPa is applied

at the stabilized temperature of 235$^{\mathrm{o}}$C. Afterward, the stress remains constant,

and the temperature is changed for two full cycles from 235-400-70-235. Then at

235 $^{\mathrm{o}}$C, the stress is raised to 425 MPa and keeps constant. Subsequently,

another two full temperature cycles of 235 $^{\mathrm{o}}$C -400 $^{\mathrm{o}}$C -70 $^{\mathrm{o}}$C -235 $^{\mathrm{o}}$C are applied.
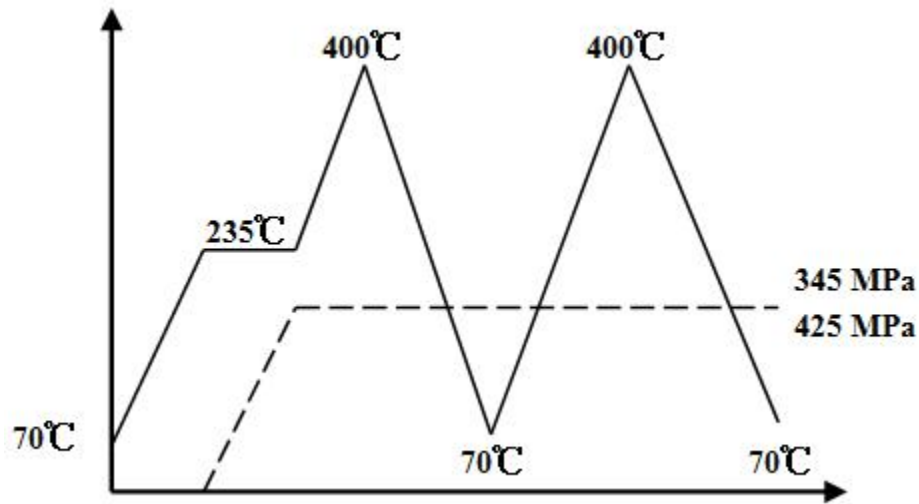
Figure 4.3 Diagram of constant stress with cyclic thermal loading

2. Uniaxial in-phase thermal-mechanical loading

The in-phase thermal-mechanical loading test was conducted to study the deformation behaviors of the coke drum material under in-phase thermal-mechanical cyclic loading condition. As shown in Fig. 4.4, the specimen is warmed up to $70\,^{\circ}C$, and the total strain and load is adjusted to zero at the steady $70\,^{\circ}C$. After that, the temperature cycling between $70\,^{\circ}C$ to $400\,^{\circ}C$ and the stress cycling from 0 MPa to 425 MPa are applied. The "in-phase" means that the temperature and the stress increase or decrease synchronistically.
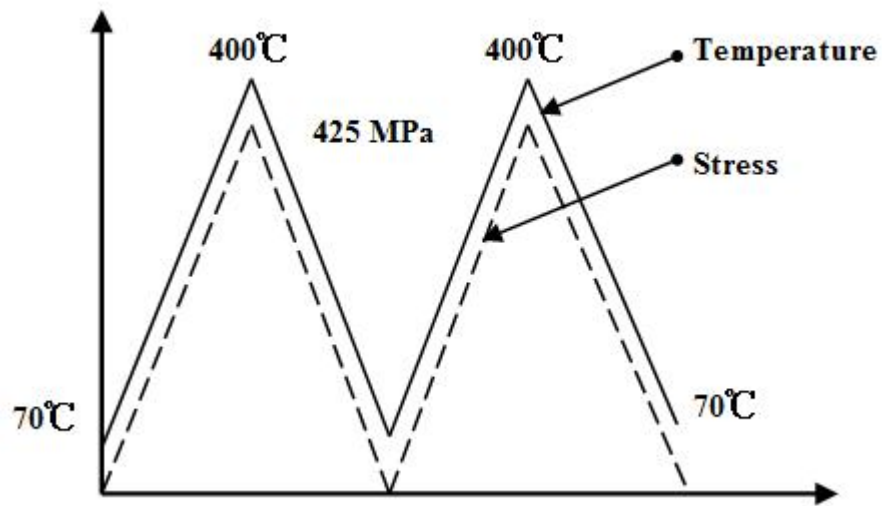
Figure 4.4 Diagram of in-phase thermal-mechanical loading

3. Uniaxial out-of-phase thermal-mechanical loading

An out-of-phase thermal-mechanical loading test was carried out according to the testing procedure expressed in Fig. 4.5. The specimen is firstly brought up to 235°C, and the stress is manually increased to 212.5 MPa. Afterwards, the test is turned into temperature-stress-controlled condition. The temperature of the specimen is cycled as 235°C - 70°C - 400 °C - 235 °C, while the stress is cycled as 212.5 MPa - 425 MPa - 0 MPa - 212.5 MPa. The "out-of-phase" means that while the stress increases or decreases the temperature is decreases or increases.
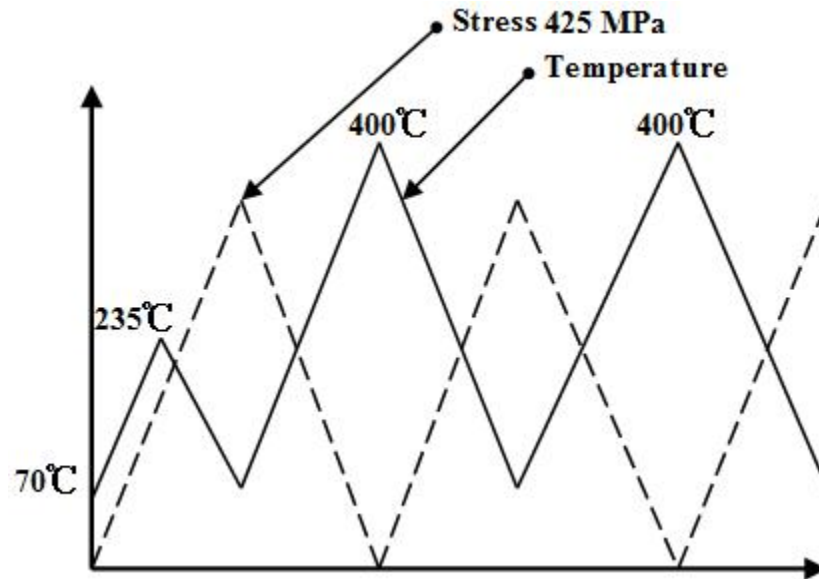
Figure 4.5 Diagram of out-of-phase thermal-mechanical loading

4. Strain-controlled fully reversed axial cycling with constant internal pressure

The tests were conducted at constant ambient temperature or at constant 427°C respectively. An internal pressure of 7.446 MPa is first applied, which generates a hoop stress of 70 MPa to the thin-walled tubular specimen. Subsequently, strain-controlled cycling of ±0.4% axial strain is executed with a period of 80 seconds per cycle. Total 100 cycles are completed for each test. Both axial and diametral strain histories are recorded.

5. Stress-controlled fully reversed axial cycling with constant internal pressure

The stress-controlled fully reversed axial cycling with constant internal pressure tests were carried out at constant ambient temperature and constant 427°C, respectively. A constant internal pressure of 7.446 MPa (same as the pressure applied in the test type 4) is applied to the thin-walled tubular specimen before applying the cyclic loading. After stabilization of the internal pressure,

stress-controlled axial cycling of ±385 MPa is added with a period of 80 seconds

per cycle and total of 100 loading cycles are completed for each test.

6. In-phase thermal-mechanical cyclic loading with constant internal pressure

Two biaxial in-phase thermal-mechanical cyclic tests, one under strain-

controlled mode and another under stress-controlled mode, were performed.

Similar to the uniaxial in-phase thermal-mechanical loading test, temperature and

axial stress/or strain increase and decrease synchronistically. A constant internal

pressure of 7.446 MPa is also firstly applied to the thin-walled tubular specimen.

Under strain-controlled condition, axial strain is cycling of ±0.4% and the

temperature is cycling between 70°C and 400°C. Under stress-controlled

condition, axial stress is cycling of ±400 MPa and the temperature is cycling

between 70 $^{\circ}$C and 400 $^{\circ}$C. Total 7 cycles were performed for the stress-controlled

test and 4 cycles were performed for the strain-controlled tests respectively.

4.4 Experimental Results and Discussions

The mechanical properties of base material of coke drum are firstly

determined at ambient and elevated temperatures, as shown in Fig. 4.6. The four

tensile tests were conducted at ambient temperature, 70°C, 235 $^{\circ}$C, and 400 $^{\circ}$C,

respectively. The yield strength and Young's modulus are obtained from the

corresponding stress-strain curves at the ambient or elevated temperatures. As the

temperature increases from 25 $^{\circ}$C to 400 $^{\circ}$C, the yield strength decreases 18%,

and the Young's modulus declines 20%.
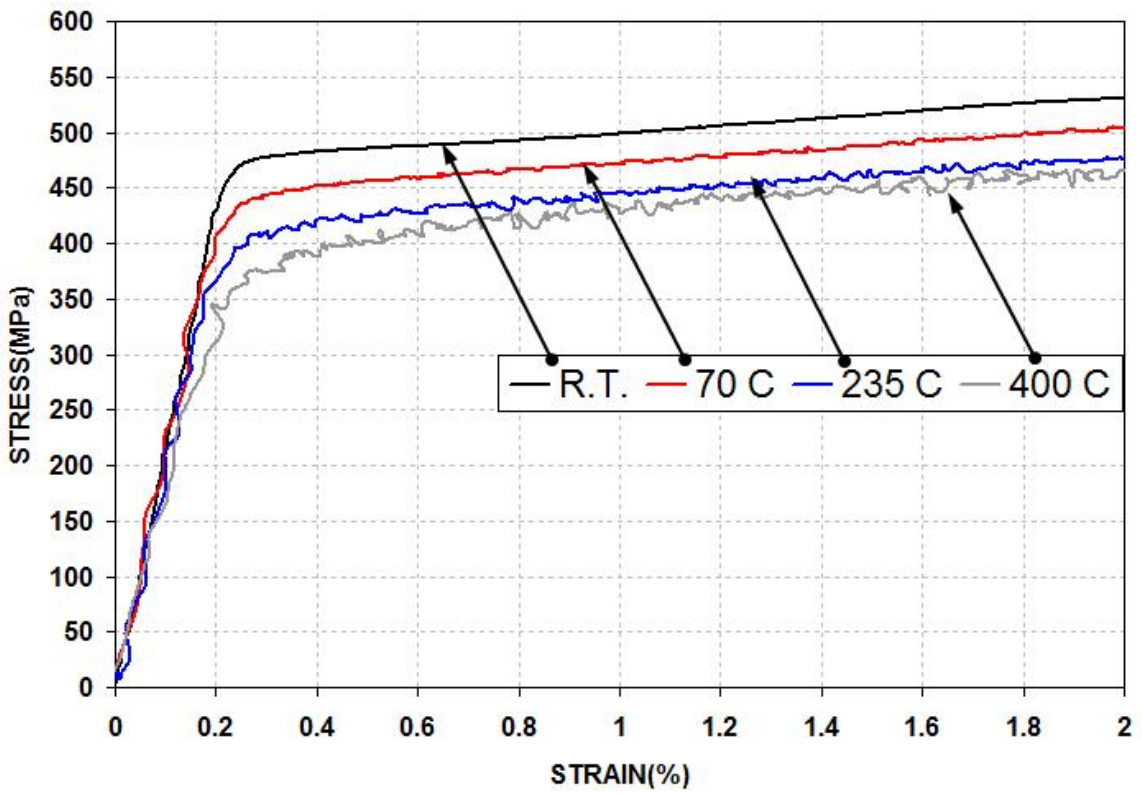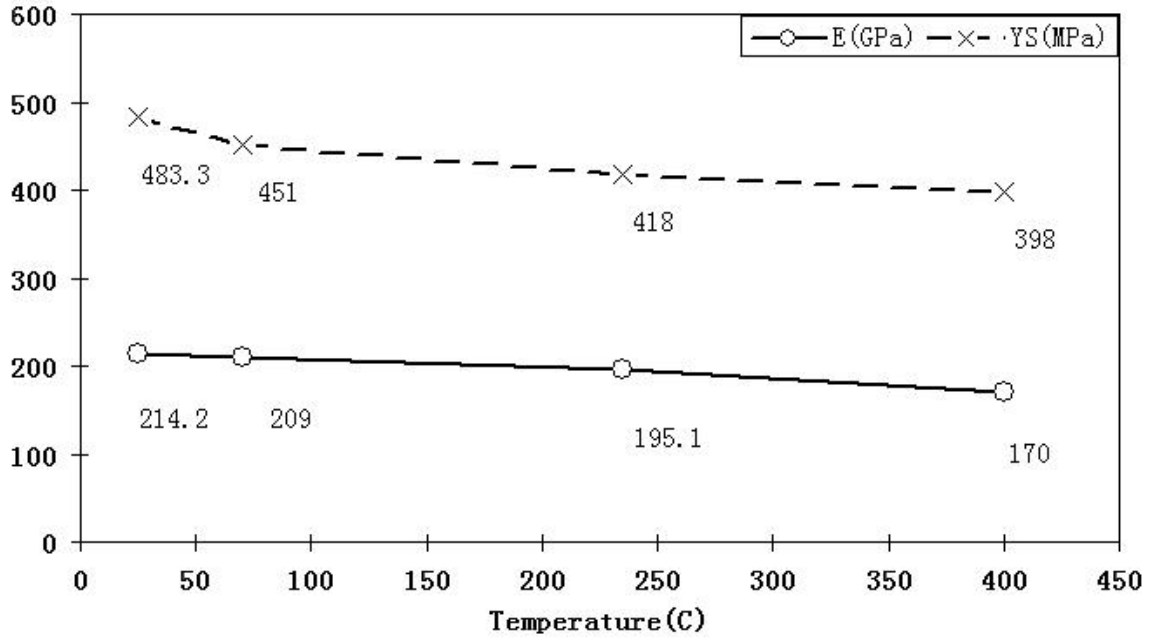
Figure 4.6 Mechanical properties and stress/strain curves of SA387-22

Free Thermal Strain

In order to determine the mechanical strain in the test results, the axial free thermal strain of ASTM SA387-22 are obtained by conducting two thermal cycles of 70-400-70-400 ^{o}C, as shown in Fig. 4.7. The specimen is under zero load condition during the thermal cycles. Therefore, the recorded strain in Fig. 4.7 is the pure free thermal strain. In the later thermal-mechanical cyclic tests, the mechanical strains can be obtained by subtraction of the free thermal strains from the total measured strains. The diametral mechanical strains could obtain in the same manner.
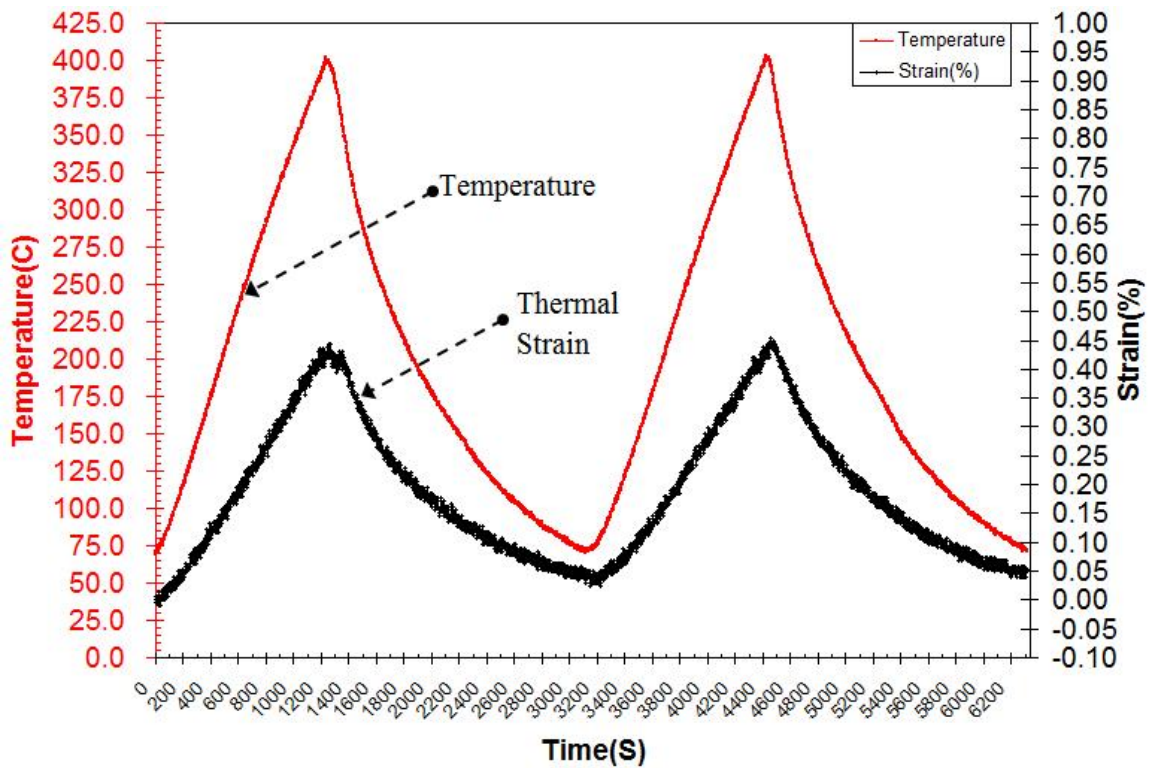
Figure 4.7 Test result of free thermal strain of SA387-22

The experimental results are presented and discussed in the same order as that in the previous section 4.3.

1. Uniaxial constant stress with cyclic thermal loading

The test result of constant stress with cyclic thermal loading is illustrated in Fig. 4.8 and 4.9. The figure 4.8 shows the total strain history while the Fig. 4.9 gives the mechanical strain history. The mechanical strain is obtained by subtracting the thermal strain from the total strain at the corresponding temperatures as showed in Fig. 4.7. The first applied constant stress is 345 MPa, which is lower than the yield strength (stress level with 0.2% plastic strain, see Fig. 4.6) of the material in the temperature range of 235ºC – 400 ºC, see Fig. 4.6. But this stress level may already be over the proportional limit of the material, i.e., a small amount of plastic deformation might be introduced. Therefore, at this stress level, during the first shot of temperature from 235 ºC to 400 ºC, a small shot of mechanical strain (A to B) is observed. After that the temperature change only causes very small change of elastic strain. Due to the relatively large noises, this change is not very clearly seen in Fig. 4.9. At the higher stress level of 425 Mpa, which is larger than the yield strength of the material at the most test temperature range between 235 ºC – 400 ºC, refer to Fig. 4.6, one can see a quite large shot of mechanical strain about 0.3% (C to D), corresponding to the first shot of temperature from 235 ºC to 400 ºC at this stress level. However, after the first increase of temperature, the strain response is mainly elastic one. The change of strain with the temperature is due to the change of elastic modulus with the temperature, refer to Fig. 4.6.
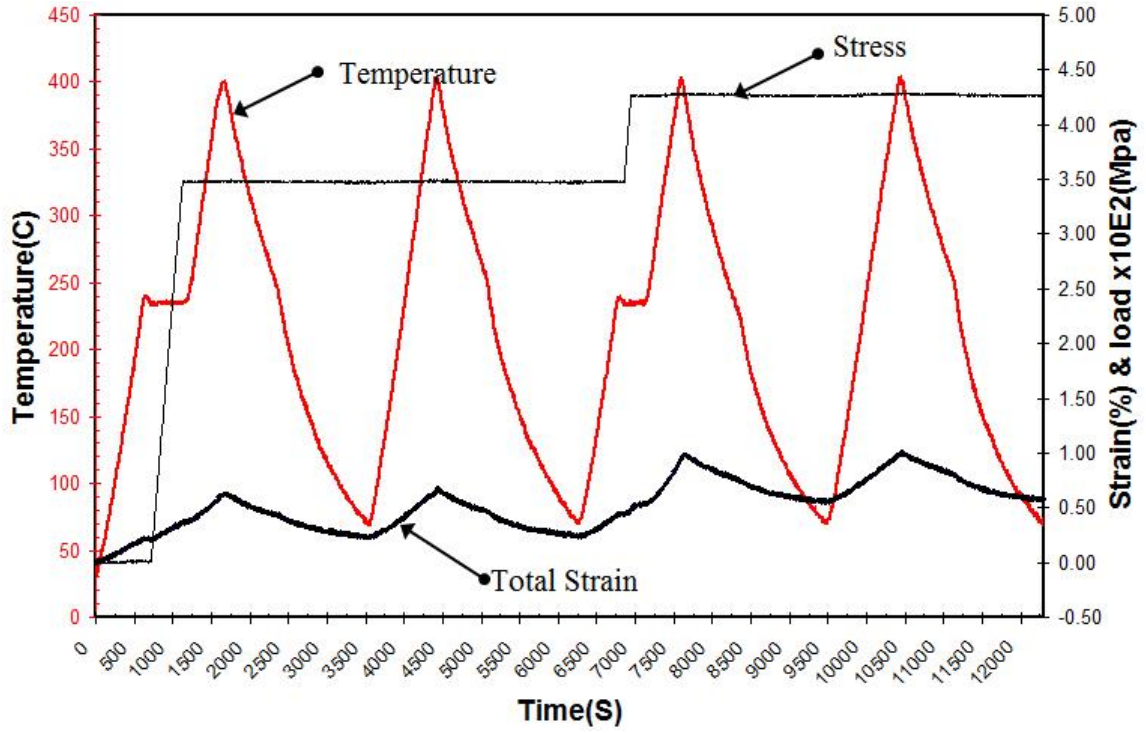
Figure 4.8 Temperature, stress and total strain history in the test of constant stress with cyclic thermal loading
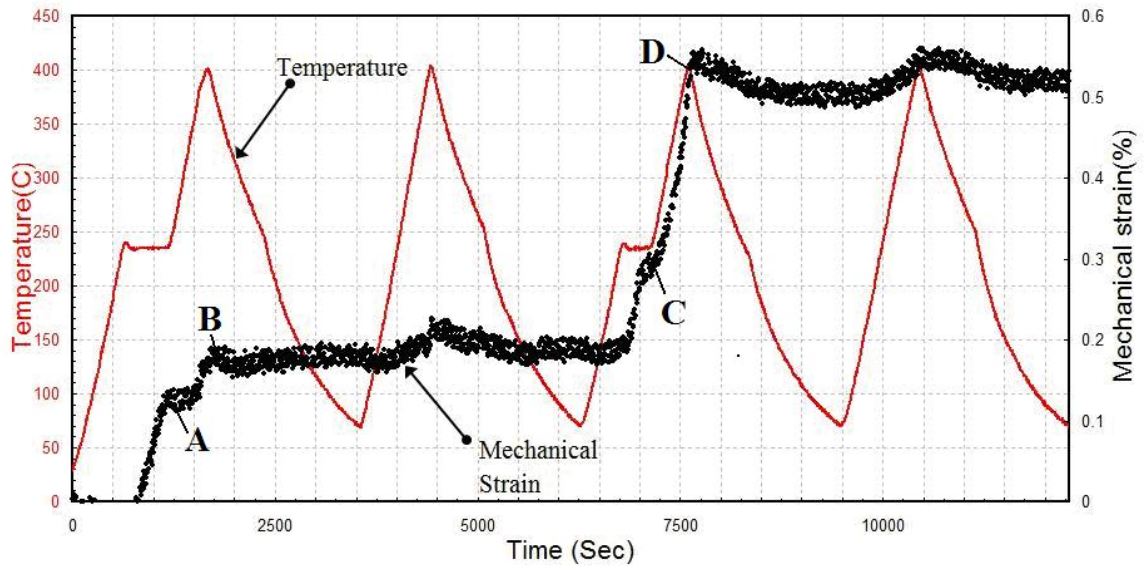
Figure 4.9 Mechanical strain history in the test of constant stress with cyclic thermal loading

2. Uniaxial in-phase thermal-mechanical loading

Figure 4.10 shows the total strain history of the test with the in-phase temperature and stress cycling. Figure 4.11 gives the mechanical strain history which is obtained by subtraction of the free thermal strain from the total strain. And Figure 4.12 presents the stress-mechanical strain response of the test.
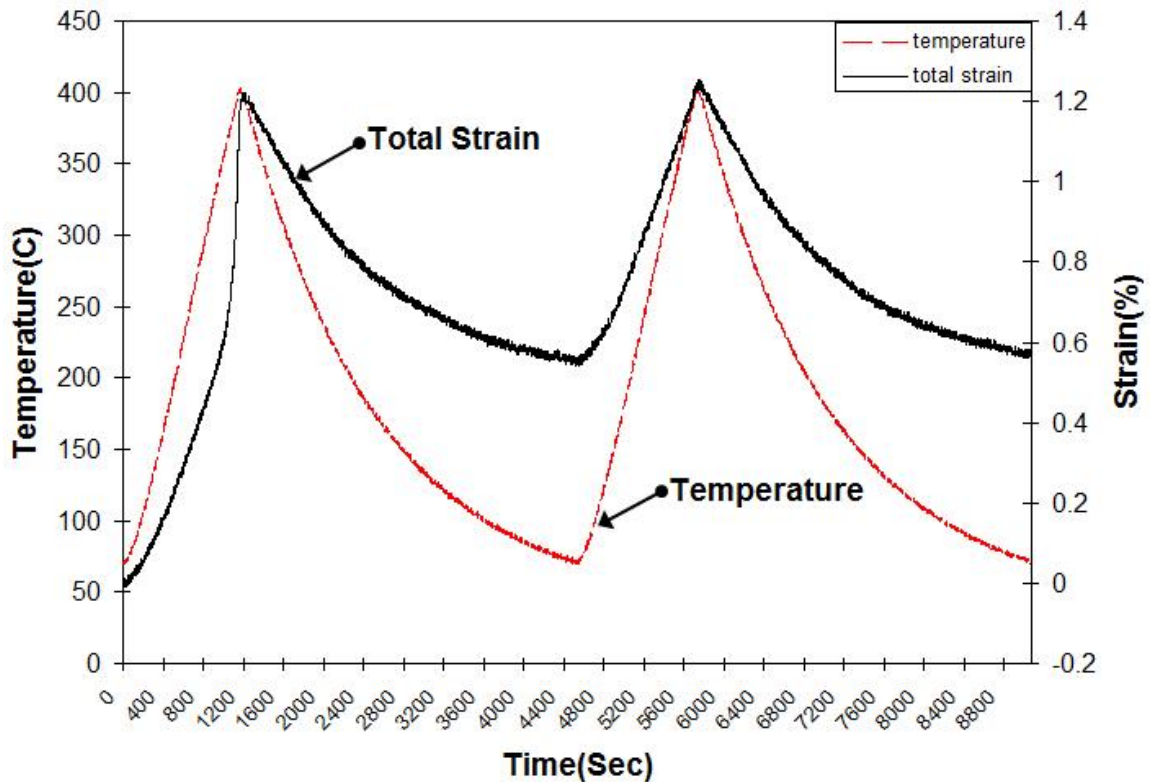
Figure 4.10 The total strain history of the in-phase thermal-mechanical loading test

From the stress-strain response of the in-phase thermal-mechanical loading test, Fig. 4.12, it is observed that the initial in-phase temperature-stress increase causes a remarkable plastic deformation (0 to A). Then the in-phase temperature-stress decrease results in an elastic unloading of the stress-strain curve (A to B). The material behaves like an elastic reloading by the subsequent in-phase temperature-stress increase. Again, the second in-phase temperature-

stress decrease results in an elastic unloading of the stress-strain state. Overall, this test result shows an elastic shakedown phenomenon, i.e. at the first increase of the thermal and mechanical load, significant plastic deformation is introduced. However, it becomes mainly an elastic stress-strain response in the thereafter cycling with the same temperature/stress range.
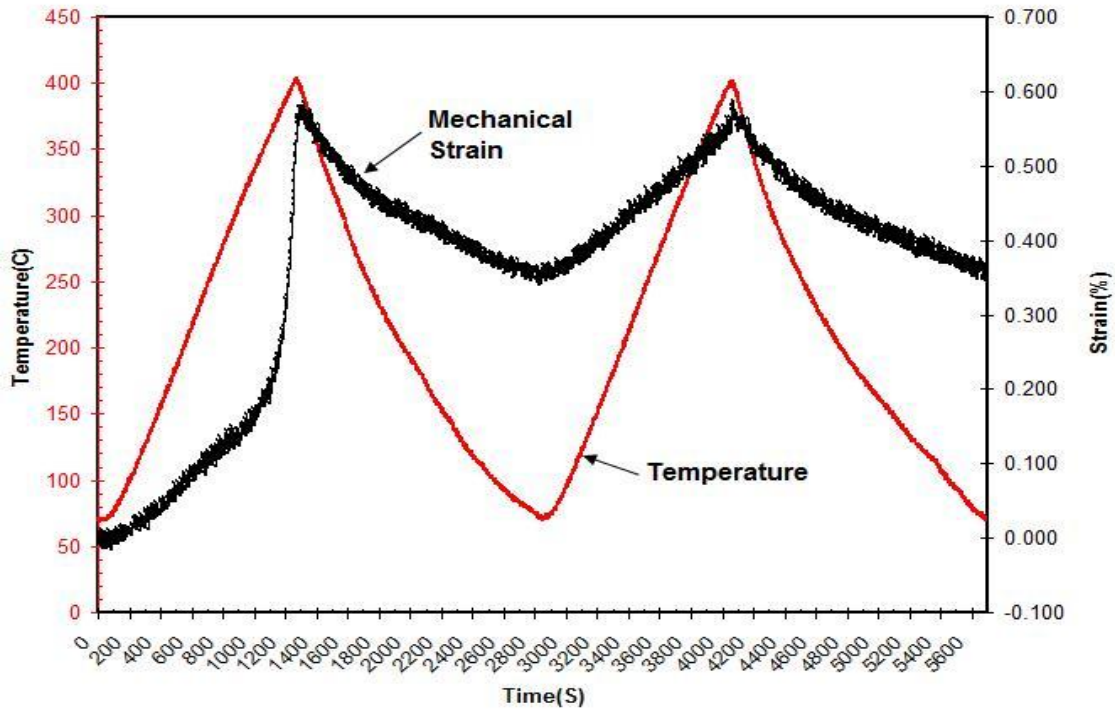
Figure 4.11 The mechanical strain history of the in-phase thermal-mechanical loading test
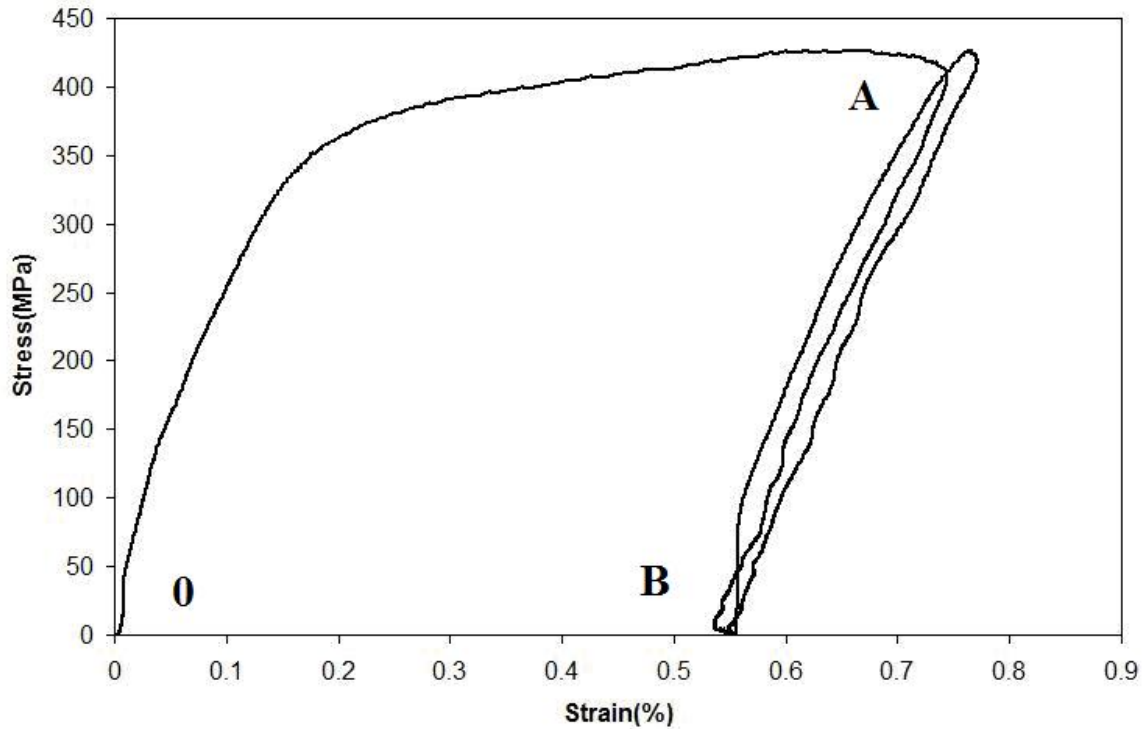
Figure 4.12 Stress-mechanical strain response of the in-phase thermal-mechanical loading test

3. Uniaxial out of phase thermal-mechanical loading

Figure 4.13 shows the total strain history of the test with the out-of-phase temperature and stress cycling. Figure 4.14 gives the mechanical strain history which is obtained by subtraction of the free thermal strain from the total strain. The maximum stress level applied is 425 Mpa which is in between proportional limit and yield strength at 70 ^{o}C (see Fig. 4.6). In the out-of-phase loadings test the material behaves like elastic deformations, and only the first out-of-phase shot of descending-temperature and rising-stress causes a little overshooting strain as seen in Fig. 4.14.
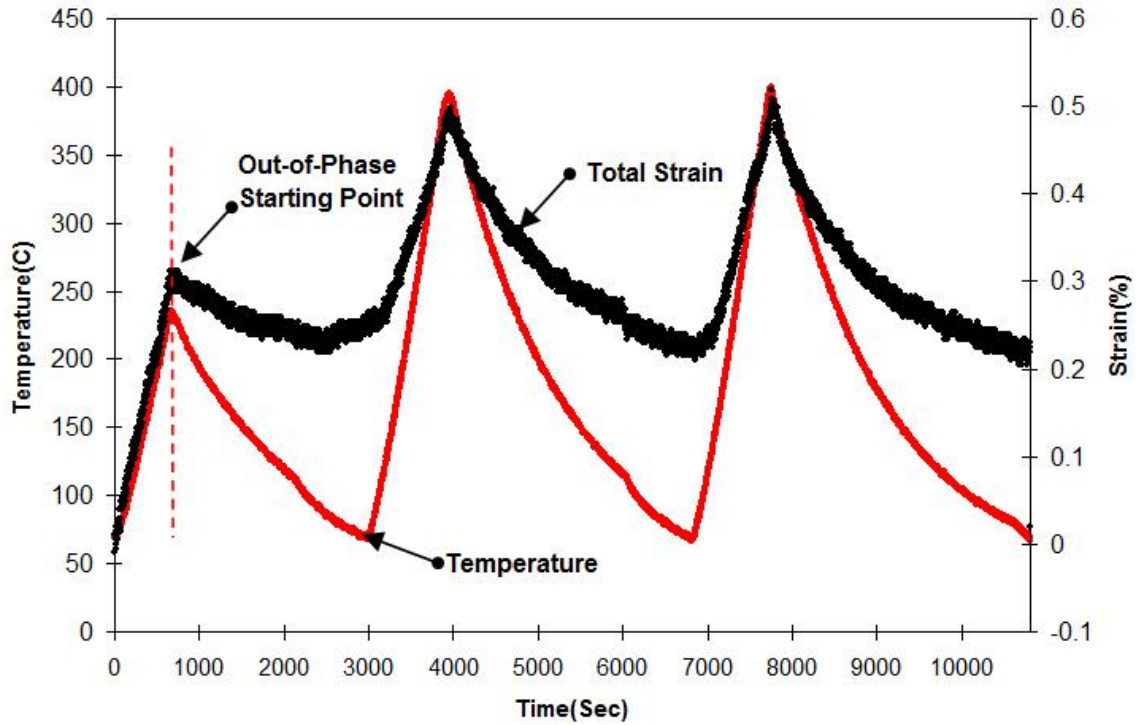
Figure 4.13 The total strain history of the in-phase thermal-mechanical loading test
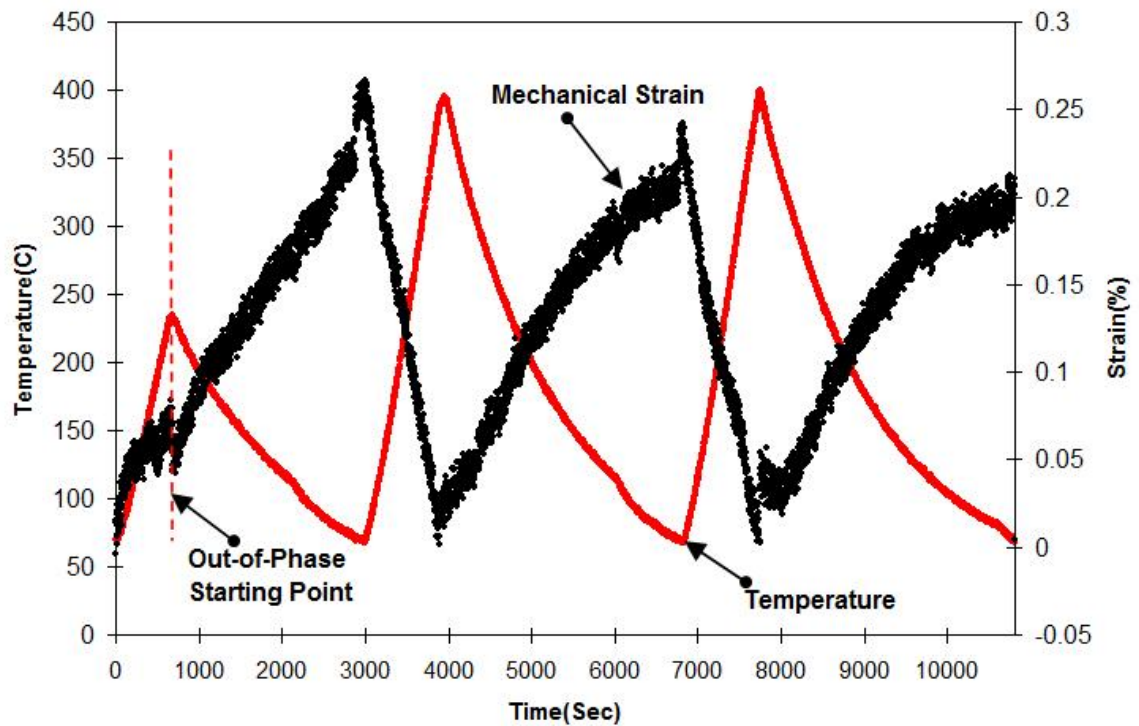
Figure 4.14 The mechanical strain history of the in-phase thermal-mechanical loading test

4. Strain-controlled fully reversed cyclic loading with constant internal pressure

Tests of strain-controlled cycling of ±0.4% axial strain with constant internal pressure 7.446 Mpa on thin-walled tubular specimens were carried out at ambient temperature and 427°C, respectively. The internal pressure generates a constant hoop stress of 70 Mpa. The results of axial stress versus diametral mechanical strain at ambient temperature and 427°C tests are shown in Fig. 4.15 and 4.16, correspondingly. Diametral ratcheting (bulging) are observed at both ambient temperature and 427°C tests. At ambient temperature, the accumulated diametral mechanical strain of 100 cycles is 0.5% while under same loading condition at 427°C the accumulated diametral mechanical strain of 100 cycles is 1.5%. It shows that higher temperature accelerates ratcheting (bulging) in diametral direction.
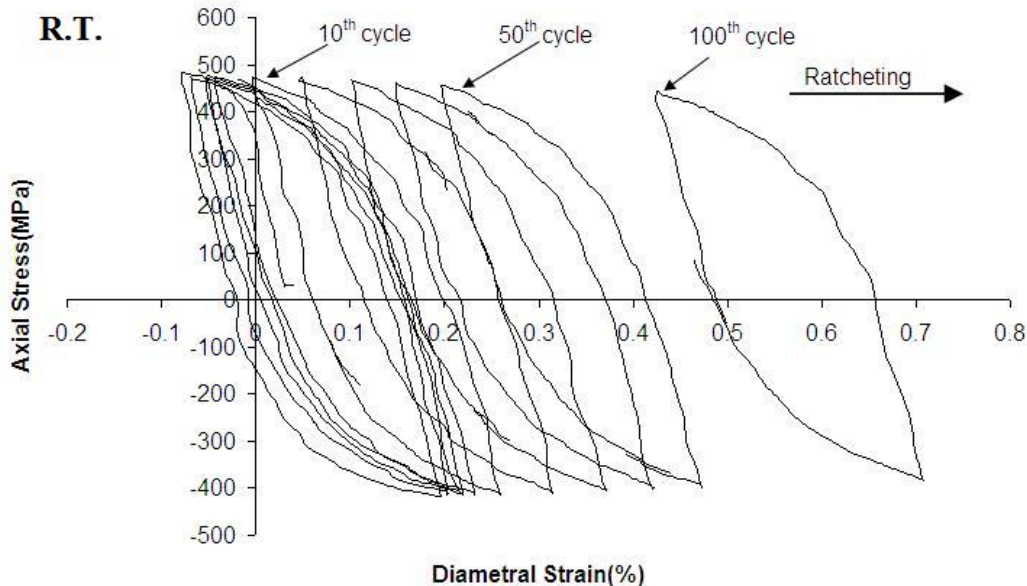
Figure 4.15 Axial stress-diametral strain response of ambient temperature strain-controlled cyclic loading with constant internal pressure test
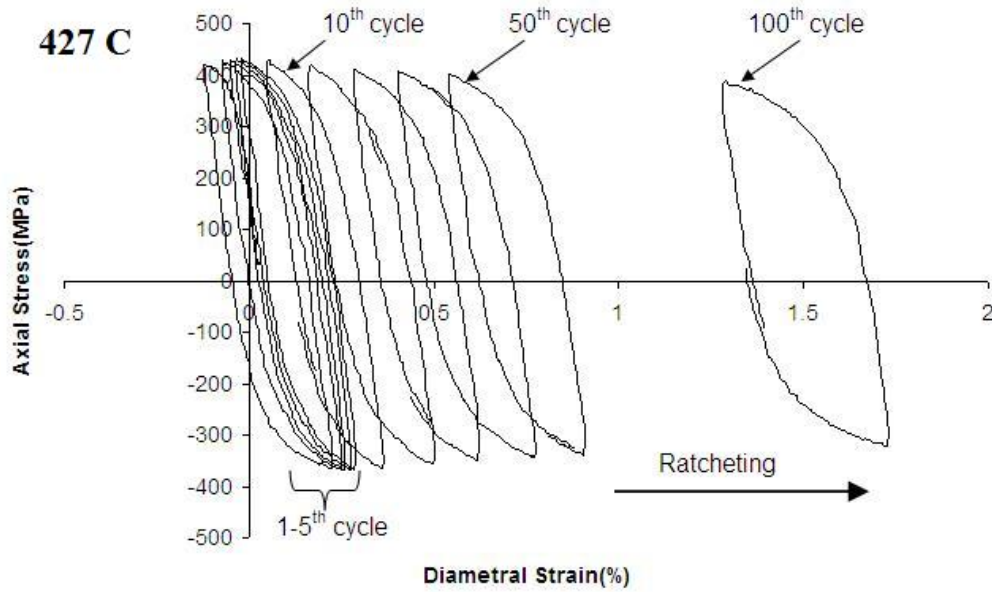
Figure 4.16 Axial stress-diametral strain response of 427 ^{o}C strain-controlled cyclic loading with constant internal pressure test

5. Stress-controlled fully reversed axial cyclic loading with constant internal pressure

Tests of stress-controlled axial stress cycling of ±385Mpa with constant internal pressure 7.446 Mpa (constant hoop stress of 70Mpa) on thin-walled tubular specimens were conducted at ambient temperature and 427°C, respectively. From the experimental results at ambient temperature (Fig. 4.17 and 4.18) and 427°C (Fig. 4.19 and 4.20), it is obviously seen that ratcheting phenomena are observed in both diametral and axial directions. At ambient temperature, the accumulated diametral mechanical strain of 100 cycles is approximate 0.06% while under same loading at 427°C the specimen collapsed at 70th cycle. Figure 4.21 shows that a circumferential shell bulging occurred at the test section of the tubular specimen.

It is noticed that the temperature increase has larger impact on accelerating ratcheting in negative axial and positive diametral directions under stress-controlled condition than in strain-controlled one. In addition, under isothermal condition, stress-controlled biaxial loading is more detrimental than strain-controlled loading due to the accumulation of ratcheting strains in negative axial and positive hoop direction simultaneously.
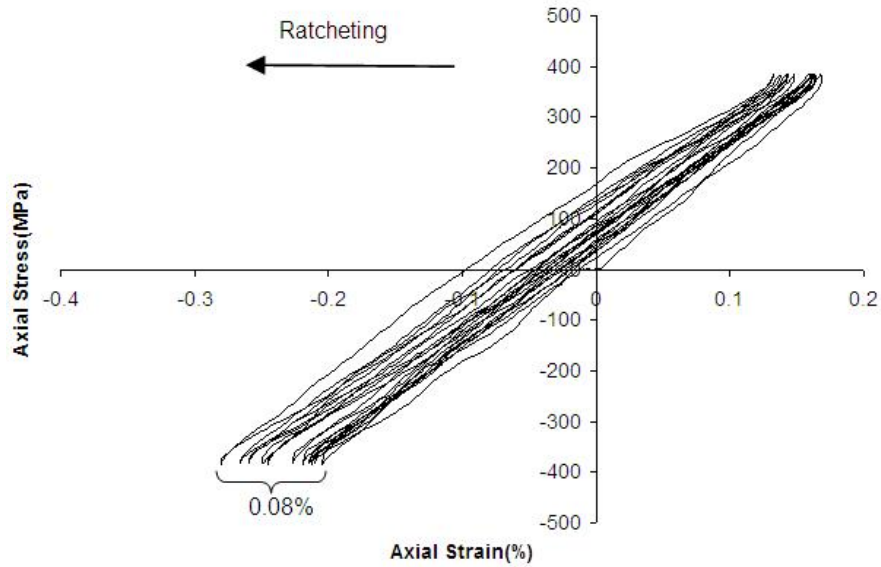
Figure 4.17 Axial stress-axial strain response of ambient temperature stress-controlled cyclic loading with constant internal pressure test
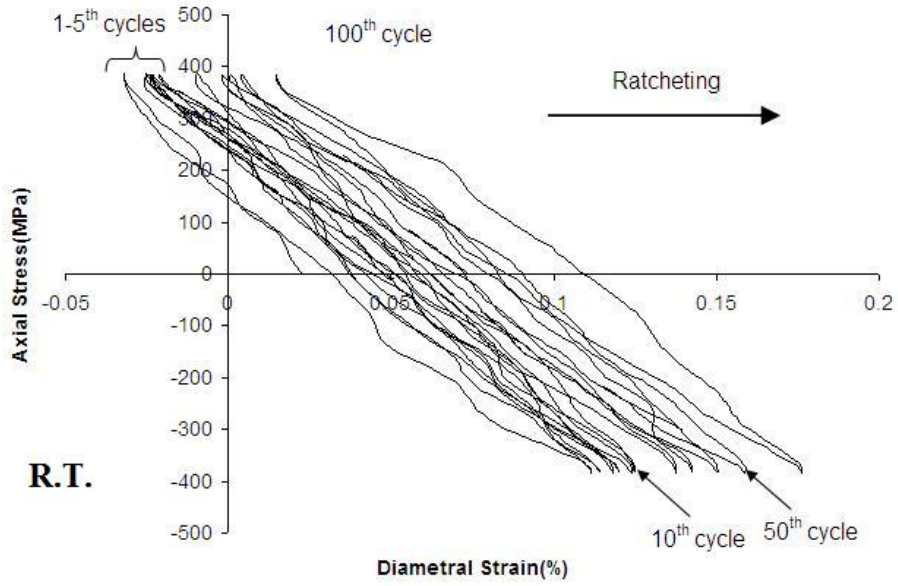
Figure 4.18 Axial stress-diametral strain response of ambient temperature stress-controlled cyclic loading with constant internal pressure test
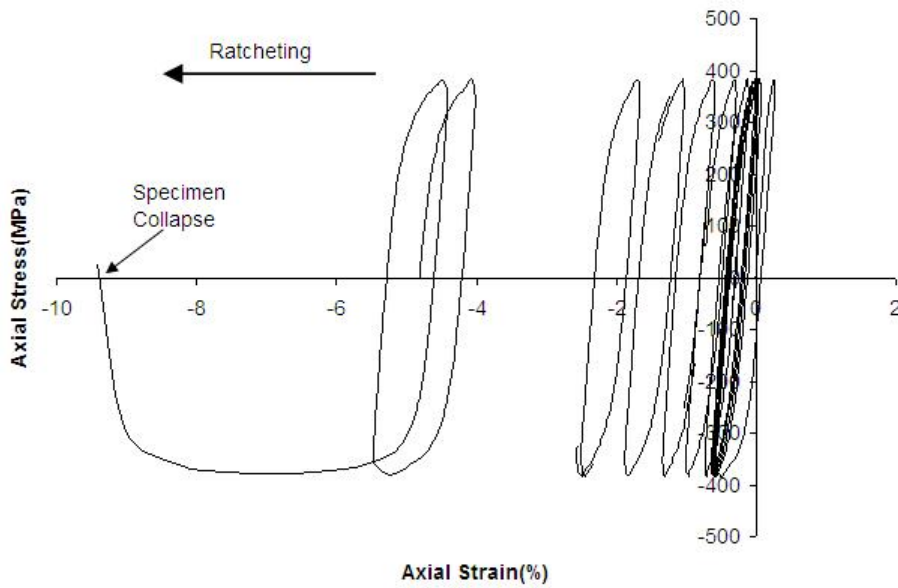
Figure 4.19 Axial stress-axial strain response of 427°C stress-controlled cyclic loading with constant internal pressure test
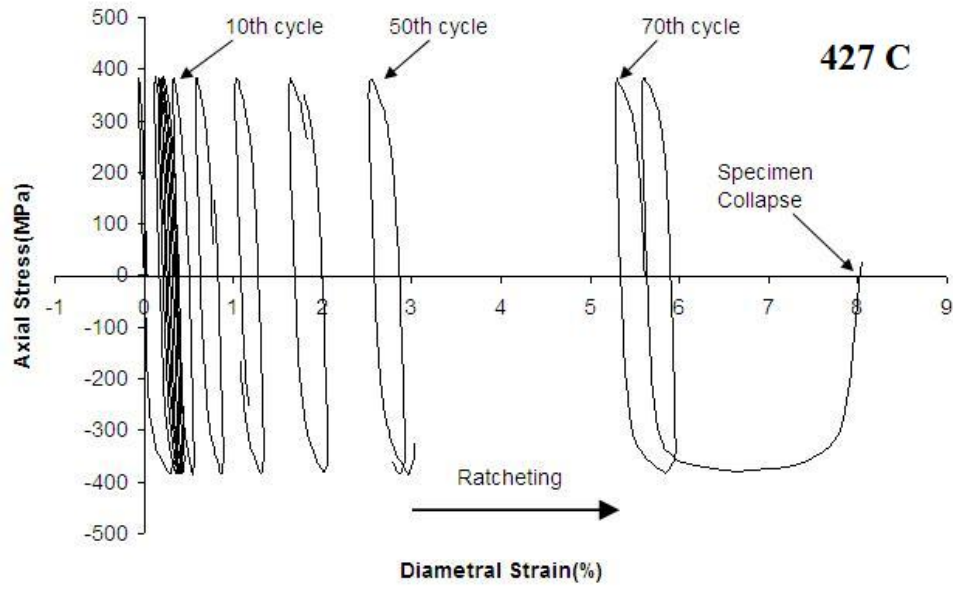
Figure 4.20 Axial stress-diametral strain response of 427°C stress-controlled cyclic loading with constant internal pressure test

Figure 4.21 Picture of collapsed tubular specimen

6. In-phase thermal-mechanical fully-reversed cyclic loading with constant

internal pressure

With 7.446 Mpa constant internal pressure (70Mpa hoop stress) applied on the thin-walled tubular specimens, two biaxial in-phase loadings of axial strain cycling of ±0.4% and axial stress cycling of ±400 Mpa while temperature cycling between 70°C and 400°C were successfully tested. Figure 4.22 and 4.23 show the result of accumulated diametral mechanical strain versus number of cycles in strain-controlled and stress-controlled bi-axial thermal-mechanical loading tests, respectively. The diametral thermal strain is subtracted from the diametral total strain. It is observed from the Fig. 4.22 that 0.05% diametral mechanical strain is accumulated during the four biaxial in-phase loading cycles. The diametral mechanical strain is steadily accumulated during each loading cycle under strain-controlled biaxial in-phase loading condition. Additionally, from the result of stress-controlled test, it is shown that the accumulated diametral mechanical strain of first loading cycle is 0.03% and of 7 cycles is 0.05%. The amount of accumulated diametral mechanical strain of each cycle is gradually decreased under stress-controlled loading condition. Overall, under in-phase biaxial thermal-mechanical cyclic loading condition, noticeable ratcheting strains are observed in spite of small number of cycles. (4-7 cycles, it was difficult to run more cycles due to long cycle time required.)
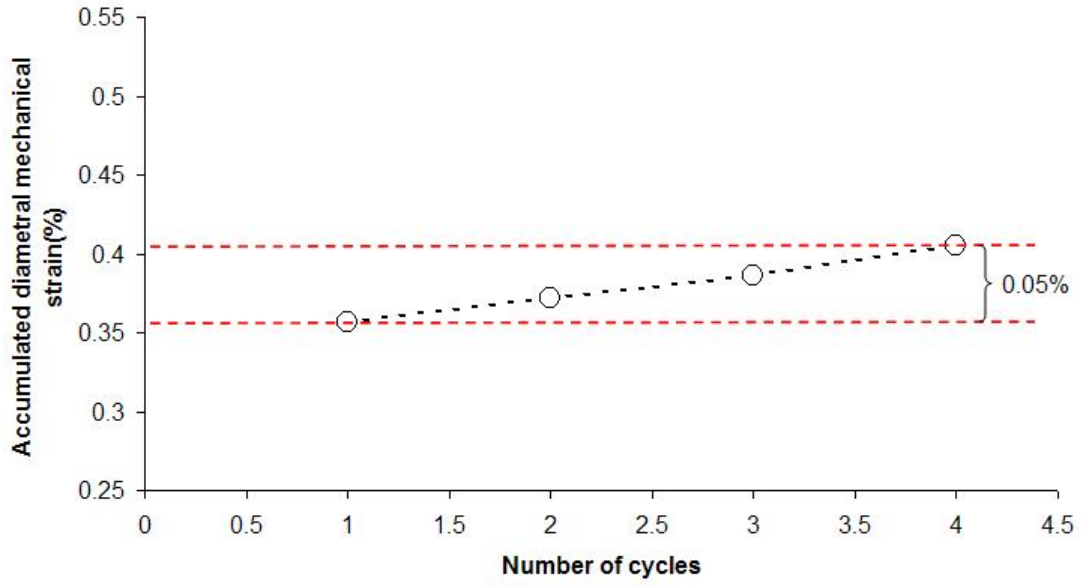
Figure 4.22 Diametral strain vs. number of cycles in strain-controlled biaxial in-phase thermal-mechanical loading test
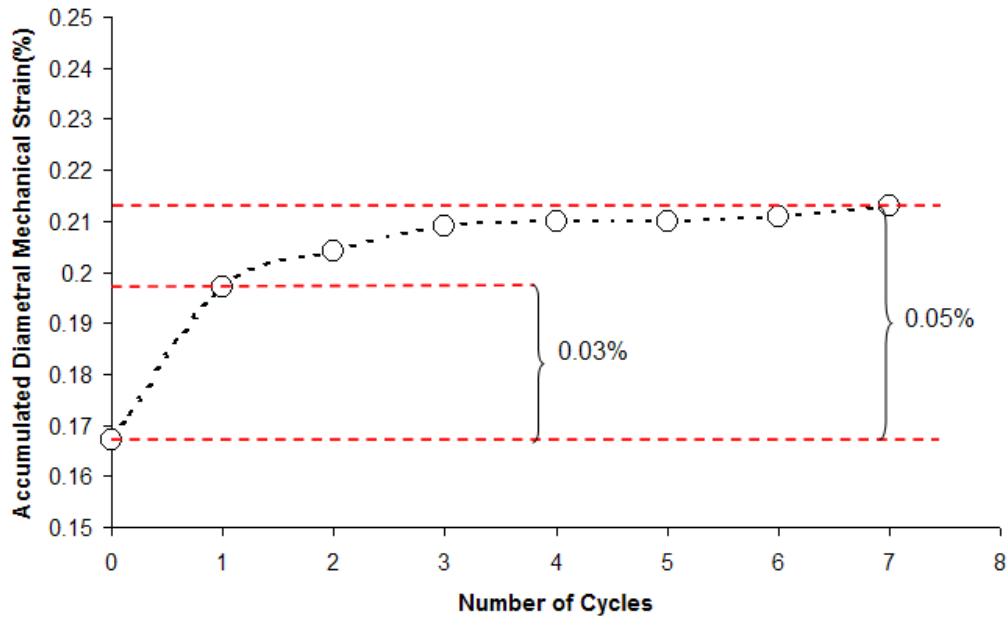
Figure 4.23 Diametral strain vs. number of cycles in stress-controlled biaxial in-phase thermal-mechanical loading test

4.5 Experimental Verification of Model Predictions

As mentioned before, one of the objectives of the current research is to provide reliable benchmark experimental data for verification of theoretical constitutive models. In the followings the predictions by the multilinear kinematic hardening model in ANSYS and by the newly-developed temperature-dependent elastoplastic constitutive model in our lab are compared to the experimental results for the three types of uniaxial thermal-mechanical loading tests.

4.5.1 Constant Stress with Cyclic Thermal Loading

The test and model prediction are carried out based on base metal of coke drum (SA387-22) under constant stress with cyclic thermal loading condition (as introduced in section 4.3, Case 1). Figure 4.24 shows the experimental and model predicted results under the same loading condition. The solid line is the experimental result, and the dash dot and dot lines are predicted by the new temperature dependent constitutive model and the multilinear kinematic model in ANSYS (commercial FEM analysis software). By comparing the results, it is found that the prediction of the new developed model is much more accurate than the multi-linear kinematic model under uniaxial constant stress with cyclic thermal loading condition.
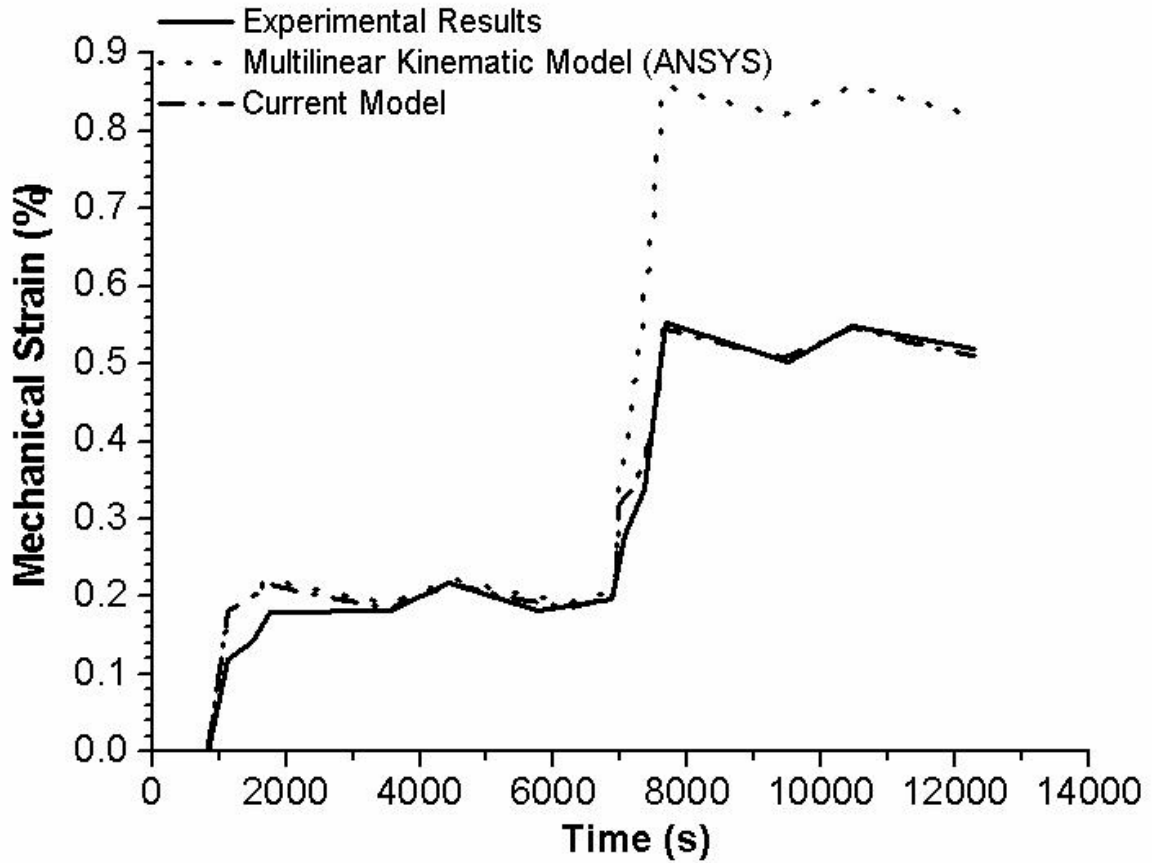
Figure 4.24 Comparison between experimental result and model predictions under constant stress with cyclic thermal loading [37]

4.5.2 In-Phase Thermal-Mechanical Cyclic Loading

The second comparison between test result and model predictions are based on uniaxial in-phase thermal-mechanical cyclic loading condition (as introduced in section 4.3, Case 2). By comparing the results of the experiment and model predictions in Fig. 4.25, it is obviously shown that the prediction of the new model is much more precise than multilinear kinematic model under unaxial in-phase thermal-mechanical loading condition as well.
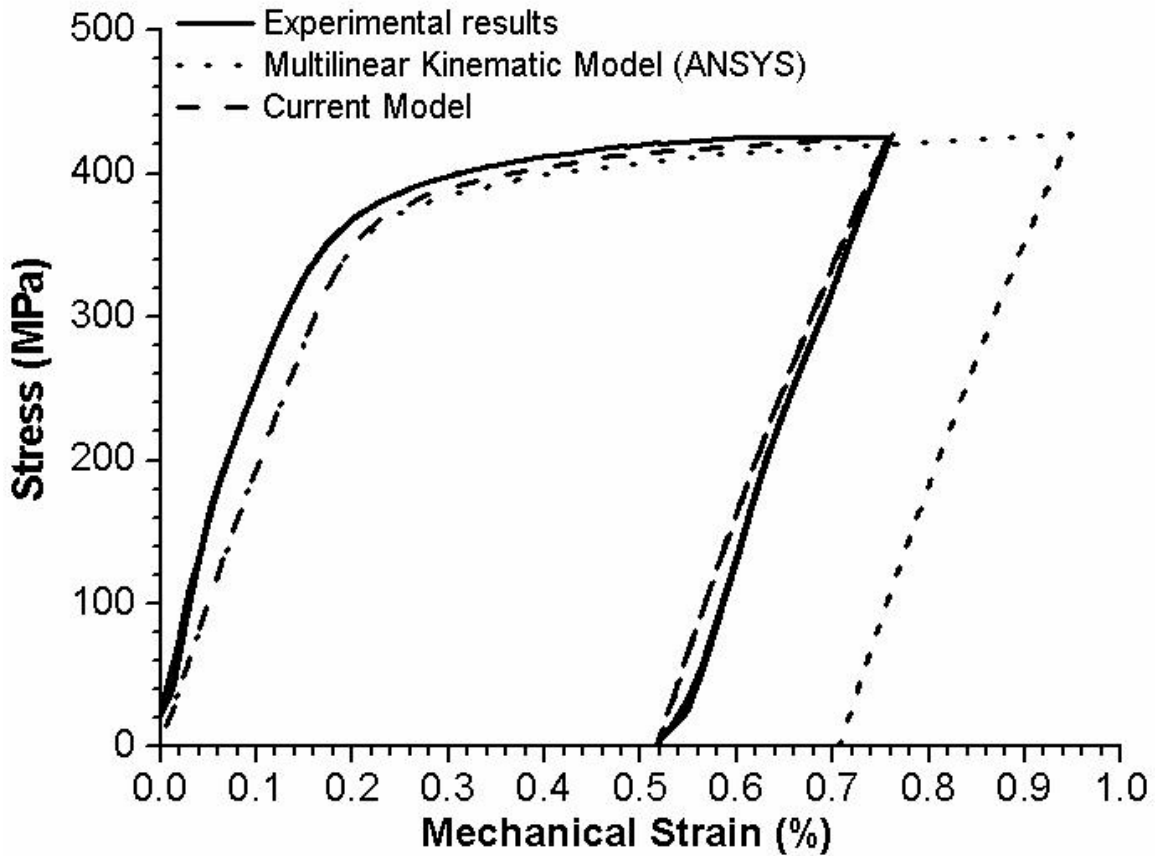
Figure 4.25 Comparison between experimental result and model predictions under in-phase thermal-mechanical loading [37]

4.5.3 Out-of-Phase Thermal-Mechanical Cyclic Loading

The third experimental verification is based on uniaxial out-of-phase thermal-mechanical cyclic loading condition (as introduced in section 4.3, Case 3). By comparing the results of the experiment and model predictions in Fig. 4.26, it is shown that both predictions of the new and the multilinear-kinematic models are close to the experimental result in out-of-phase thermal-mechanical loading condition.
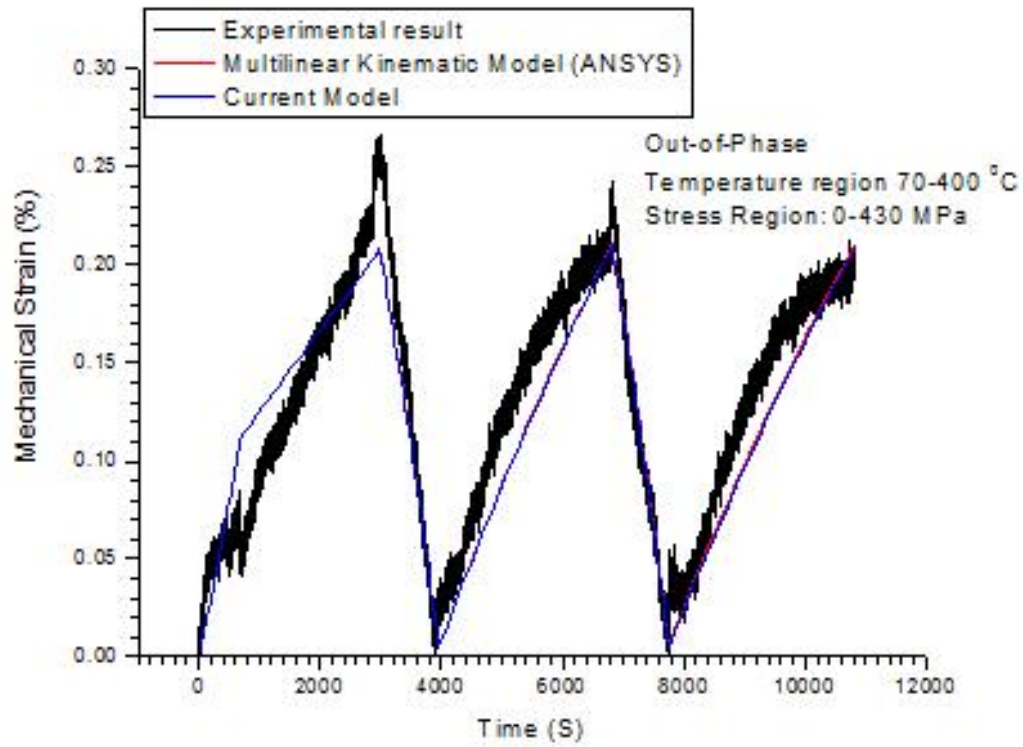
Figure 4.26 Comparison between experimental result and model prediction under out-of-phase thermal-mechanical loading [37]

4.6 Summary

Material deformation behaviors of SA387-22 under uniaxial and biaxial complex thermal-mechanical loading conditions were experimentally investigated. Under uniaxial constant stress with cyclic thermal loading, the first shot of temperature increase will cause a noticeable plastic deformation, and the rest of thermal cycling will result in elastic deformation. Under uniaxial in-phase thermal-mechanical loading condition, the initial in-phase temperature-load increase will cause a significant plastic deformation, and the subsequent in-phase thermal-mechanical cycling will result in an elastic unloading-reloading behavior. In addition, under uniaxial out-of-phase thermal-mechanical loading case, the out-of-phase thermal-mechanical cycling will not cause noticeable plastic deformation but only elastic one. From the biaxial thermal-mechanical loading tests, it is shown that the diametral mechanical strain can be accumulated under either axial strain or axial stress-controlled cycling. This experimental observation is in good agreement with the one experimentally investigated on 304 stainless steel by Z. Xia and F. Ellyin [39]. Under isothermal condition, stress-controlled biaxial loading is more detrimental than strain-controlled loading. Under same loading condition, the ratcheting strain is accumulated more at higher temperature. In addition, under biaxial in-phase loading tests, the small number of in-phase thermal-mechanical cycling will yield noticeable ratcheting strain. Finally, by experimental verification of the new developed temperature dependent constitutive model (developed by Dr. Y. Jiang.) for the three uniaxial loading cases, one can see that the predictions of the newly developed model has better

agreement with the experimental results than the one currently available in ANSYS code.

Chapter 5 Conclusions

5.1 Summary

In order to better understand the failure mechanisms of coke drum, experimental study of elastoplastic mechanical properties of typical coke drum materials has been carried out. A biaxial thermal-mechanical material testing system is developed. The newly-developed material testing system mainly consists of the modified MTS testing system, a furnace, a water cooled gripping system, a set of extensometers, and a data acquisition and control system. A servo-controlled electro-hydraulic closed-loop system, a modified MTS system, is used as the base system. The furnace with controller has the capability of adjusting the temperature inside the furnace to any desired value between ambient temperature and 500°C. The designed water-cooled gripping system can adopt different geometries of specimens. The water cooled fixtures are mounted in between the load cell and the grip to eliminate the thermal effect to the measurement and response of the load cell. The designed axial and diametral extensometers with extension quartz rods are capable of measuring strains in axial and diametral directions at elevated temperatures. Strain-controlled, stress-controlled, temperature-strain controlled, or temperature-stress controlled tests can be achieved by MTS and house-built control systems. Commercial software, LabView SignalExpress, is used as a tool for test data acquisition through out all tests.

The basic mechanical properties of SA387-11 (base material) and alloy SA 240 type 410S (cladding material) are determined from the experimental results of both monotonic and stepped fully-reversed cyclic tests. Firstly, both yield strength and Young's modulus at ambient and elevated temperatures are satisfied with specified values. As the temperature changes from $25\,^{\circ}\text{C}$ to $427\,^{\circ}\text{C}$, both the yield strength and Young's modulus of the base and cladding materials approximately decrease from 10% to 30%, respectively. Additionally, comparisons of mechanical properties and stress-strain curves of the coke drum materials are presented to characterize the cyclic mechanical behaviours of the coke drum materials. It is found that the base and cladding material at ambient temperature and the cladding at elevated temperature have mixed cyclic behaviours (initially cyclic softening, then cyclic hardening or vice versa). The base material at elevated temperature has distinguished cyclic hardening behaviour. The different rates of straining of the coke drum materials in monotonic tensile tests are compared to identify the strain-rate dependence of the coke drum materials. It is found that, at room temperature, the base and cladding materials of the coke drum is strain-rate insensitive, and the base material of the coke drum is also strain-rate insensitive at $427\,^{\circ}\text{C}$. The creep tests of base material were tested at two constant temperatures $427\,^{\circ}\text{C}$ and $500\,^{\circ}\text{C}$. From the experimental results, it is shown that SA387-22 (base material) has a negligible creep at a stress level up to 385 Mpa and at a temperature up to 427°C. However, at a higher temperature of $500\,^{\circ}\text{C}$, the creep is obvious at the stress level of 385 Mpa.

In addition, complex thermal-mechanical cyclic loading tests were performed to understand the material deformation behaviour under thermal-mechanical loading conditions. Firstly, the uniaxial constant stress with thermal cyclic loading test was conducted. The first wave of temperature increasing causes a noticeable plastic deformation and the rest of the thermal cycling results in elastic responses. Secondly, uniaxial in-phase thermal-mechanical loading test is performed. The temperature is increased from 70 ^{o}C to 400 ^{o}C and decreased from 400 ^{o}C to 70 ^{o}C, while the stress is controlled by temperature with a cycling of 0-425-0 Mpa. From the experimental results, it is observed that the initial in-phase temperature-stress increasing causes a significant plastic deformation, and the rest of the in-phase thermal-mechanical cycling results in elastic unloading-reloading behaviors. Uniaxial out-of-phase thermal-mechanical loading test was carried out. The amplitude of temperature-controlled stress is decreasing from 0 to 425 Mpa as the temperature increases from 70 to 400 ^{o}C, and vice versa. The experimental result shows that the out-of-phase thermal-mechanical loading yields consistent elastic loading-unloading cycles, and it does not cause noticeable plastic deformation. From the biaxial thermal-mechanical loading tests, it is shown that the diametral mechanical strain can be accumulated under either axial strain or axial stress-controlled cycling with constant internal pressure. Under isothermal condition, stress-controlled biaxial loading is more detrimental than strain-controlled loading since the ratcheting strains are accumulated in both negative axial and positive diametral directions. The ratcheting strain is accumulated more at higher temperatures. In addition, under biaxial in-phase

loading tests, the small number of in-phase thermal-mechanical cycling can yield noticeable ratcheting strain.

A temperature-dependent elastoplastic constitutive model is developed. Comparisons between experimental results and the constitutive models are performed. It is found that the prediction of the new developed model is more accurate than the multilinear kinematic model in ANSYS code.

There are several factors that may affect the accuracy of the test results. The shortage of the consistent specimens and repeated tests may affect the consistency of the test results. Instrumental factors that can affect the test results include: the stiffness, the natural frequency, and the mass of moving parts of the tensile test machine, the accuracy of the load cell, the specimen installation, the calibration of extensometers, the heat effect to the strain gage of the extensometers and so on. Material factors that may affect the test results include: inhomogeneity of the test material and defect in the material. In addition, measurement error and data post-processing also may affect the accuracy of the test result.

5.2 Future Work

This thesis work mainly focuses on development of new biaxial thermal-mechanical material testing system, experimental characterization of mechanical properties of coke drum materials at ambient and elevated temperatures, and experimental study of coke drum material behaviour under complex thermal-mechanical loading conditions. The monotonic test, cyclic test, and uniaxial complex thermal-mechanical loading tests are categorized into uniaxial tests. Coke drums are pressure vessels which are subjected simultaneously to an internal pressure and a cyclic axial loading, and they may develop a fair amount of ratcheting deformation. In order to deeply study the material behaviour under thermal/mechanical cyclic loading conditions with internal pressure, more multiaxial ratcheting tests should be considered to simulate practical loading conditions of coke drum structures. Furthermore, the reliability of the developed constitutive model could be verified from more experimental results. In addition, the creep test for the cladding material has not been carried out. More creep tests are necessarily for both base and cladding materials in order to determine what are the temperature ranges and the stress levels that the coke drum will not experience obvious creep deformation in the operation.

Bibliography

[1] J.A. Penso, etc., "Understanding Failure Mechanisms to Improve Reliability of Coke   Drums", PVP-Vol.395, Operations, Applications, and Components, ASME 1999

[2] Weil N.A. and Rapasky F.S., "Experience with vessels of Delayed – Coking Units", API 23rd Midyear Meeting, 1958

[3] C.J. Pieper, L.R. Shockley and C.W. Stewart, "Coke Drum Design-Longer Life through Innovation", AIChE 2000 Spring National Meeting, Atlanta, GA, March 5-9, 2000

[4] Richard Boswell, "Coke Drum Bulges", Stress Engineering Services, May, 2001

[5] Boswell R.S., Ferraro T., "Remaining Life Evaluation of Coke Drums", Plant Engineering, Design and Responsibility Symposium, Energy Engineering Conference, 1997

[6] API Proceedings "1996 APE Coke Drum Survey-Final Report", 1996 American Petroleum Institute, Washington, DC

[7] D.K. Rutt, R.D. Clark, "Stress Analysis Using Actual Coke Drum Bulge Profiles a Case Study", AIChE 2000 Spring National Meeting, Atlanta, GA, March 5-9, 2000

[8] C. Allevato, R.S. Boswell, "Assessing the Structural Integrity and Remaining Life of Coke Drums with Acoustic Emission Testing, Strain Gaging, and Finite Element Analysis", 1999 Engineering Sources Technology Conference & Exhibition, Houston, Texas

[9] ASME Section II parts A & C, plus Plate and Electrode Manufacturers Brochures and CB&I data

[10] A. Ramos, C. Rios and J. Vargas, "Mechanical Integrity Evaluation of Delayed Coke Drums", PVP-Vol.359, Fitness for Adverse Environments in Petroleum and Power Equipment, ASME 1997

[11] A. Ramos, C. Rios, etc., "Delayed Coke Drum Assessment Using Field Measurements and FEM", PVP-Vol.368, Analysis and Design of Composite, Process, and Power Piping and Vessels, ASME 1999

[12] A. J. Ramos, C. Rios and J.A.R. Vargas. "Fatigue Life Prediction of Delayed Coke Drums", Vision Techenologica, Vol.6, 1999: 93-100

[13] J. Chen, B. Young, "Stress-Strain Curves for Stainless Steel at Elevated Temperatures", Engineering Structures, Vol.28, 2006: 229-239

[14] Z. Xia, F. Ellyin, "Nonproportional Multiaxial Cyclic Loading: Experiments and Constitute Modeling", Journal of Applied Mechanics, Vol.113, 1991
[15] F. Ellyin, K. Golos and Z. Xia, "In-Phase and Out-of-Phase Multiaxial Fatigue", Journal of Engineering Materials and Technology, Vol.113, 1991

[16] Z. Xia, F. Ellyin, "A Constitutive Model with Capability To Simulate Complex Multiaxial Ratcheting Behaviour of Materials", International Journal of Plasticity, Vol.13, No. ½, 1997:127-142

[17] F. Ellyin, K.W. Neale, "Effect of Cyclic Loading on the Yield Surface", Journal of Pressure Vessel Technology, Vol. 101, 1979

[18] F. Ellyin, Z. Xia and K. Sasaki, "Effect of Rate and Rate History on Plastic Deformation: Experiments and Constitutive Modelling", International Journal of Plasticity, Vol.9, 1993:951-959

[19] Y. Ohashi, M. Kawai and T. Kaito, "Inelastic Behavior of Type 316 Stainless Steel Under Multiaxial Nonproportional Cyclic Stressings at Elevated Temperature", Journal of Engineering Materials and Technology, Vol.107, 1985

[20] X. Chen, R. Jiao, "Modified Kinematic Hardening Rule for Multiaxial Ratcheting Prediction", International Journal of Plasticity Vol.20, 2004:871-898

[21] Ben R. Gossick, "Design of Extensometer for Creep Studies", The Review of Scientific Instruments, Volume 25, Number 9, 1954

[22] ASTM, "Standard Practice for Verification and Classification of Extensometer Systems", E 83-06, 2006

[23] National Instruments Corporation, "NI LabVIEW SignalExpress ", August 2007

[24] ASME, "Section II Part A Ferrous Material Specifications", ASME Boiler and Pressure Vessel Code for 2007, New York, NY

[25] ASTM, "Specification for Pressure Vessel Plates, Alloy Steel, Chromium-molybdenum", SA-387/SA-387M, section II, 2004

[26] ASTM, "Standard Specification for Chromium and Chromium-Nickel Stainless Steel Plate, Sheet, and Strip for Pressure Vessels and for General Applications", A 240/A 240M-09a, 2009

[27] The A to Z of Materials website,
http://www.azom.com/details.asp?ArticleID=4835

[28] Masteel website,
http://www.masteel.co.uk/a387-grade-22-class-2.htm

[29] M.K. Booker, "Analytical Representation of Mechanical Properties Data for 2 ¼ Mo Steel", Nuclear Systems Materials Handbook, 1977

[30] ASME, "Section II Part D Properties", ASME Boiler and Pressure Vessel Code for 2001, New York, NY

[31] ASTM, "Standard Test Methods for Tension Testing of Metallic Materials", E 8/E 8M-08, 2008

[32] ASTM, "Standard Test Method for Young's Modulus, Tangent Modulus, and Chord Modulus", E 111-04, 2004

[33] ASTM. "Standard Test Methods for Elevated Temperature Tension Tests of Metallic Materials", E 21-09, 2009

[34] H.E. Boyer, "Atlas of Stress-Strain Curves", ASM International, Metals Park Ohio, 1987

[35] W.F. Hosford, "Mechanical Behavior of Materials", Cambridge University Press, 2005

[36] ASTM, "Standard Terminology Relating to Methods of Mechanical Testing", E 6-08a, 2008

[37] Y.J. Jiang, Z. Xia and J. Chen, "Consitutive Modeling for Temperature-Dependent Elasto Plastic Materials Under Cyclic Thermal-Mechanical Loading", To be submitted to International Journal of Plasticity

[38] ASTM, "Standard Practice for Strain-Controlled Axial-Torsional Fatigue Testing with Thin walled Tubular Specimens", E 2207-08, 2008

[39] Z. Xia, F. Ellyin, "Biaxial Ratcheting under Strain or Stress-Controlled Axial Cycling with Constant Hoop Stress", ASME J. Appl. Mech., Vol.61, 1994:422-428

Appendix A Cantilever Beam Design

Please refer Fig 2.3 and 2.4 for schematics of the cantilever beam

Calculation by Spreadsheet

Assume max 15% strain along 0.0508 m gauge length, which leads to 0.00381 m deflection on one end of extensometer
Aluminum alloy 6061-T6 at room temperature, young's modulus (E) = 70Gpa
L_1 – length of solid rod (0.127 m)
L_2 – length of bending beam
h – thickness of bending beam
b – width of bending beam
I – moments of inertia of bending beam
F – force applied on the tip of solid rod
m – total deflection of extensometer
e – strain on point C

the strain at point C is maximum, therefore, the measured strain of strain gage which is mounted little far from point C (reasonable) should be less than max strain and strain at point C is 0.0015 should be used (recommended by Mr. Bernie).

Example of Iteration by Spreadsheet

Criteria							· 0.00381	· 0.0015 ·
Variable	L_1 (m)	L_2 (m)	h (m)	b (m)	I (m^4)	F (N)	m (m)	e
	0.127	0.019	0.0012	0.009525	1.37E-12	0.767219	0.003777	0.0007
	0.1	0.019	0.0011	0.009525	1.06E-12	0.790949	0.003706	0.0007
√	0.127	0.02	0.0009	0.009525	5.79E-13	0.306161	0.00383	0.0005
	0.1	0.02	0.0008	0.009525	4.06E-13	0.296333	0.003889	0.0005

The selected dimension of the cantilever beam gives fairly less vertical force and

aimed total deflection (m=0.00381) of the extensometer arm.

All dimensions are in inch;
Material: Aluminum (alloy 6061-T6);
Quantity: 4;

SCALE 2.000

.59
2.10
.59
.0354
R.065

Ø.089
.29
.10
.15
.375
.79
R.065
2-56
.15
.08
TOP_4
.50
TOP_4
.29
.1575
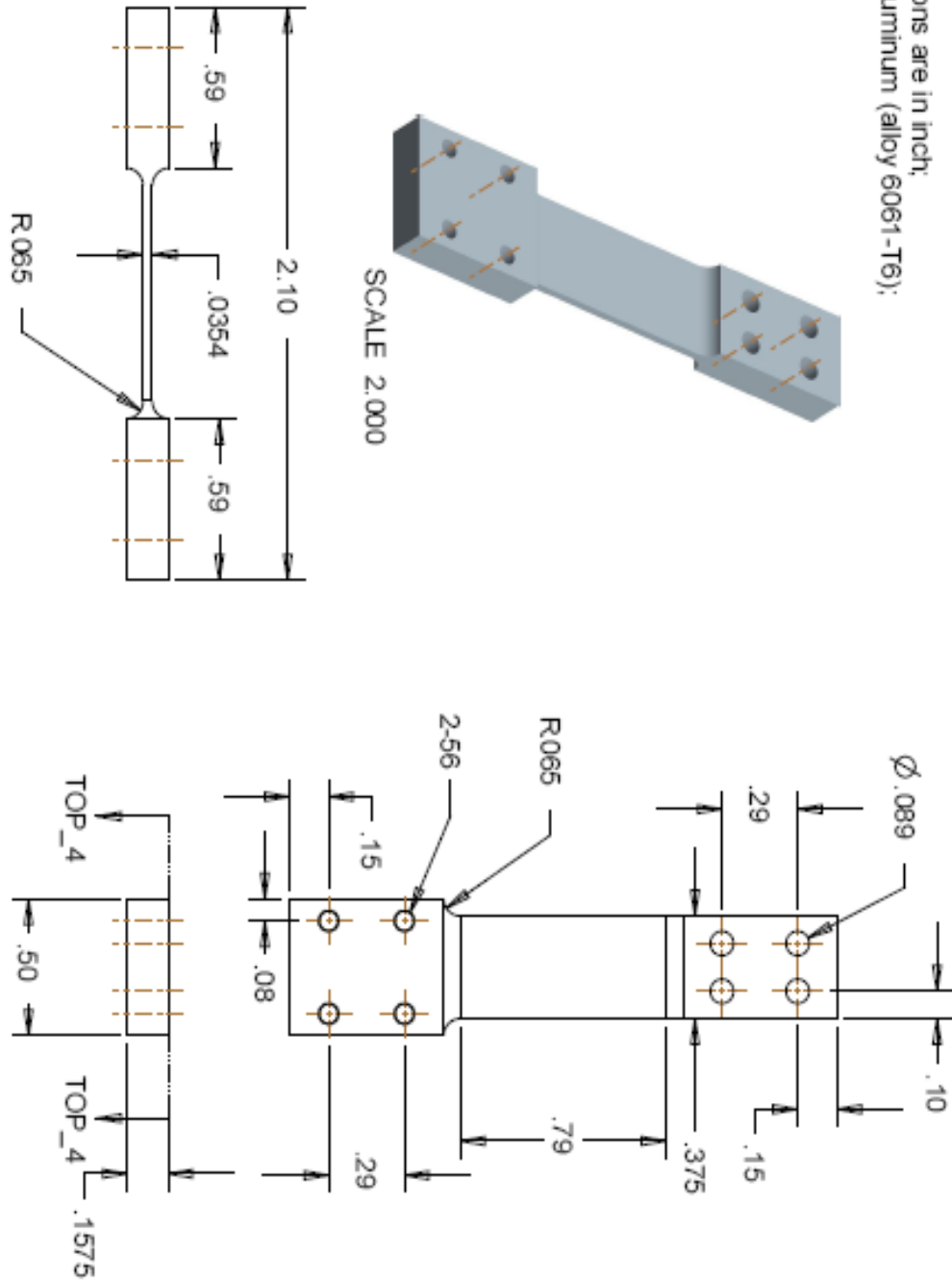
Figure A.1 Engineering drawing of the designed cantilever beam

Appendix B Buckling Consideration of Solid Specimens

Buckling Calculation of circular cross-section specimen

Formulas:

$$P_{Cr} = \frac{\pi^2 EI}{L_e^2}$$

$$\sigma_{Cr} = \frac{\pi^2 E}{(L_e / r)^2}$$

For two fixed end: $L_e = L/2$, $I = \frac{1}{4}\pi r^4$

Therefore, the equations become:

$$P_{Cr} = \frac{\pi^3 E r^4}{L^2}$$

$$\sigma_{Cr} = \frac{4\pi^2 E}{(L / r)^2}$$

For Steel, E=200 Gpa (Modulus of elasticity)

Dimension of solid cylindrical specimen(Figure 3.1):

r=0.00635 m, gauge length (L) = 0.057

$$P_{Cr} = \frac{\pi^3 (200x10^9)(0.00635)^4}{(0.057)^2} = 3103.3 kN = 697686 lbs$$

$$\sigma_{Cr} = \frac{4\pi^2 (200x10)^9}{(0.057 / 0.00635)^2} = 98 GPa$$

r=0.00317 m (0.125 inch in radius), gauge length (L) = 0.019 m (0.75 inch)

$$P_{Cr} = \frac{\pi^3 (200x10^9)(0.00317)^4}{(0.019)^2} = 1734.6 kN = 389982 lbs$$

$$\sigma_{Cr} = \frac{4\pi^2 (200x10)^9}{(0.019 / 0.00317)^2} = 220 GPa$$

In the elastic range, the critical uniaxial stress is much higher than loading stress level.

For material entering plastic range, use tangent modulus, E_t, instead of elastic modulus
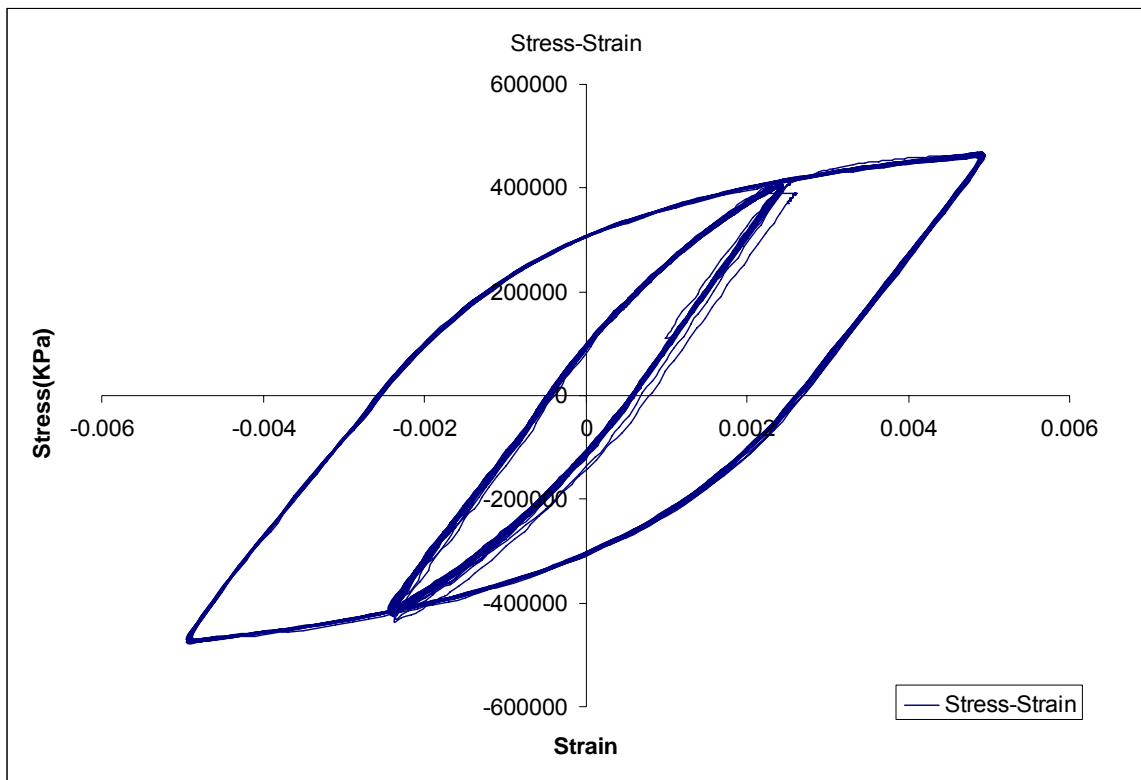
Figure B.1 Room temperature cyclic test result of a cylindrical solid specimen

E= 32.5 GPa (tangential modulus between 0.002 and 0.004, see Fig. B.1)

Same cylindrical specimen (Figure 3.1) was analyzed based on cyclic stress/strain curve (shown in B.1) – up to 0.5% strain

Dimension of the specimen: r=0.00635 m, gauge length (L) = 0.057

$$P_{Cr} = \frac{\pi^3 (32.5 x 10^9)(0.00635)^4}{(0.057)^2} = 504.3 kN = 113374 lbs$$

$$\sigma_{Cr} = \frac{4\pi^2(32.5x10^9)}{(0.057\ /0.00635)^2} = 16GPa$$

The critical uniaxial stress is much higher than loading stress level.

The modified round stepped cyclic test specimen (Figure 3.3):

r=0.00317 m (0.125 inch in radius), gauge length (L) = 0.019 m (0.75 inch)

$$P_{Cr} = \frac{\pi^3(32.5x10^9)(0.00317)^4}{(0.019)^2} = 281.9kN = 63371lbs$$

$$\sigma_{Cr} = \frac{4\pi^2(32.5x10^9)}{(0.019\ /0.00317)^2} = 35.72GPa$$

Based on the calculation, the critical bulking stress of modified round stepped cyclic test specimen is twice higher than non-modified specimen under same loading case.
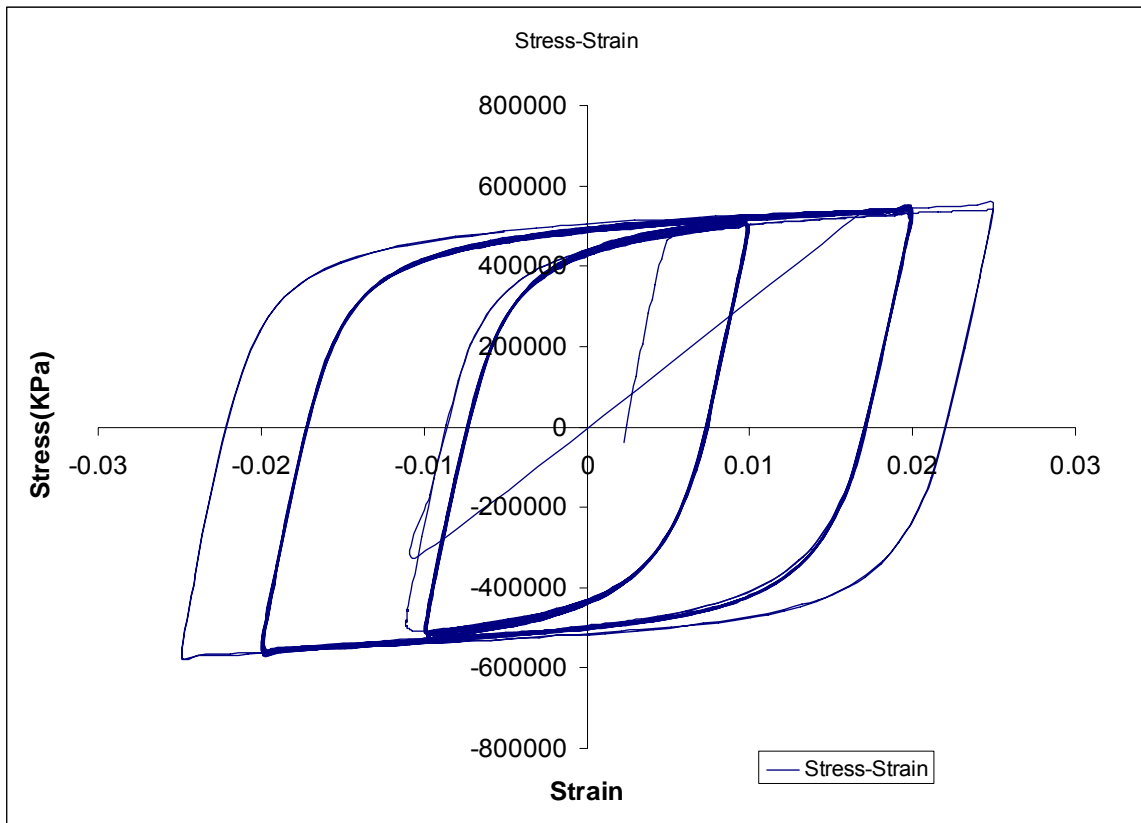
Figure B.2 Room temperature cyclic test result of a cylindrical solid specimen

Both critical buckling stresses of cylindrical (Figure 3.1) and modified round stepped cyclic test specimen (Figure 3.3) were analyzed based on cyclic stress/strain curve (shown in B.2) – up to 2.5% strain

E= 2.1 GPa (tangential modulus between 2% and 2.5%)

Solid Cylindrical specimen (Figure 3.1):

r=0.00635 m, gauge length (L) = 0.057

$$P_{Cr} = \frac{\pi^3 (2.1 x 10^9)(0.00635)^4}{(0.057)^2} = 32.6 kN = 7325.7 lbs$$

$$\sigma_{Cr} = \frac{4\pi^2(2.1x10^9)}{(0.057 \ /0.00635)^2} = 1GPa$$

Modified round stepped cyclic test specimen (Figure 3.3)

r=0.00317 m (0.125 inch in radius), gauge length (L) = 0.019 m (0.75 inch)

$$P_{Cr} = \frac{\pi^3(2.1x10^9)(0.00317)^4}{(0.019)^2} = 18.2kN = 4095lbs$$

$$\sigma_{Cr} = \frac{4\pi^2(2.1x10^9)}{(0.019 \ /0.00317)^2} = 2.31GPa$$

From the above calculations of critical stress for both solid cylindrical specimens, it is also observed that the modified round stepped cyclic test specimen (Figure 3.3) has higher critical buckling stress than non-modified one (Figure 3.1). Therefore, in order to reduce the buckling effect to the test results, the modified round stepped cyclic test specimen should be used for fully reversed cyclic loading tests.

Buckling Calculation-rectangular cross section

Formulas:

$$P_{Cr} = \frac{\pi^2 EI}{L_e^2}$$

$$\sigma_{Cr} = \frac{\pi^2 E}{(L_e / r)^2}$$

For two fixed end: $L_e = L/2$
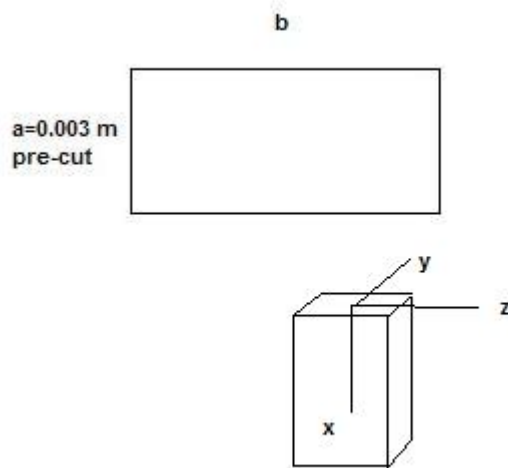
Figure B.3 Cross section of a flat specimen

Determine the relation between L and b regarding to buckling

$$I_x = \frac{1}{12} ba^3, A = ab$$

Since, $I_z = Ar_z^2, r_z^2 = \frac{I_z}{A} = \frac{\frac{1}{12}ba^3}{ab} = \frac{a^2}{12} \Rightarrow r_z = \frac{a}{\sqrt{12}}$

$$r_z = \frac{0.003}{\sqrt{12}} = 0.000866m \text{ (Assume b>a, radius of gyration for the weak axis,}$$

buckling occurs in x-y plane)

The effective slenderness ratio of the column with respect to buckling in the x-y plane is

$$\frac{L_e}{r_z} = \frac{0.5L}{a/\sqrt{12}} = \frac{0.5L}{0.000866} = 577.35L$$

$$\sigma_{Cr} = \frac{\pi^2 E}{(L_e/r)^2} = \frac{\pi^2 E}{[L/(2r_z)]^2} = \frac{4\pi^2 E}{(L/r_z)^2} = \frac{\pi^2 E}{(577.4L)^2}$$

For 1Cr-1/2 Mo, base material

From previous test, at 2% strain, load = 17.7 kN

Tangential modulus calculated at 2% strain is 2.11GPa.

$$L_{cr} = \sqrt{\frac{\pi^2 E}{(577.35)^2 \sigma_{cr}}} = \sqrt{\frac{\pi^2 (2.11*10^9)}{(577.35)^2 (\frac{17700}{0.0000317})}} = 0.0106m$$

The limitation of extensometer, 0.0122 m gauge length will be used. Since the critical length (0.0106 m) of the test section is smaller than gauge length of the test specimen (Figure 3.4). The specimen is more likely to buckle at 2% strain during the compressive loading. However, due to the limitation of the precut materials, the buckling effect was minimized by this geometry (Figure 3.4)

Appendix C Buckling Consideration of Thin-Walled Tubular Specimens
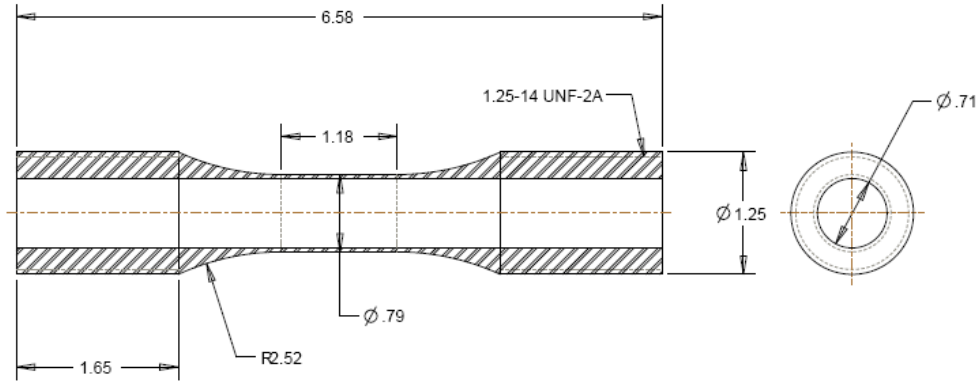
Figure C.1 Engineering drawing of thin-walled tubular specimen
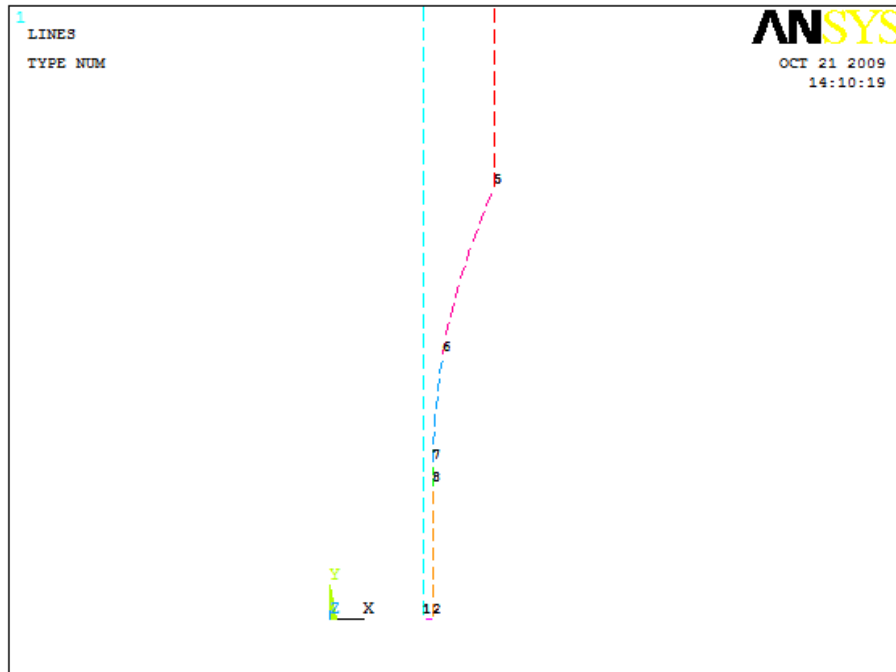
Figure C.2 Schematic of a quarter cross section of the tubular specimen

Fig. C.2. shows a quarter cross section of the designed tubular specimen. Point 1 and point 8 are selected as analyzing reference point for cylindrical tubular specimen buckling analysis. Point 1 and 2 are constraint in y-direction. The distance between 2 and 8 is the half span of the uniaxial extensometer. Point 7 is one end of the gage length of the test section on the specimen. Point 1 is the botton node point of the model, when buckling occurs, the x-displacement of this point will increase dramatically when small amount of load increases.

Point 8 is half inch above the horizontal symmetric line (line 1-2).

Case 1

Compressive loading without internal pressure applied
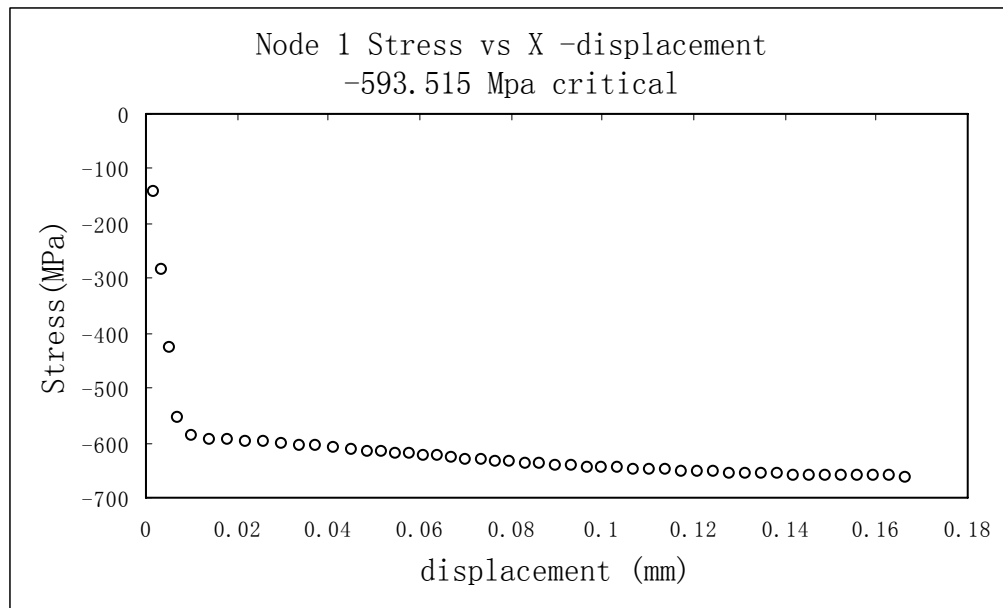
Figure C.3 Stress/displacement curve of point 1

From figure C.3, the x-displacement of point 1 rapidly increases at -593.5 MPa which sets as a critical buckling load level. At this moment the point 8 has a strain value of *-0.51%* which means that a compressive strain less than 0.51% will not yield buckling. Therefore, in biaxial thermal-mechanical loading tests the maximum cycling of ± 0.4% strain was selected to avoid buckling effect.

Case 2

Compressive loading with 7.4 MPa (1 ksi) internal pressure
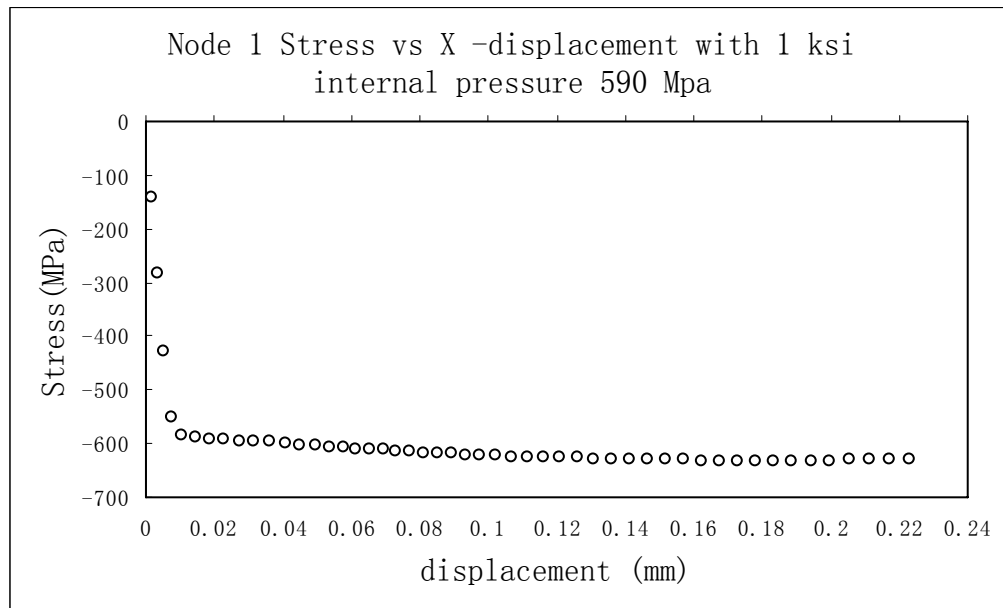
Figure C.4 Stress/displacement curve of point 1 (with internal pressure)

From figure C.4, the x-displacement of point 1 rapidly increases at -590 MPa which sets as a critical buckling load level. At this moment the point 8 has a strain value of -0.52% which means that a compressive strain less than 0.52% will not yield buckling. Therefore, in biaxial thermal-mechanical loading tests the maximum cycling of ± 0.4% strain was selected to avoid buckling effect.